PTNSS

1/2016 (164)

COMBUSTION ENGINES

INSTYTUT TECHNICZNY WOJSK LOTNICZYCH

ul. Księcia Bolesława 6, 01-494 Warszawa, skr. poczt. 96
tel.: 22 685 10 13; tel./faks: 22 836 44 71
www.itwl.pl e-mail: poczta@itwl.pl

ULEPSZYMY KAŻDĄ TECHNOLOGIĘ

COMBUSTION ENGINES

A Scientific Magazine/*Czasopismo naukowe*

1/2016 (164)

Rok LV

PL ISSN 2300-9896

Editor/*Wydawca*:

Polskie Towarzystwo Naukowe Silników Spalinowych
43-300 Bielsko-Biała, ul. Sarni Stok 93, Polska
tel.: +48 33 8130402, fax: +48 33 8125038
E-mail: sekretariat@ptnss.pl
WebSite: http://www.ptnss.pl

Editorial/*Redakcja*:
Instytut Silników Spalinowych i Transportu
Politechnika Poznańska
60-965 Poznań, ul. Piotrowo 3
tel.: +48 61 2244505, +48 61 2244502
E-mail: silniki@ptnss.pl

prof. dr hab. inż. Jerzy Merkisz (Editor-in-chief/*Redaktor Naczelny*)
dr hab. inż. Miłosław Kozak (Editorial Secretary for Science/*Sekretarz Naukowy Redakcji*) – papers@ptnss.pl
dr hab. inż. Ireneusz Pielecha, prof. PP (Technical Editor/*Redaktor Techniczny*)
mgr Krystyna Bubacz (Proofreading Editor/*Redaktor Językowy*)
prof. dr hab. inż. Wojciech Serdecki (Statistical Editor/*Redaktor Statystyczny*) and Associate Editors/*oraz Redaktorzy Tematyczni*

Contents/*Spis treści*

Deklaracja wersji pierwotnej
Wersją pierwotną czasopisma Combustion Engines jest wersja drukowana.

Publikacje naukowe drukowane w kwartalniku
Combustion Engines
otrzymują **13 punktów**
zgodnie z Komunikatem Ministra Nauki
i Szkolnictwa Wyższego z dnia 31 grudnia 2015 r.

Editor/*Wydawca*
Polish Scientific Society
of Combustion Engines
43-300 Bielsko-Biała, Sarni Stok 93 Street, Poland
tel.: +48 33 8130402, fax: +48 33 8125038
E-mail: sekretariat@ptnss.pl
WebSite: http://www.ptnss.pl

Subscriptions/*Prenumerata*
Send subscription requests to the Publisher's address.
Cost of a single issue PLZ25 + postage and packing.
Zamówienia należy kierować na adres Wydawcy.
Cena numeru czasopisma wynosi 25 zł + koszty wysyłki.

Preparation for print/*Przygotowanie do druku*
ARS NOVA Publishing House/*Wydawnictwo ARS NOVA*
60-782 Poznań, ul. Grunwaldzka 17/10A

Circulation/*Nakład*: 700 egz.

Printing and binding/*Druk i oprawa*
Print Group Szczecin, ul. Mieszka I 63/64

Wydawnictwo rejestrowane
w bazie danych o zawartości
polskich czasopism technicznych
– **BAZTECH** www.baztech.icm.edu.pl

Czasopismo indeksowane
w międzynarodowej bazie
IC Journal Master List
– **Index Copernicus** www.indexcopernicus.com

As recommended by the *Ministry of Science and Higher Education*, the panel of associate paper reviewers will be listed in each year's last issue of the magazine./*Zgodnie z zaleceniami Ministerstwa Nauki i Szkolnictwa Wyższego lista recenzentów współpracujących publikowana będzie w ostatnim w danym roku numerze czasopisma.*

Cover/*Okładka*
I – Mercury Mercruiser 4.3L V6 engine (*fot. www.mercurymarine.com*),
background (Monaco, dawn, city – *www.bestwallpapers-hd.com*)
IV – Toyota Prius 2016 1.8L 2ZR-FXE engine
(*fot. www.hybridcars.com*)

Article citation info:
WOŚ, P. et al. Technical and operating problems yielded from setting up the optimum value of geometric compression ratio in piston engines. *Combustion Engines*. 2016, **164**(1), 3-14. ISSN 2300-9896.

Paweł WOŚ
Artur JAWORSKI
Hubert KUSZEWSKI
Kazimierz LEJDA
Adam USTRZYCKI

PTNSS-2016-101

Technical and operating problems yielded from setting up the optimum value of geometric compression ratio in piston engines

The article discusses the problem of choosing the optimal compression ratio value in internal combustion engines at their design phase, according to today's development trends toward high economy and ecology of road transportation and the divers' expectations in vehicle use and performance. Because the variable compression ratio technology VCR is not yet developed well enough to be implemented into the mass production of engines in the near future, the choice of compression ratio value is always a serious task for constructors to find a compromise between the functional engine properties, operational characteristics, engine efficiency, the powertrain design complexity, and finally the exhaust emission level. Therefore, the paper examines the impact of the compression ratio on the combustion engine parameters mentioned above and presents some innovative designs, where the settings of the compression ratio value beyond the conventional range is connected with using additional solutions in design structure and control systems, with modifications corresponding to the working process in these engines.

Key words: *compression ratio, variable compression ratio engine, VCR*

Uwarunkowania techniczne i eksploatacyjne związane z wyborem optymalnej wartości geometrycznego stopnia sprężania w silnikach tłokowych

W artykule omówiono problem wyboru optymalnej wartości stopnia sprężania przy konstruowaniu silników spalinowych, zgodnie z trendami rozwojowymi w zakresie spełnienia wskaźników ekonomiki i ekologii transportu drogowego oraz ze współczesnymi oczekiwaniami użytkowników pojazdów w zakresie ich osiągów i eksploatacji. Ponieważ technologia zmiennego stopnia sprężania VCR (ang. Variable Compression Ratio) nie jest jeszcze na tyle zaawansowana, aby można było oczekiwać w najbliższym czasie jej wdrożenia do produkcji seryjnej, wybór wartości stopnia sprężania jest dla konstruktorów zawsze zadaniem znalezienia kompromisu pomiędzy założonymi parametrami użytkowymi, cechami eksploatacyjnymi, sprawnością silnika, złożonością konstrukcji i poziomem emisji szkodliwych składników spalin. W artykule przedstawiono zatem przeanalizowany wpływ wartości stopnia sprężania na wymienione wyżej parametry silników spalinowych oraz podano przykłady innowacyjnych konstrukcji, w których ustalenie wartości stopnia sprężania poza konwencjonalnym zakresem uwarunkowane jest zastosowaniem dodatkowych rozwiązań konstrukcyjnych i systemów sterujących, odpowiednio modyfikujących przebieg procesu roboczego w tych silnikach.

Słowa kluczowe: *stopień sprężania, silnik o zmiennym stopniu sprężania, VCR*

1. Introduction

Current and future development of internal combustion engines is conditioned primarily by the ecological and economic issues related to transportation that are clearly reflected by the limits of exhaust gas emission including carbon monoxide CO, hydrocarbons HC, nitric oxides NO_x, particulates PM, smoke, and carbon dioxide CO_2. All the emissions, particularly CO_2, are directly related to the amount of fuel consumed by the vehicle. Although carbon dioxide is not considered a toxic gas but many believes it plays a significant role in generating the greenhouse effect. Therefore, a permanent trend is to strive to further increasing the efficiency of propulsion systems for automotive vehicles and progressive substitution of fossil fuels with renewable energy sources.

The primary piston engine design parameter affecting the previously mentioned operational indicators is the compression ratio ε. It is defined as the ratio of minimum

1. Wprowadzenie

Obecny i przyszły rozwój silników spalinowych uwarunkowany jest przede wszystkim względami ekologicznymi i ekonomiką transportu. Wymagania w tym zakresie wyraźnie odzwierciedlają limity emisji składników spalin, tj. tlenku węgla CO, węglowodorów HC, tlenków azotu NO_x, cząstek stałych PM, zadymienia, a także dwutlenku węgla CO_2, którego emisja pozostaje w bezpośredniej relacji z ilością zużywanego przez pojazd paliwa. Dwutlenek węgla wprawdzie nie jest gazem toksycznym, lecz sądzi się, że odgrywa on znaczącą rolę w generowaniu efektu cieplarnianego. Z tego względu stałym trendem jest dążenie do dalszego podniesienia sprawności układów napędowych pojazdów samochodowych oraz sukcesywne zastępowanie paliw pochodzenia kopalnego paliwami odnawialnymi.

W silnikach tłokowych podstawowym parametrem konstrukcyjnym, wpływającym na wcześniej wspomniane wskaźniki pracy, jest stopień sprężania ε. Określony jest on

combustion chamber volume V_{min} at top dead center (TDC) piston position and the maximum volume of combustion chamber V_{max}, at the bottom dead center (BDC) piston position. For engines currently manufactured, this parameter is structurally set fixed but not at the value ensuring optimum efficiency, especially for wide range of speeds and loads at which traction motors operate. Due to high complexity of the phenomena involved in the entire engine work cycle, the choice of compression ratio value that design engineers have to make together with many other decisions on structural and regulation parameters of the new engine is the result of a multifaceted compromise between expected engine performance and other operational factors, mainly the emission of harmful exhaust components. A brief analysis of the compression ratio values for mass-produced engines, both medium- and high-speed ones, shows that they are chosen from the range of 9.0 to 12.0 (for spark ignition engines) and from 16.0 to 21.0 (for compression-ignition engines). The main constraints for setting the compression ratio at lower limits is the decrease in total engine efficiency below an acceptable level, and for compression-ignition engines also the deterioration of self-ignition stability of the injected fuel and difficulties with cold start. Instead, the constraints for setting the compression ratio at upper limits is intensification of the knocking in spark ignition engines and increasing dynamic loads of the crankshaft and the cylinder group mechanisms in compression-ignition engines.

As a result of efforts towards avoiding unfavorable design compromises in modern reciprocating engines, a few years

przez stosunek minimalnej objętości komory spalania V_{min} w zwrocie zewnętrznym (ZZ) tłoka, lub inaczej – górnym martwym położeniu tłoka (GMP), do maksymalnej objętości przestrzeni nadtłokowej V_{max} odpowiednio w zwrocie wewnętrznym (ZW), tj. w dolnym martwym położeniu tłoka (DMP). W silnikach obecnie stosowanych w produkcji seryjnej parametr ten jest ustalony konstrukcyjnie na stałe, co nie jest rozwiązaniem zapewniającym optymalną efektywność silnika, zwłaszcza w zmiennych warunkach prędkości i obciążenia, w jakich operują w szczególności silniki trakcyjne. Złożoność zjawisk w całym cyklu roboczym silnika powoduje, że dobór przez konstruktora wartości stopnia sprężania, jak również wielu innych parametrów konstrukcyjnych i regulacyjnych silnika, jest wynikiem określonego kompromisu pomiędzy osiągami silnika a innymi wskaźnikami pracy, przede wszystkim emisją szkodliwych składników spalin. Pobieżna analiza wartości stopnia sprężania w seryjnych silnikach średnio- i szybkoobrotowych wskazuje, że mieszczą się one przeważnie w zakresie od 9,0 do 12 (dla silników z zapłonem iskrowym) oraz od 16 do 21 (dla silników z zapłonem samoczynnym). Podstawowymi ograniczeniami w ustaleniu granicznych dolnych wartości stopnia sprężania jest związany z tym spadek sprawności ogólnej silnika poza akceptowalny poziom, a dla silników z zapłonem samoczynnym również pogorszenie pewności samozapłonu dawki paliwa i procesu rozruchu. Natomiast ograniczeniami "z góry" jest, w przypadku silników z zapłonem iskrowym, nasilenie się zjawiska spalania stukowego, a w odniesieniu do silników z zapłonem samoczynnym również wzrost obciążeń dynamicznych układu T–P–C (tłok–pierścienie–cylinder).

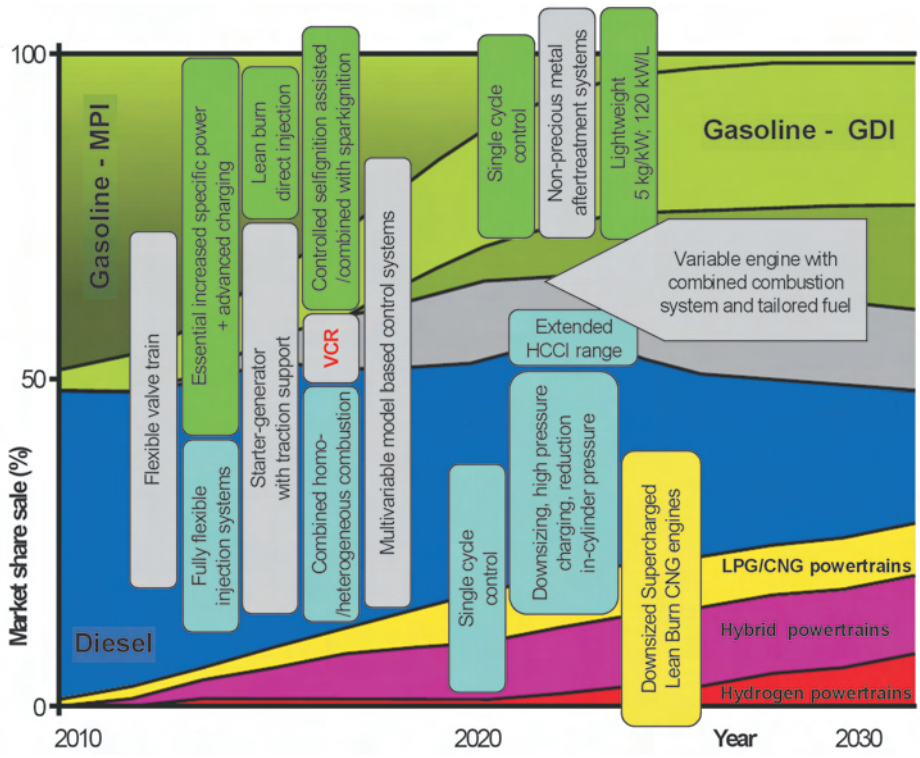

Fig. 1. The forecasts for the development and market share of chosen advanced technologies in automotive combustion powertrains according to [2]

Rys. 1. Prognozy w zakresie rozwoju i udziału wybranych zaawansowanych technologii w spalinowych źródłach napędu pojazdów samochodowych wg [2]

W wyniku dążeń do uniknięcia niekorzystnych kompromisów konstrukcyjnych we współczesnych silnikach tłokowych, kilka lat temu pojawiła się koncepcja, będąca jedną z bardziej zaawansowanych dróg rozwoju silników spalinowych, a odpowiadająca wspomnianym wyżej kierunkom poprawy ich ekologii i efektywności energetycznej, m.in. przez umożliwienie szerszego wykorzystania paliw alternatywnych lub niskotemperaturowych procesów spalania [14]. Chodzi mianowicie o konstrukcje silników, w których stopień sprężania jest parametrem regulacyjnym i może być zmieniany bezstopniowo w szerokim zakresie i stosunkowo krótkim czasie. Technologia ta określana jest mianem VCR (ang. *Variable Compression Ratio* – zmienny stopień sprę-

ago a concept has been proposed that is one of the more advanced development paths for combustion engines. It corresponds to the above-mentioned directions for improving environmental impact and energy efficiency of the engines by, among others, allowing wider use of alternative fuels or low-temperature combustion processes [14]. Namely, there are engine designs where the compression ratio is a regulated parameter and can be changed continuously over a wide range and in a relatively short time. This technology is called VCR – Variable Compression Ratio. Works on the development of this type of power drives are conducted by a few research and development centers in the world [3, 9], including the authors' team [12, 13]. While the idea of VCR engines shows a certain complexity of construction and technology and can cause some operational problems, it is expected [2, 10], that it could become the standard design for reciprocating engines in the near future, mainly due to the well-established constraints of fixed compression ratio engines (Fig. 1).

2. The compression ratio as a parameter shaping the performance and operating processes in internal combustion engines

The compression ratio is a value which heavily influences the thermodynamic parameters in the combustion chamber at the end of the compression stroke, as well as the further course of the combustion process. Increasing the compression ratio decreases specific fuel consumption and increases engine power. This is the result of increased theoretical efficiency of cycle η_t, which may be expressed mathematically in the simplest form for the Otto cycle (Eq. 1):

$$\eta_t = 1 - 1/(\varepsilon^{\kappa-1}) \tag{1}$$

where: η_t – Otto cycle theoretical efficiency, ε – compression ratio, κ – polytropic index.

However, the freely increasing the engine efficiency this way is limited, due to the structural and durability constraints as well as the unfavorable changes to the fuel combustion process that appear in spark-ignition engines with compression ratio raised above the permissible limit. In compression ignition engines it is also not possible to increase the compression ratio freely; too high value causes excessive mechanical losses that are greater than the profit resulting from improved overall engine efficiency.

To choose an appropriate compression ratio value many factors must be taken into account. Among them, the most important are:
– octane/cetane number of fuel,
– the material that the piston and piston head are made of,
– combustion chamber design,
– harmful pollutant emissions.

In diesel engines the prerequisite to ignite the fuel injected into the combustion chamber is high pressure and temperature of the cylinder charge at the end of the compżania). Prace nad tego typu jednostkami napędowymi są prowadzone przez nieliczne ośrodki badawczo-rozwojowe na świecie [3, 9], w tym przez zespół autorów publikacji [12, 13]. Pomimo tego, że idea silników o zmiennym stopniu sprężania VCR wiąże się z pewnym skomplikowaniem konstrukcyjno-technologicznym oraz problemami eksploatacyjnymi, z uwagi na ograniczenia silników o stałym stopniu sprężania, ocenia się [2, 10], że może stać się ona w niedalekiej przyszłości standardem konstrukcyjnym w silnikach tłokowych (rys. 1).

2. Stopień sprężania jako parametr determinujący właściwości eksploatacyjne i przebieg procesów roboczych silników spalinowych

Stopień sprężania jest wielkością, od której zależą w zasadniczej mierze parametry termodynamiczne ładunku w cylindrze pod koniec suwu sprężania oraz dalszy przebieg procesu spalania. Wraz ze wzrostem stopnia sprężania maleje jednostkowe zużycie paliwa i wzrasta moc silnika. Jest to skutkiem wzrostu sprawności teoretycznej obiegu η_t, którą można wyrazić zależnością matematyczną, przedstawioną w najprostszej postaci dla obiegu Otto równaniem (1): gdzie: η_t – sprawność teoretyczna obiegu Otto, ε – stopień sprężania, κ – wykładnik politropy.

Jednak możliwości dowolnego zwiększania tym sposobem sprawności silników są ograniczone ze względów konstrukcyjnych, wytrzymałościowych oraz przez niekorzystny przebieg spalania paliw w silnikach z zapłonem iskrowym o podniesionym ponad dopuszczalną granicę stopniu sprężania. W silnikach z zapłonem samoczynnym nie jest również możliwe dowolne zwiększanie stopnia sprężania; zbyt wysoka jego wartość powoduje nadmierne straty mechaniczne, które są większe niż zysk wynikający z poprawy sprawności ogólnej silnika.

Aby dobrać odpowiednią wartość stopnia sprężania, należy wziąć pod uwagę wiele czynników. Do najważniejszych należą:
– liczba oktanowa/cetanowa użytego paliwa,
– materiał głowicy i tłoka,
– konstrukcja komory spalania,
– emisja szkodliwych składników spalin.

W silnikach o zapłonie samoczynnym warunkiem koniecznym do zapłonu paliwa wtryśniętego do komory spalania jest odpowiednio wysokie ciśnienie i wysoka temperatura ładunku cylindra w końcu suwu sprężania. Najtrudniejsze warunki do osiągnięcia odpowiednich wartości tych parametrów istnieją podczas zimnego rozruchu silnika. Na ciśnienie sprężania, oprócz stopnia sprężania, pewien wpływ ma również prędkość obrotowa rozruchu silnika; stąd istotna jest też sprawność układu rozruchowego silnika.

W rezultacie bazowania na teorii silników tłokowych, znana jest zależność termodynamiczna na temperaturę czynnika roboczego w końcu suwu sprężania T_2 w funkcji stopnia sprężania, o postaci (2), gdzie: T_1 – temperatura ładunku cylindra na początku suwu sprężania, T_2 – tempe-

pression stroke. The most difficult conditions to achieve appropriate values for these parameters exist during engine cold start. Here, the end-of-stroke compression pressure is affected generally by the compression ratio and motor starting speed; hence the effectiveness of the engine starter system is also important.

Based on the theory of piston engines, there is a known thermodynamic dependence of working charge temperature at the end of the compression stroke T_2 as a function of compression ratio in the form:

$$T_2 = T_1 \varepsilon^{m_1-1} \tag{2}$$

where: T_1 – in-cylinder temperature at the beginning of compression stroke, T_2 – in-cylinder temperature at the end of compression stroke, ε – compression ratio, m_1 – average polytropic index at compression stroke.

Experimental studies on the effect of the compression ratio on the diesel engine starting process were performed by Abramek [1]. The author gives, among others, the relationship between the temperature in the combustion chamber at the end of the compression stroke and the time of cold starting of the engine as a function of compression ratio. According to the expectations based on the previously cited theoretical equations, the temperature of cylinder charge increases as the compression ratio is increased (Fig. 2), while the time required to start-up the cold engine decreases (Fig. 3).

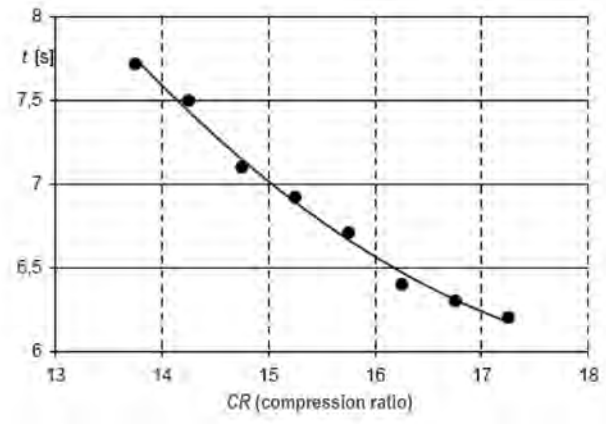

Fig. 3. Effect of compression ratio on the time required for start-up the cold diesel engine [1]

Rys. 3. Wpływ stopnia sprężania na czas zimnego rozruchu silnika z zapłonem samoczynnym [1]

Going further, an equally important effect on the process of fuel injection and atomization in the combustion chamber is the effect of the compression ratio, in particular the compression pressure. Appropriate relationships and experimental results are given by Zablocki in his fundamental work [15]. These interactions have implications for the subsequent stages of the operating cycle, and one can say that in light of the current technical accounts and legislations in the development of internal combustion engines, the most significant is the effect of compression

ratura ładunku cylindra w końcu suwu sprężania, ε – stopień sprężania, m_1 – średni wykładnik politropy sprężania.

Badania doświadczalne nad wpływem wartości stopnia sprężania na proces rozruchu silnika z zapłonem samoczynnym prowadził Abramek [1]. Autor podał m.in. zależność temperatury ładunku w cylindrze w końcu suwu sprężania oraz czasu zimnego rozruchu silnika w funkcji stopnia sprężania. Zgodnie z przewidywaniami na podstawie wcześniej przytoczonych zależności teoretycznych, wraz ze wzrostem stopnia sprężania rośnie temperatura ładunku w cylindrze (rys. 2), maleje natomiast czas wymagany do rozruchu zimnego silnika (rys. 3).

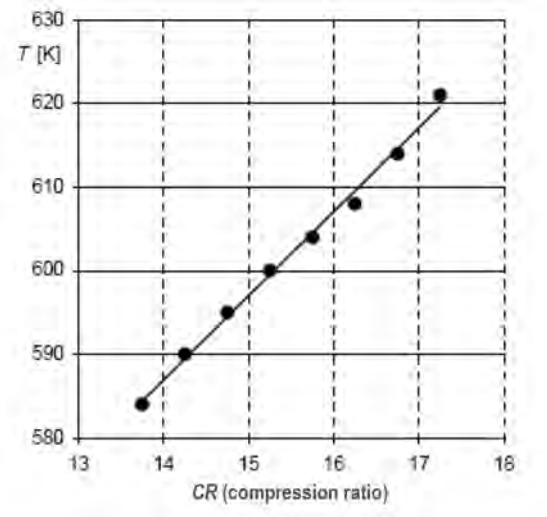

Fig. 2. Effect of the compression ratio on the in-cylinder temperature at the end of the compression stroke [1]

Rys. 2. Wpływ stopnia sprężania na temperaturę ładunku w cylindrze w końcu suwu sprężania [1]

Także istotny jest wpływ stopnia sprężania, a w szczególności ciśnienia sprężania na przebieg procesu wtrysku i rozpylenia paliwa w komorze spalania (odpowiednie zależności i wyniki badań doświadczalnych podaje w swej fundamentalnej pracy Zabłocki [15]). Oddziaływania te mają implikacje dla kolejnych etapów cyklu roboczego i można powiedzieć, że w świetle obecnych uwarunkowań technicznych i prawnych w rozwoju silników spalinowych najbardziej znaczącym jest wpływ wartości stopnia sprężania na przebieg i efekty procesu spalania, tj. parametry użytkowe, ekonomikę pracy i emisję szkodliwych składników spalin. Jeśli chodzi o dwa pierwsze wymienione efektów, to korzystne jest stosowanie wyższych wartości stopnia sprężania z uwagi na towarzyszący temu wzrost sprawności obiegu, a w rezultacie wzrost średniego ciśnienia indykowanego. Wskazują na to, prócz jałowych zależności teoretycznych, również wyniki przeprowadzonych symulacji (rys. 4) z użyciem pakietu Diesel-RK [6, 7] dla prototypowego silnika o zmiennym stopniu sprężania VCR, wg autorskiego [12, 13] projektu i konstrukcji, pracującego w trybie zapłonu samoczynnego.

Przeprowadzone obliczenia w zakresie emisyjności spalin wskazują jednak na kontradykcyjny efekt stopnia

ratio on the course and effects of the combustion process, i.e. output performances, operation efficiency and harmful emissions. As for the first two of these effects, it is preferred to use higher values of the compression ratio because of the increased cycle efficiency resulting in an increased mean indicated pressure. Apart from clean theoretical dependencies this is also proven by the results of the simulations (Fig. 4) using Diesel-RK package [6, 7] for a prototype engine of variable compression ratio VCR according to the authors' own design and construction that operates as the compression-ignition engine [12, 13].

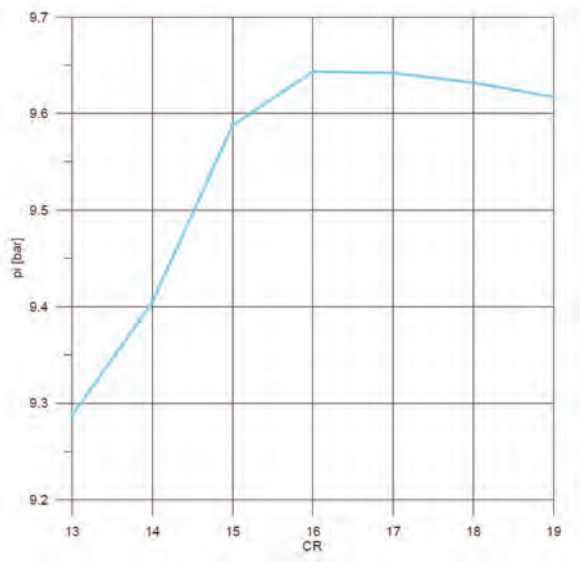

Fig. 4. Effect of compression ratio on mean indicated pressure for variable compression ratio VCR engine

Rys. 4. Wpływ stopnia sprężania na wartość średniego ciśnienia indykowanego w silniku o zmiennym stopniu sprężania VCR

However, the calculations for exhaust gas emission show the contradictions between the compression ratio and the analyzed indicators. This is mostly evident for changes in particulate PM (Fig. 5) and nitrogen oxides NO_x (Fig. 6) emissions.

From analysis of the presented curves it can be concluded that finding an appropriate constructional setting of compression ratio value is not an obvious problem. On the one hand, to follow high energy conversion efficiency and positive environmental effects on particulate matter emissions, the optimum compression ratio should be set around the value of 16.0. Such values are generally standard sets for modern compression-ignition engines; it guarantees proper engine operating characteristics, for example the easy and reliable engine start-up in low temperatures. However, considering the significant problem of nitrogen oxide emissions, it would be better to lower the values of the compression ratio, even below 14.0, which, as the further discussion will show, involves the use of additional advanced systems that ensure a stable operation of the engine, especially during the warm-up phase.

sprężania w obszarze analizowanych wskaźników. Najbardziej widoczne jest to w zestawieniu przebiegu zmian emisji cząstek stałych PM (rys. 5) i tlenków azotu NO_x (rys. 6).

Analizując przedstawione przebiegi, można stwierdzić, że ustalenie konstrukcyjnej wartości stopnia sprężania

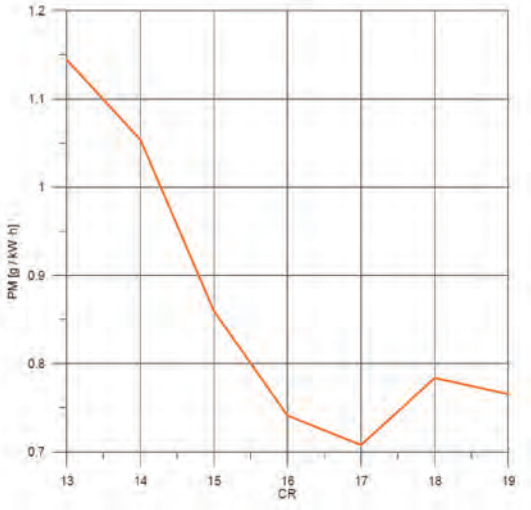

Fig. 5. Effect of compression ratio on particulate matter PM specific emission for variable compression ratio VCR engine

Rys. 5. Wpływ stopnia sprężania na emisję jednostkową cząstek stałych PM w silniku o zmiennym stopniu sprężania VCR

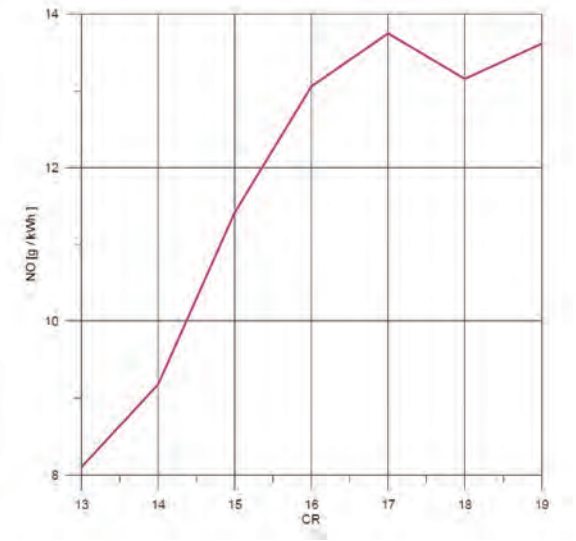

Fig. 6. Effect of compression ratio on nitric oxides NO_x specific emission (recalculated as NO emission) for variable compression ratio VCR engine

Rys. 6. Wpływ stopnia sprężania na emisję jednostkową tlenków azotu NO_x (w przeliczeniu na NO) w silniku o zmiennym stopniu sprężania VCR

nie jest zagadnieniem jednoznacznym. Gdy weźmie się pod uwagę pozytywny efekt energetyczny i ekologiczny w zakresie emisji cząstek stałych, optymalne wartości stopnia sprężania oscylują wokół liczby 16. Takie wartości są z reguły standardowymi stopniami sprężania dla współ-

3. Problem synthesis based on the selected internal combustion engine layouts

SkyActiv engines used in Mazda vehicles are examples of modern internal combustion engines where a constructional layout quite different from the current standards has been adopted, including the value of the compression ratio [8]. The characteristic feature of this family of engines is the value of the compression ratio set at 14.0, the same for both gasoline and diesel units. According to the manufacturer, these engines belong to the conceptually new system of components and powertrains of Mazda cars, designed in accordance with the idea of an innovative technology platform under the marketing name SkyActiv. They were introduced for the first time to the world markets in 2012 in the CX-5 and 6 car models. Among the wide range of engines especially interesting is the compression-ignition

3. Synteza problematyki na przykładzie wybranych konstrukcji silników spalinowych

Przykładami nowoczesnych silników spalinowych, dla których przyjęto odbiegającą od obecnych standardów strategię założeń konstrukcyjnych, m.in. w zakresie stopnia sprężania, są silniki SkyActiv, stosowane w pojazdach marki

Table 1. Technical specifications of MAZDA 2.2 SKYACTIV-D engine [8]

Tabela 1. Charakterystyka techniczna silnika MAZDA 2.2 SKYACTIV-D [8]

Engine type/*rodzaj silnika*	direct injection compression-ignition, turbocharged/*turbodoładowany, z zaplonem samoczynnym i wtryskiem bezpośrednim*
Cylinder number and layout/*liczba i układ cylindrów*	4, inline/*4 w układzie rzędowym*
Total engine capacity/*pojemność skokowa*	2191 cm^3
Cylinder bore × piston stroke/ *średnica cylindra × skok tłoka*	86.0 mm × 94.3 mm
Compression ratio/*stopień sprężania*	14.0
Max. power/*moc maks.*	110 or 129 kW at 4500 rpm
Max. torque/*maks. moment obrotowy*	380 or 420 N·m
Valve layout/*układ rozrządu*	DOHC, 4 valves per cylinder
Valve train/*napęd zaworów*	two overhead camshafts DOHC; main valve train with single row machine chain, mid-camshaft train with two gears, fixed-phase inlet valves timing, two-phase exhaust valves timing with on-demand opening of half number of valves during inlet stroke using triple cams and switchable roller finger followers/*dwa wałki krzywkowe zamontowane w głowicy – układ DOHC; napęd jednego wałka łańcuchem maszynowym jednorzędowym od wału korbowego, napęd międzywałkowy przekładnią zębatą, stałe fazy rozrządu zaworów ssących, dwufazowy rozrząd zaworów wydechowych z aktywowaną na żądanie fazą uchylenia połowy zaworów wydechowych w suwie ssania za pomocą potrójnych krzywek i podwójnych, przełączalnych dźwigni zaworowych*
Turbocharging system/*system doładowania*	two turbochargers working together or separately, air cooling system intercooler/ *dwie turbosprężarki pracujące łącznie lub niezależnie, układ chłodzenia powietrza doładowującego intercooler*
Fuel system/*układ zasilania*	DENSO common-rail, multihole piezoelectric injectors, splitting fuel dose up to 9 parts, max. fuel injection pressure 2000 bar/*DENSO typu common-rail, wtryskiwacze piezoelektryczne wielootworkowe, umożliwiające podział dawki paliwa na 9 części, maksymalne ciśnienie wtrysku paliwa 2000 bar*
Exhaust aftertreatment system/*system ograniczania emisji spalin*	cooled exhaust gas recirculation EGR, oxidation catalyst and diesel particulate filter periodically cleaned due to temperature increase through additional fuel injection during exhaust stroke/*układ recyrkulacji spalin EGR z chłodnicą spalin, układ wydechowy z katalizatorem utleniającym i filtrem cząstek stałych, okresowe oczyszczanie filtra cząstek stałych metodą termiczną przez dodatkowy*
Exhaust emission standard/*poziom emisji spalin*	Euro 6
Lubrication system/*układ olejenia*	under circulation, full-flow oil filter, pressurized lubrication of crankshaft bearings, the rest of pairs lubricated by oil splashing, cooling oil spray on the bottom of piston head/ *obiegowy, filtr pełnego przepływu, łożyska ślizgowe smarowane pod ciśnieniem, pozostałe pary trące smarowane rozbryzgowo, chłodzący natrysk oleju pod denka tłoków*
– oil filter type/*typ filtra oleju*	Mazda SHY1 14 302 – alternately also MAHLE OC1182, BluePrint ADM52123, WIX WXWL7516, Filtron OP 597/1
– recommended oil class and type/*zalecany typ I klasa oleju smarującego*	Mazda Original Oil Supra DPF 0W-30 Mazda Original Oil Ultra DPF 5W-30

engine marked as SkyActiv-D. Its displacement is 2.2 L and maximum power is 129 kW at 4500 rpm. It is worth noting that despite the global trend towards "downsized" engines, the SkyActiv engines are developed according to different concepts involving, among others, on reducing the compression ratio of the engine. A more complete SkyActiv-D engine specification is given in Table 1.

The relatively low for a compression ignition engine geometric compression ratio of 14.0, allows for reduced mechanical loads of main parts of the engine structure, thus the engine block, for example, can be made of less strength but much lighter alloys. According to the manufacturer, the overall engine weight is decreased by about 25 kg compared to previous, similarly sized engines.

Another, yet definitely the most important benefit of lowered compression ratio is the reduction of nitrogen oxides NO_x emissions. Thanks to low CR value, the engine can meet the current limits on nitrogen oxides emissions (Euro 6, for example) without the need to use the expensive and problematic aftertreatment systems in exhaust duct like selective reduction of nitrogen oxides SCR/AdBlue®. This gives it a significant advantage, mainly from the point of view of the end users.

Unfortunately, reducing the compression ratio in diesel engines too much brings many negative consequences. In order to compensate the drop in indicated efficiency of the work cycle, and to further ensure appropriate parameters for power, torque, and engine dynamics in a wide range of engine speeds and loads, it was necessary to supercharge the engine with an efficient and fast, low inertia device. Thus the SkyActiv-D engine is equipped with a pair of two turbochargers (Fig. 7), working together or independently.

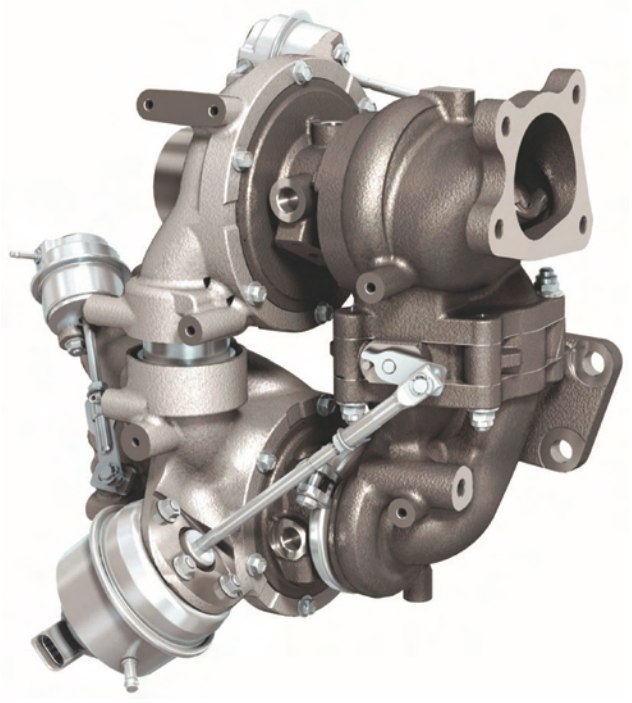

Fig. 7. Turbocharging unit of SkyActiv-D engine [4]

Rys. 7. Zespół turbosprężarek silnika SkyActiv-D [4]

Mazda [8]. Ich cechą charakterystyczną jest wartość stopnia sprężania ustalona na poziomie 14 i jest ona jednakowa zarówno dla jednostki napędowej z zapłonem iskrowym, jak i z zapłonem samoczynnym. Jak podaje producent, silniki te należą do koncepcyjnie nowego systemu podzespołów i układów funkcjonalnych samochodów marki Mazda, zaprojektowanych zgodnie z ideą innowacyjnej platformy technologicznej o marketingowej nazwie SkyActiv. Wprowadzone zostały po raz pierwszy na rynki światowe w 2012 r. w modelach CX-5, Mazda 6. Wśród szerokiej gamy jednostek napędowych na szczególną uwagę zasługuje wersja silnika z zapłonem samoczynnym, oznaczana jako SkyActiv-D, o pojemności skokowej 2,2 l i mocy maksymalnej 129 kW przy 4500 obr/min. Warto zaznaczyć, że pomimo ogólnoświatowego trendu w kierunku tzw. downsizingu, jednostki napędowe SkyActiv są rozwijane wg odmiennej koncepcji, polegającej m.in. na wyraźnym odprężeniu silnika. Pełniejszą charakterystykę techniczną silnika SkyAcyiv-D podano w tabeli 1.

Stosunkowo niski, jak na silnik z zapłonem samoczynnym, geometryczny stopień sprężania o wartości 14 pozwala na uzyskanie zredukowanych obciążeń mechanicznych elementów roboczych silnika, stąd np. kadłub silnika może być wykonany z mniej wytrzymałych, ale za to znacznie lżejszych stopów lekkich. Według informacji producenta, uzyskano zmniejszenie ogólnej masy silnika o około 25 kg w stosunku do poprzednich, porównywalnych konstrukcji.

Kolejną, najważniejszą korzyścią wynikającą z zastosowania zmniejszonego stopnia sprężania jest obniżenie emisji tlenków azotu NO_x. Dzięki temu silnik może spełnić obecne limity emisji tlenków azotu (tj. na poziomie normy Euro 6) bez konieczności stosowania w układzie wydechowym kosztownego i problematycznego w eksploatacji systemu selektywnej redukcji tlenków azotu SCR/AdBlue®, co jest istotną zaletą, chociażby z punktu widzenia użytkownika końcowego.

Radykalne obniżenie stopnia sprężania w silniku z zapłonem samoczynnym powoduje jednak wiele niekorzystnych konsekwencji. Celem zrekompensowania spadku sprawności indykowanej obiegu, a w dalszej konsekwencji dla zapewnienia właściwych parametrów mocy, momentu obrotowego, dynamiki silnika w szerokim zakresie prędkości obrotowej i zmian obciążenia itd., konieczne było zastosowanie wydajnego układu doładowania o małej bezwładności. Silnik SkyActiv-D wyposażono zatem w układ dwóch turbosprężarek (rys. 7), pracujących łącznie lub niezależnie.

Turbosprężarka o większej wydajności (a także bezwładności działania), uaktywniana jest przy większych obciążeniach; druga, o mniejszej wydajności, ale też o mniejszej bezwładności działania, pozwala na utrzymanie żądanego przebiegu momentu obrotowego przy nagłych zmianach obciążenia. Sterowanie włączaniem poszczególnych turbin i sprężarek odbywa się za pomocą sterowanych klap upustowych, zarówno po stronie spalin, jak i powietrza doładowującego (rys. 7).

Zastosowanie obniżonego stopnia sprężania powoduje znaczne zmniejszenie zdolności rozruchowych silnika oraz

The turbocharger with a higher efficiency (and also with higher device inertia) is activated at higher loads; the second one with a lower efficiency, but also with lower device inertia, allows to maintain the desired rate of torque at quick load changes. Controlling the activation of individual turbines and compressors is done using controlled pressure relief valves on both the exhaust and supercharged air sides (Fig. 7).

The use of low compression ratio results in a significant deterioration in motor starting capability and leads to unstable operation due to ignitability problem, known as the "misfire" phenomenon, especially during start-up and initial phase of the engine warming up. Therefore, in order to make starting the SkyActiv-D engine easier, efficient ceramic glow plugs are placed directly in the combustion chamber and the appropriate fuel injection strategy is implemented as well.

To ensure the stability of the combustion process in the engine warm-up phase, an "on demand" control strategy for hot exhaust gas recirculation has also been applied. It is performed by a mechanical double lift of a half of exhaust valves system IDEVA. The function of double exhaust valve lift is achieved by a triple-cam of the camshaft and a switchable, double rocker arm (Fig. 8).

The first opening of the exhaust valves takes place normally during the exhaust stroke. The second opening – a slight gap of one exhaust valve for each cylinder occurs during the intake stroke, and it is intended to provide the cylinders with a small portion of hot gases to raise the in-cylinder temperature assuring reliable self-ignition of the fuel (Fig. 9).

The single-alloy camshaft is made of ductile iron; cam surfaces are hardened through induction heating process. The sliding surfaces of rocker arms that co-work with

prowadzi do niestabilnej pracy w postaci tzw. zjawiska wypadania zapłonów (*ignitability problem*), zwłaszcza podczas rozruchu i w początkowej fazie rozgrzewania się silnika. Aby zatem ułatwić rozruch w silniku SkyActiv-D zastosowano wydajne, ceramiczne świece żarowe umieszczone w komorze spalania oraz dostosowano odpowiednią strategię wtrysku paliwa.

Do zapewnienia stabilności procesu spalania w fazie nagrzewania się silnika zastosowano strategię sterowania "na żądanie" gorącą recyrkulacją spalin przez układ mechaniczny podwójnego wzniosu połowy zaworów wydechowych IDEVA. Funkcja podwójnego wzniosu zaworów wydechowych realizowana jest za pomocą potrójnych krzywek wałka rozrządu i przełączalnych, podwójnych dźwigni zaworowych (rys. 8).

Pierwsze otwarcie zaworów wydechowych standardowo występuje podczas suwu wydechu. Drugie, nieznaczne uchylenie jednego z zaworów wydechowych następuje w suwie ssania i ma na celu dostarczenie do cylindrów niewielkiej porcji gorących spalin, aby zwiększyć temperaturę ładunku do wartości zapewniającej pewny samozapłon paliwa (rys. 9).

Wałek rozrządu jednolity wykonany jest z żeliwa sferoidalnego; powierzchnia krzywek jest utwardzana indukcyjnie. Powierzchnie ślizgowe dźwigni zaworowych, współpracujące z zewnętrznymi krzywkami, z uwagi na duże naciski jednostkowe i występowanie tarcia ślizgowego są utwardzane azotkiem chromu w procesie cieplno-chemicznym, podczas którego wytwarzana jest bardzo twarda, lecz stosunkowo cienka warstwa ślizgowa o handlowej nazwie producenta dźwigienek zaworowych TriondurCN [11].

Złożoność konstrukcyjna, technologiczna i mechatroniczna układu rozrządu w silniku SkyActiv-D, choć godna uwagi, może w pewnych warunkach pracy silnika stwarzać określone problemy eksploatacyjne.

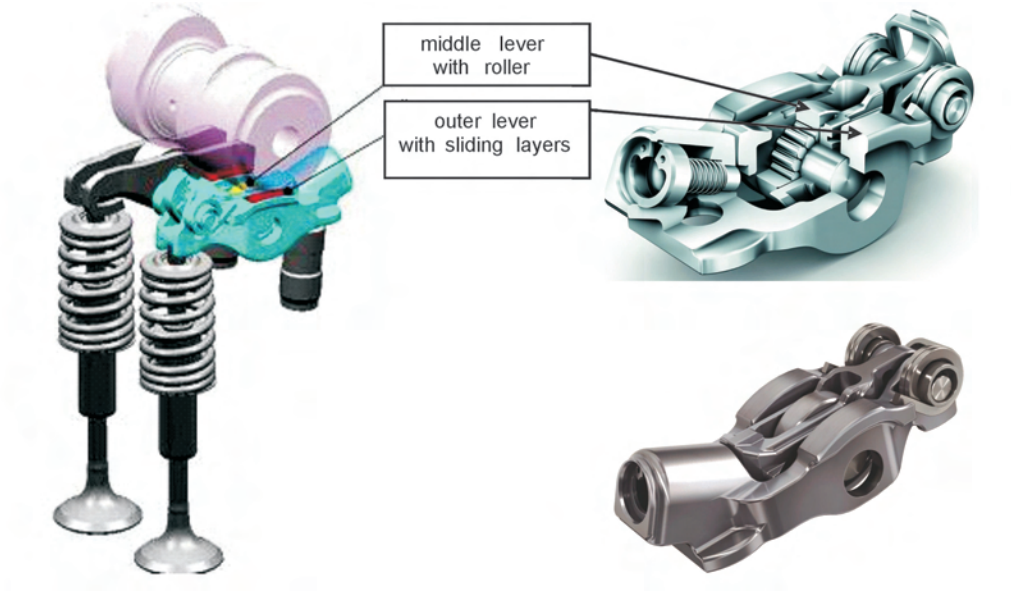

Fig. 8. Design of the two-phase exhaust valve lift system in the engine SkyActiv-D with "on-demand" hydro-electric switchable arms [5, 11]

Rys. 8. Konstrukcja dwufazowego układu rozrządu zaworów wydechowych w silniku SkyActiv-D z elektrohydraulicznie przełączalnymi "na żądanie" dźwigienkami zaworowymi [5, 11]

4. Podsumowanie

Dobór konstrukcyjny optymalnej wartości stopnia sprężania jest zagadnieniem złożonym. Wybierając ustawienia odpowiednie pod względem przewidywanych parametrów użytecznych silnika, nie można zagwarantować właściwych wartości dla innych, istotnych np. z punktu widzenia ochrony środowiska naturalnego, parametrów roboczych i wyjściowych silnika. Pewne dodatkowe możliwości kompensacji niekorzystnych efektów, wynikających z założonych wartości

outer cams, due to their operation under high unit pressure and sliding friction, are treated by chromium nitride in a thermo-chemical process, which creates a very hard but relatively thin sliding layer under the rocker manufacturer trade name TriondurCN [11].

The noteworthy complexity in design, technology, and mechatronics of SKYACTIV-D engine valve lifting system, may also cause specific technical problems under certain engine operating conditions.

4. Conclusions

Constructional selection of the optimum compression ratio value is a complex issue. Choosing the appropriate settings with regards to expected engine output parameters can not guarantee appropriate values for other parameters important from the point of view of environmental protection, engine operation and its output characteristics. Some possible compensation of adverse effects resulting from the fixed value of geometric compression ratio can be derived from simultaneously coupled extended control of supercharging, cold and hot exhaust gas recirculation, valve lifting and timing, and finally the use of complex maps of fuel injection characteristics and powerful functionality of individual engine components affecting engine working process. However, this results in a considerable growth in complexity of the engine working systems and its auxiliaries. A promising alternative, which might give many more advantages at simplifying the entire powerdrive system construction, is the still-under-development technology of variable compression ratio in VCR engines.

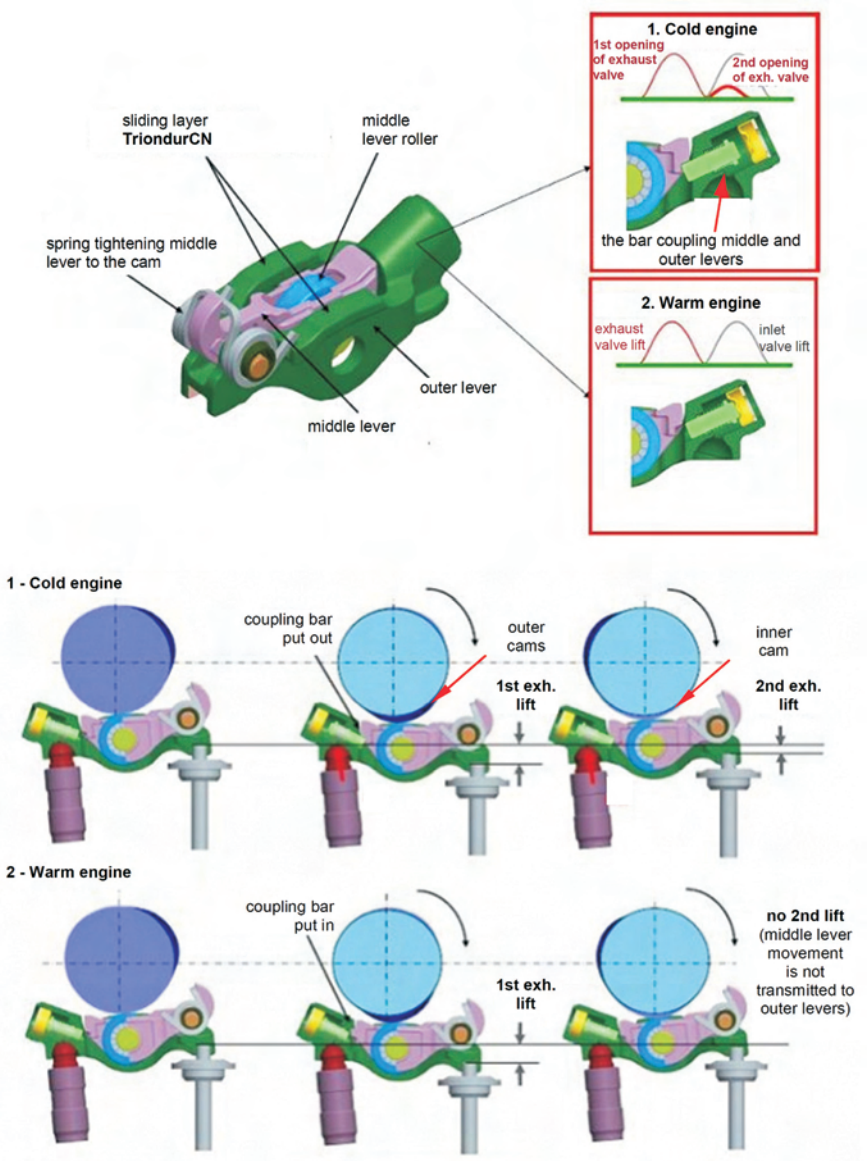

Fig. 9. Principle and operation modes of the two-phase exhaust valve lift system in the engine SkyActiv-D with "on-demand" hydro-electric switchable arms [5]

Rys. 9. Zasada i tryby działania dwufazowego układu rozrządu zaworów wydechowych w silniku SkyActiv-D z elektrohydraulicznie przełączalnymi "na żądanie" dźwigienkami zaworowymi [5]

Acknowledgements

The authors wish to thank the authors of Diesel RK program from N.E. Bauman Moscow State Technical University for the opportunity to use their software in simulation tests.

Podziękowania

Autorzy artykułu dziękują autorom programu Diesel-RK z Moskiewskiego Państwowego Uniwersytetu Technicznego im. N. E. Baumana za możliwość wykorzystania ich oprogramowania w badaniach symulacyjnych.

geometrycznego stopnia sprężania, daje jednoczesne połączenie ze sobą rozszerzonego sterowania doładowaniem, chłodnej i gorącej recyrkulacji spalin, napędu zaworów, czy zastosowanie złożonych map sterowania wtryskiem paliwa i rozbudowanych funkcjonalności poszczególnych podzespołów mających wpływ na proces roboczy silnika. Wiąże się to jednak ze znacznym skomplikowaniem układów roboczych w silniku i jego osprzęcie. Obiecującą alternatywą, a mogącą dać znacznie więcej korzyści, przy jednoczesnym uproszczeniu konstrukcji całego układu napędowego, jest wciąż rozwijana technologia zmiennego stopnia sprężania w silnikach typu VCR.

Nomenclature/*Skróty i oznaczenia*

MPI	MultiPoint Injection/*wtrysk wielopunktowy benzyny (pośredni)*
GDI	Gasoline Direct Injection/*wtrysk bezpośredni benzyny*
HCCI	Homogenous Charge Compression Ignition/*samozapłon ładunku homogenicznego*
VCR	Variable Compression Ratio/*zmienny stopień sprężania*
DI	Direct Injection/*wtrysk bezpośredni*
CNG	Compressed Natural Gas/*sprężony gaz ziemny*
LPG	Liquified Petrolum Gas/*gaz skroplony*
CR	Compression ratio/*stopień sprężania*
TDC/ZZ	top dead center/*zwrot zewnętrzny tłoka*
BDC/ZW	bottom dead center/*zwrot wewnętrzny tłoka*
NO	Nitrogen oxide/*tlenek azotu*
NO_x	Nitrogen oxides/*tlenki azotu*
PM	Particulatte matter/*cząstki stałe*

Bibliography/*Literatura*

[1] Abramek K.F. Zmiana stopnia sprężania i jej wpływ na właściwości rozruchowe silników z zapłonem samoczynnym. Zeszyty Naukowe Akademii Morskiej w Szczecinie, nr 10/2006.

[2] EUCAR R&D for Europe, The European Council for Automotive R&D Conference, 2006, www.eucar.be.

[3] Habermann K. Demonstration Vehicle with Continuously Variable Compression Ratio (VCR). FEV Magazine "Spectrum", Issue 22, 2003: www.fev.com.

[4] Hitomi M., Nakai E., Terazawa Y., Takamatsu H., Shimo D. Development of a New Generation Clean Diesel Engine (2.2L) which Achieves both Driving Pleasure and Environmental Performance – Realization of a concept for ultra-low compression ratio of 14.0. Mazda Motor Corporation, 2013.

[5] http://mechanical tech.jp/book/export/html/4810.

[6] Kuleshov A.S. Use of Multi-Zone DI Diesel Spray Combustion Model for Simulation and Optimization of Performance and Emissions of Engines with Multiple Injection. SAE Technical Paper No. 2006-01-1385, SAE International, Warrendale, PA, USA, 2006.

[7] Kuleshov A.S. Diesel-RK Engine Simulation Software User Manual. Moscow 2004.

[8] Mazda Motor Corporation Tech Newsletters: http://www.mazda.pl.

[9] MCE-5 Development Tech Newsletters: www.mce-5.com.

[10] Rault A. Mid and Long Term Powertrains Evolution. Presentation at EUCAR Conference, 2002.

[11] Scheidt M., Lang M. Pure Efficiency. Developing combusting engines from the perspective of a supplier. 10th Schaeffler Symposium, April 3/4–2014, Schaeffler Technologies AG & Co. KG, 2014.

[12] Woś P., Balawender K., Jakubowski M., Kuszewski H., Lejda K., Ustrzycki A. Design of Affordable Multi-Cylinder Variable Compression Ratio (VCR) Engine for Advanced Combustion Research Purposes. SAE Technical Paper No. 2012-01-0414, SAE International, Warrendale, PA, USA, 2012.

[13] Woś P., Jakubowski M. Silnik tłokowy o zmiennym stopniu sprężania. Zgłoszenie patentowe nr P.389951 z dnia 18-12-2009 r. Biuletyn Urzędu Patentowego RP, nr 13/2011 (978), Warszawa 2011.

[14] Woś P. Procesy spalania niskotemperaturowego w silnikach tłokowych, [w:] Lejda K. (red.): Systemy i środki transportu samochodowego – wybrane zagadnienia. Seria: Transport, nr 3, Oficyna Wyd. Politechniki Rzeszowskiej, s. 229-234, Rzeszów 2012.

[15] Zabłocki M. Wtrysk i spalanie w silnikach wysokoprężnych. WKiŁ, Warszawa 1976.

Paweł Woś, DEng. – Assistant Professor in the Faculty of Mechanical Engineering and Aeronautics at Rzeszów University of Technology.

Dr inż. Paweł Woś – adiunkt na Wydziale Budowy Maszyn i Lotnictwa Politechniki Rzeszowskiej.

e-mail: *pwos@prz.edu.pl*

Hubert Kuszewski, DEng. – Assistant Professor in the Faculty of Mechanical Engineering and Aeronautics at Rzeszów University of Technology.

Dr inż. Hubert Kuszewski – adiunkt na Wydziale Budowy Maszyn i Lotnictwa Politechniki Rzeszowskiej.

e-mail: *hkuszews@prz.edu.pl*

Artur Jaworski, DEng. – Assistant Professor in the Faculty of Mechanical Engineering and Aeronautics at Rzeszów University of Technology.

Dr inż. Artur Jaworski – adiunkt na Wydziale Budowy Maszyn i Lotnictwa Politechniki Rzeszowskiej.

e-mail: *ajaworsk@prz.edu.pl*

Adam Ustrzycki, DEng. – Assistant Professor in the Faculty of Mechanical Engineering and Aeronautics at Rzeszów University of Technology.

Dr inż. Adam Ustrzycki – adiunkt na Wydziale Budowy Maszyn i Lotnictwa Politechniki Rzeszowskiej.

e-mail: *austrzyc@prz.edu.pl*

Prof. Kazimierz Lejda, DSc., DEng. – Professor in the Faculty of Mechanical Engineering and Aeronautics at Rzeszów University of Technology.

Prof. dr hab. inż. Kazimierz Lejda – profesor na Wydziale Budowy Maszyn i Lotnictwa Politechniki Rzeszowskiej.

e-mail: *klejda@prz.edu.pl*

Article citation info:
DZIUBAK, T., KARCZEWSKI, M. Operational malfunctions of turbochargers – reasons and consequences. *Combustion Engines*. 2016, **164**(1), 13-21. ISSN 2300-9896.

Tadeusz DZIUBAK
Mirosław KARCZEWSKI

PTNSS-2016-102

Operational malfunctions of turbochargers – reasons and consequences

The paper discusses the most frequently occurring types of damage in turbochargers fitted in modern combustion engines and their influence on the engine basic operational indexes. The following causes of turbocharger malfunctions have been discussed: no lubrication, low lubricant pressure, reduced lubricant quality, foreign objects in the charged air and in the exhaust gas. Example malfunctions resulting from the said causes have been shown. The experimental part discusses the influence of a reduction of the charging pressure resulting from a leakage in the intake system on the effective parameters of a diesel engine fitted in light-duty and heavy-duty vehicles. The leakage in the intake system has been simulated by boring holes of the diameter of 3 and 12 mm in the intake manifold downstream of the turbocharger. The influence has been determined of the leakage of the turbocharging system on the value of the charging pressure, maximum effective power, engine torque, unit and hourly fuel consumption and the concentration of the exhaust components. A significant impact has been observed of the leakage of the turbocharging system on the effective parameters of the tested diesel engine and exhaust gas composition.

Key words: *combustion engine, intake system, turbocharger, operational malfunctions*

Niesprawności eksploatacyjne turbosprężarek, ich przyczyny i skutki

W artykule wskazano najczęściej występujące uszkodzenia turbosprężarek stosowanych we współczesnych silnikach spalinowych oraz przedstawiono ich wpływ na podstawowe wskaźniki operacyjne silników. Omówiono takie niesprawności turbosprężarek, jak: brak smarowania lub zbyt małe ciśnienie czynnika smarującego, jakość oleju smarującego, obecność ciał obcych w powietrzu i w spalinach. Przedstawiono przykładowe niesprawności spowodowane poszczególnymi czynnikami. W części doświadczalnej oceniono wpływ zmniejszenia ciśnienia doładowania spowodowanego nieszczelnością układu dolotowego na parametry użyteczne silnika o zapłonie samoczynnym, stosowanego w samochodach dostawczych oraz osobowych. Nieszczelność układu dolotowego została zamodelowana przez wykonanie otworów o średnicy 3 i 12 mm w kolektorze dolotowym za turbosprężarką. Określono wpływ nieszczelności układu doładowania na wartość ciśnienia doładowania, maksymalną moc użyteczną, moment obrotowy silnika, jednostkowe i godzinowe zużycie paliwa oraz stężenie składników toksycznych w spalinach. Stwierdzono istotny wpływ nieszczelności układu doładowania na parametry użyteczne i skład spalin silnika o zapłonie samoczynnym.

Słowa kluczowe: *silnik spalinowy, układ dolotowy, turbosprężarka, niesprawności eksploatacyjne*

1. Introduction

The operating conditions of turbochargers are characterized by: high pressure of the incoming exhaust gas, high speeds of the rotor reaching 120 000–240 000 rpm, high temperature of the propellant exhaust gas (on average, 800 °C for diesel engines and 1000 °C for a spark ignition engines) acting on the turbine rotor and variable dynamic loads. An additional disadvantageous phenomenon influencing the operation of turbochargers is the pulsating pressure of the exhaust gas resulting from the firing order of individual cylinders [4].

For the said reasons the components of a turbocharger are subject to great mechanical and thermal stress. Turbocharger is, thus, an assembly extremely sensitive to any deviations from the designed conditions of operation. When designing turbochargers, the engineers constantly try to minimize their size, thus reducing the turbocharger rotating mass and its moment of inertia while increasing the effective range of turbocharger speeds. The main turbocharger components such as the rotors, shrouds, the shaft and slide bearings must be made from durable materials resistant to exhaust gas under arduous operating conditions.

1. Wstęp

Warunki pracy turbosprężarek charakteryzują: duże ciśnienie napływających spalin, duże prędkości obrotowe ich wirników wynoszące 120 000–240 000 obr/min oraz wysoka temperatura napędzających spalin (średnio 800 °C dla silnika ZS oraz 1000 °C dla ZI), działająca na wirnik turbiny, jak również zmienne obciążenia dynamiczne. Do niekorzystnych zjawisk wpływających na pracę turbosprężarek należą także pulsacje ciśnienia spalin w kolektorze wydechowym związane z kolejnością pracy poszczególnych cylindrów [4].

Ze wskazanych powodów elementy turbosprężarki poddane są dużym obciążeniom mechanicznym i cieplnym. Turbosprężarka jest więc zespołem bardzo czułym na wszelkie odstępstwa od przyjętych warunków eksploatacji. Przy konstruowaniu turbosprężarek dąży się do ciągłego minimalizowania ich gabarytów, co powoduje zmniejszenie mas wirujących i ich momentu bezwładności przy jednoczesnym zwiększeniu użytecznego zakresu prędkości obrotowych turbozespołu. Dlatego główne elementy turbosprężarki, tj. wirniki oraz kadłuby turbiny, sprężarki, wałek oraz łożyska ślizgowe, muszą być wykonane z materiałów, które w tych

A properly operated and serviced turbocharger can work trouble-free for many years. Only external factors and improper operation and maintenance may be the cause of malfunctions or premature wear. Turbocharger malfunctions are most frequently caused by the following:
– no lubrication or insufficient lubrication pressure,
– poor lubricant quality,
– exceeded maximum speed of the rotating assembly,
– unbalanced turbine and compressor,
– contamination of air and exhaust gas,
– foreign objects in the intake air and in the exhaust gas,
– atmospheric corrosion,
– leakage in the intake manifold – upstream and downstream of the turbocharger,
– high exhaust gas temperature at the outlet of the turbine.

2. No lubrication or insufficient lubrication pressure

Insufficient lubrication of the turbocharger bearings may result from low lubricant feed pressure or low lubricant quality. This may be caused by a malfunction in the oil lubrication system as turbochargers and engine share the same system. High rotor speeds require constant lubrication with clean engine oil of appropriate quality and pressure. Properly fed engine oil, aside from its lubricating properties, also serves the purpose of a turbocharger coolant. The reason for an insufficient oil pressure may be blockage of the oil feed lines or malfunctioning turbocharger oil valve. Poor oil quality may be caused by its dilution with fuel or coolant. This leads to a loss of the lubricating properties, fading of the oil film and, eventually, premature wear of the turbocharger journal-bearing assembly. Excessively low lubricating pressure or its instantaneous lack contributes to the damage of the bearings (Fig. 1) and the turbocharger rotating assembly (Fig. 2).

The reason for excess wear of the resistance bearing may also be the reduced flow of exhaust gas through the exhaust system (clogged DPF or catalytic converter), which, again generates axial forces acting on the turbine rotor.

Excessive wear of the bearing and the shaft results in a greater play in this pair. It may be the cause of radial tilt which leads to scratching of the blades of the turbine/compressor rotors against the shroud leading to their twist

a) b)

Fig. 1. Scratches caused by low quality and insufficient pressure of the lubricant or foreign objects in the lubricating oil: a) on the bearing race, b) on the resistance bearing [5]

Rys. 1. Zarysowania spowodowane złą jakością i małym ciśnieniem oleju silnikowego lub ciałami obcymi w oleju: a) na bieżni łożyska wzdłużnego, b) na łożysku oporowym [5]

trudnych warunkach zachowają dużą wytrzymałość i odporność na oddziaływujące spaliny.

Prawidłowo użytkowana i obsługiwana turbosprężarka jest zdolna do niezawodnej pracy przez wiele lat. Tylko czynniki pochodzące spoza turbosprężarki (z zewnątrz) oraz niewłaściwa eksploatacja mogą być przyczyną jej przedwczesnego zużycia lub awarii. Niesprawności turbosprężarek spowodowane są najczęściej następującymi przyczynami:
– brak smarowania lub zbyt małe ciśnienie czynnika smarującego,
– zła jakość oleju smarującego,
– niewyrównoważenie zespołu sprężarki i turbiny,
– zanieczyszczenia powietrza i spalin:
– obecność ciał obcych w powietrzu wlotowym i w spalinach,
– korozja atmosferyczna,
– nieszczelność układu zasilania powietrzem – przed i za turbosprężarką,
– wysoka temperatura spalin na wylocie z turbiny.

2. Brak smarowania lub zbyt małe ciśnienie smarowania

Niewystarczające smarowanie łożysk turbosprężarki może być spowodowane zbyt małym ciśnieniem dopływającego oleju lub jego złą jakością, co jest wynikiem niedomagania układu smarowania silnika, gdyż turbosprężarka smarowana jest olejem z tego układu. Duża prędkość obrotowa wirnika turbosprężarki wymaga stałego smarowania czystym olejem silnikowym o odpowiedniej jakości i właściwym ciśnieniu. Prawidłowo doprowadzony olej silnikowy poza właściwościami smarującymi pełni także funkcję chłodzenia turbosprężarki. Przyczyną niedostatecznego ciśnienia oleju może być niedrożność przewodów doprowadzających lub niewłaściwe działanie zaworu olejowego turbosprężarki. Zła jakość oleju może być spowodowana jego rozcieńczeniem przez paliwo lub płyn chłodniczy. Powoduje to utratę właściwości smarnych oleju, zanik filmu olejowego, a w efekcie przyspieszone zużycie skojarzenia czop–panewka wałka turbosprężarki. Zbyt małe ciśnienie smarowania lub chwilowy jego brak przyczyniają się do uszkodzenia łożysk (rys. 1) i zespołu wirującego turbosprężarki (rys. 2).

a) b)

Fig. 2. Damaged air compressor wheel after hitting: a) the shroud, b) the iron housing caused by increased bearing play [5]

Rys. 2. Uszkodzone koło sprężarki powietrza po uderzeniu: a) o korpus sprężarki, b) łopatek wirnika o żeliwną obudowę w wyniku zwiększenia luzu ułożyskowania turbosprężarki [5]

or breaking (Fig. 2a). Under extreme conditions a total seizure or breaking of the turbine/compressor rotor may occur (Fig. 2b).

A very sudden engine stop (before the engine speed is reduced and the temperature drops), particularly after operation at high loads, is detrimental for the life of a turbocharger. As at the moment of the engine stop, the compressor and the turbine are still rotating at high speeds (up to 240 thousand rpm), the oil feed to the compressor bearings is inhibited as the lubrication comes under pressure from the operating engine. The oil film fades, which leads to a wear of the shaft and a continuous increase in the play of the bearings. This leads to a damage of the rotor seal and the oil begins to penetrate the engine intake system.

a) b)

Fig. 3. Damage of the turbine rotor: a) surface overheat zone visible (purple-blue) caused by insufficient lubrication, b) breaking of the turbine rotor shaft caused by a seizure of the turbocharger bearings [5]

Rys. 3. Uszkodzenia wirnika turbiny: a) widoczna strefa przegrzania powierzchni (fioletowo-niebieski kolor) spowodowana niedostatecznym smarowaniem, b) pęknięcie wałka wirnika turbiny spowodowane zatarciem łożysk turbosprężarki [5]

At the moment of sudden stop of the engine operating at high speeds and loads, the rotating assembly has a high temperature, which, with no lubrication of the shaft i.e. its chilling, leads to overheating (Fig. 3a) and burning of the residual oil.

Prolonged operation of the turbocharger with insufficient lubrication may lead to breaking of the turbine rotor shaft (Fig. 3b). This type of damage occurs when the bearings seize or the structure of the material changes following prolonged overheating.

3. Quality of the lubricating oil

The turbocharger shaft bearings are lubricated with the oil from the engine lubrication system. The quality of the lubricant is chiefly determined by the level of contaminants. The main engine oil contaminants are:

– mineral dust penetrating the oil by the air/fuel feed system,
– coolant getting through leakage in the lubrication system,
– fuel getting to the crankcase from the combustion chamber where it failed to burn due to injection system malfunction,
– remains of the wear of metal components of engine friction pairs,
– products of chemical transformation of the oil generated as a result of oxidation, thermal decomposition or polymerization of oil hydrocarbon compounds.

Przyczyną nadmiernego zużycia łożyska oporowego może być także przydławiony przepływ spalin przez układ wydechowy (np. niedrożny filtr cząstek stałych lub reaktor katalityczny), co z kolei prowadzi do powstania sił osiowych działających na wirnik turbiny.

Nadmierne zużycie łożysk i wałka to zwiększony luz w tym skojarzeniu. Może on być przyczyną odchylenia promieniowego wirnika, co w efekcie prowadzi do ocierania łopatek wirnika turbiny lub sprężarki o powierzchnię korpusu, a w następstwie tego do ich zużycia, wygięcia lub wyłamania (rys. 2a). W ekstremalnych warunkach może wystąpić całkowite zablokowanie lub pęknięcie wirnika sprężarki albo turbiny (rys. 2b).

Bardzo duże znaczenie dla pracy turbosprężarki, szczególnie gdy silnik pojazdu był eksploatowany z dużym obciążeniem, ma zbyt szybkie unieruchomienie silnika, zanim nastąpi zwolnienie obrotów turbosprężarki oraz częściowe obniżenie jej temperatury. W chwili unieruchomienia silnika sprężarka i turbina obracają się jeszcze z dużą prędkością (do 240 tys. obr/min), zanika dopływ oleju do łożysk turbosprężarki, gdyż są one smarowane pod ciśnieniem tylko podczas pracy silnika. Następuje zanik filmu olejowego, co powoduje zużycie wałka oraz systematyczne powiększanie luzu w łożyskach. Prowadzi to do uszkodzenia uszczelnienia wirnika i przedostawania się oleju do układu dolotowego silnika.

W chwili nagłego unieruchomienia silnika pracującego z dużą prędkością obrotową i pod dużym obciążeniem zespół wirujący ma wysoką temperaturę, co przy braku smarowania wałka, a tym samym jego chłodzenia, powoduje przegrzewanie (rys. 3a) i spalanie się oleju pozostałego w sprężarce.

Zbyt długa praca turbosprężarki z niedostatecznym smarowaniem może doprowadzić do pęknięcia wałka wirnika turbiny (rys. 3b). Tego typu uszkodzenie następuje w wyniku zatarcia łożysk lub zmian struktury materiału na skutek długotrwałego wpływu wysokiej temperatury.

3. Jakość oleju smarującego

Łożyska wałka turbosprężarki smarowane są olejem z układu smarowania silnika. O jakości oleju silnikowego w znacznym stopniu decydują zanieczyszczenia w nim zawarte. Głównymi zanieczyszczeniami oleju silnikowego są:

– pył mineralny przedostający się do oleju przez układ zasilania wraz z powietrzem i paliwem,
– płyn chłodzący dostający się przez nieszczelności układu smarowania,
– paliwo przedostające się do skrzyni korbowej z komory spalania, gdzie nie uległo spaleniu w wyniku niesprawności układu wtryskowego,
– produkty zużycia metalowych elementów skojarzeń współpracujących ciernie,
– produkty chemicznych przemian oleju powstałe w wyniku utleniania, rozkładu termicznego i polimeryzacji związków węglowodorowych oleju.

Zła jakość oleju może być wynikiem przedłużonego okresu wymiany oleju silnikowego, co skutkuje zwiększoną zawartością zanieczyszczeń, a w efekcie końcowym

Poor oil quality may be a result of extended oil change intervals, which results in an increased amount of contaminants, and, eventually, premature friction-related wear of the turbocharger shaft and its bearings (Fig. 4).

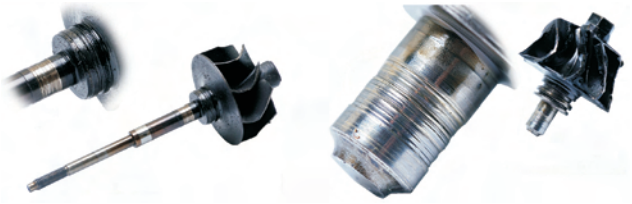

Fig. 4. Damage of the journal surface of the turbocharger shaft following lubrication with contaminated oil [5]

Rys. 4. Uszkodzenia powierzchni czopa wałka turbosprężarki w sytuacji smarowania nadmiernie zanieczyszczonym olejem [5]

A instant shutdown of an engine operating at high loads may lead to a situation when carbon deposits on the bearing. This leads to premature wear of the bearing surface and a reduced life of the turbocharger. Figure 5a shows a new bearing (1) and a used one (2) with visible traces of deposits.

One of the very frequently occurring malfunctions is the blockage of the line returning the oil from the turbocharger. If the oil cannot return, the lubrication and the cooling processes are disturbed and leakage may occur (Fig. 5b). Most often the oil begins to penetrate the turbocharger box or the shroud. Alternatively, the oil may remain in the turbocharger and, resulting from high temperatures carbon deposits will form on the turbine rotor, which may lead to a significant wear of the bearings, their housings and the turbine seal ring.

The oil, apart from its purpose of lubricating the friction pairs, also cools them. Insufficient oil pressure or its poor quality may lead to the turbocharger overheating, as a result of which the bearing will deform and scratch and the oil holes and grooves will be damaged. These malfunctions may lead to secondary damage such as:

– Seizure of the compressor and turbine rotors,
– Bending or breaking of the turbocharger shaft,
– Damage of the seals on the turbocharger shroud,
– Damage of the resistance or transverse bearings.

4. Foreign objects in the air and exhaust gas

Damage of the compressor or turbine rotors caused by foreign objects usually happens when foreign objects from the exhaust or intake systems get to the turbocharger (Fig. 6).

In most of the cases these are parts of the air cleaner case or the air filter element itself, parts of the fitting straps or if the engine itself fails – its consequences – fragments of valves, piston rings pistons, glow plugs or carbon deposits from the combustion chamber [3]. Following a hit of a foreign object on the blades of the turbine or the compressor they are usually mechanically damaged (deformation, breaking of one or several blades, scratching of the front part), which leads to unbalancing of the turbine and a reduction of the efficiency and service life of the turbocharger and eventually a serious damage.

przyspieszonym ściernym zużyciem wałka i łożysk turbosprężarki (rys. 4).

Natychmiastowe wyłączanie obciążonego silnika może spowodować, że w łożysku będzie osadzać się nagar. Powoduje to przyspieszone zużycie powierzchni łożyska i skrócony okres użytkowania turbosprężarki. Na rysunku 5a pokazano łożysko nowe (1) i używane (2) z widocznymi śladami nagaru na powierzchni.

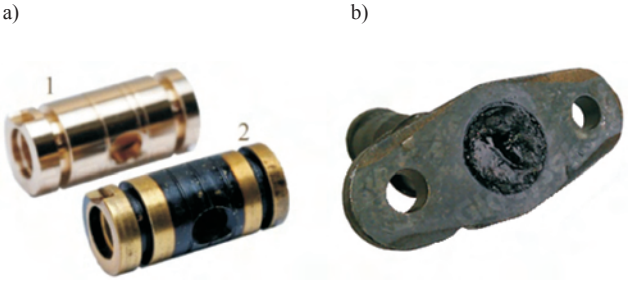

Fig. 5. Consequences of precipitation and influence of carbon deposits on the turbocharger components: a) deposition of carbon on the surface of the bearing, b) blockage of the oil return line from the turbocharger [5]

Rys. 5. Skutki wydzielania i oddziaływania nagaru na elementach turbosprężarki: a) osadzanie się nagaru na powierzchni łożyska wzdłużnego, b) zatkanie nagarem przewodu spływu oleju z turbosprężarki [5]

Jedną z częstych awarii jest zablokowanie przewodu odprowadzającego olej z turbosprężarki. Brak możliwości spływu oleju przez zablokowany przewód (rys. 5b) uniemożliwia prawidłowe smarowanie i chłodzenie turbosprężarki oraz powoduje utratę jej szczelności. Najczęściej olej zaczyna wydostawać się do skrzyni wlotowej sprężarki lub do obudowy turbiny. W drugim przypadku istnieje ryzyko, że w wyniku działania wysokiej temperatury utworzy się nagar na powierzchni wirnika turbiny, który może spowodować znaczne zużycie łożysk, obudowy łożyskowań oraz pierścienia uszczelniającego turbiny.

Olej, poza smarowaniem współpracujących powierzchni dwóch elementów, ma również za zadanie ich chłodzenie. Niedostateczne ciśnienie oleju lub zła jego jakość mogą być przyczyną przegrzania turbosprężarki, w wyniku czego łożyska będą zdeformowane i porysowane, a otwory olejowe i rowki uszkodzone. Niesprawności te mogą powodować wtórne uszkodzenia, np.:

– zakleszczenie i uszkodzenie wirnika sprężarki lub turbiny,
– zgięcie lub pęknięcie wałka turbosprężarki,
– zniszczenie uszczelnień w obudowie,
– niszczenie łożysk oporowych i poprzecznych.

4. Obecność ciał obcych w powietrzu i w spalinach

Uszkodzenia wirnika sprężarki lub turbiny spowodowane przez obcy materiał występują najczęściej w wyniku przedostania się wraz z powietrzem do turbosprężarki elementów pochodzących z układu dolotowego lub wydechowego silnika (rys. 6).

W większości są to elementy obudowy filtra powietrza lub samego filtra, części opasek montażowych, a w przy-

a) b) c)

Fig. 6. Damage of the rotor blade from the front side as a result of: a) a single hit of a foreign object [5], b) metal strap left in the intake system following an improper assembly [6], c) a foreign object present in the intake system

Rys. 6. Uszkodzenie łopatki wirnika sprężarki od strony czołowej wskutek: a) jednorazowego uderzenia niewielkim ciałem obcym [5], b) pozostawienia stalowej opaski montażowej w układzie dolotowym po nieprawidłowym montażu [6], c) dostania się do układu dolotowego ciała obcego

Damage of the turbine or the compressor rotor may also occur if the intake system is not airtight – cracked intercooler or leaking air feed lines. In such a case, contaminants (dust, salt etc.) may be sucked into the system. The contaminants in the exhaust gas (most often soot) are a frequent cause of malfunctions of the variable geometry system of the turbocharger. Following a deposition of contaminants, seizure and blockage of the variable geometry system occurs (Fig. 7).

Inaccurate control of the VGT blades results in surges of the charging pressure, hence improper turbocharger operation. A factor contributing to the formation of products of incomplete combustion is cold engine operation (coolant temperature < 70 °C). In extreme cases the variable geometry system seizes rendering the engine inoperative.

5. Tightness of the charging system

Tightness of the charging system is an important element that directly influences the operating parameters of a turbocharger. Loss of exhaust gas or air through the leakage leads to a drop in the charging pressure, which changes the engine operating parameters. Tests have been performed on a diesel engine – Renault G9T. This is a V_{ss} = 2.188 dm^3 Garett turbocharged engine commonly used in passenger and light-duty trucks. In the tests, the injectors, the turbocharger and the engine control unit were taken from a 66 kW/3000 rpm engine of maximum torque of 290 N·m at 1750 rpm.

The engine tests were performed on a typical engine dynamometer. The engine was loaded with a Schenck W 230 brake of the power of 230 kW. The torque produced by the engine was measured by a tensometric converter. The engine speed was recorded using a pulse converter cooperating with a toothed wheel rim located at the brake coupling. For the measurement of the fuel consumption, AVL Fuel Balance was used that allowed sampling of the fuel consumption with the resolution of 5 s. The airflow through the intercooler was generated by two fans. The temperature of the coolant was maintained on the level of 80–85 °C using an external heat exchanger.

For the analysis of the exhaust gas components the authors used CEBII – 2000 analyzers. It is fully automated, computer controlled measurement equipment. The shares of such exhaust components as nitrogen oxides NO and NO_x

padku awarii silnika i jej następstw np. fragmenty zaworów, pierścieni, drobne części tłoków, świec żarowych lub nagar z komory spalania [3]. W wyniku uderzenia materiału obcego w łopatki sprężarki lub turbiny ulegają one najczęściej awarii w sposób mechaniczny (deformacja, oderwanie jednej lub kilku łopatek, starcie części czołowej sprężarki), co powoduje niewyrównoważenie turbiny, obniżenie sprawności i trwałości turbosprężarki, a w konsekwencji poważną awarię.

Uszkodzenia wirnika sprężarki lub turbiny mogą również powstać w sytuacji użytkowania pojazdów z nieszczelnym układem dolotowym, np. z pękniętą chłodnicą powietrza doładowującego „intercoolera" lub nieszczelnymi przewodami doprowadzającymi powietrze do silnika. Istnieje wtedy możliwość zassania do układu dolotowego zanieczyszczeń, takich jak pył, sól itp.

Znajdujące się w spalinach zanieczyszczenia, najczęściej sadza, są częstą przyczyną niesprawności układu sterowania napływem spalin na łopatki turbiny w sprężarkach ze zmienną geometrią. W wyniku osadzania się zanieczyszczeń następuje zatarcie i blokowanie mechanizmu sterującego wychyleniem łopatek kierownicy (rys. 7).

a) b) c)

Fig. 7. Damage of the moving blades of the variable geometry system: a) a hit by a broken fragment of the turbine rotor blade [5], b, c) blockage caused by carbon deposit [7]

Rys. 7. Uszkodzenie ruchomych łopatek kierownicy turbiny w wyniku: a) uderzenia przez oderwany fragment łopatki wirnika turbiny [5], b, c) zablokowania przez nagromadzony nagar [7]

Nieprecyzyjne sterowanie kierownicami powoduje skoki ciśnienia doładowania, a tym samym niewłaściwą pracę sprężarki. Czynnikiem sprzyjającym powstawaniu produktów niezupełnego spalania jest praca silnika nierozgrzanego, czyli przy niskiej (< 70 °C) temperaturze czynnika chłodzącego. W skrajnych przypadkach dochodzi do zablokowania układu sterowania turbiny, co uniemożliwia użytkowanie pojazdu.

5. Szczelność układu doładowania

Szczelność układu doładowania jest ważnym elementem, który bezpośrednio wpływa na parametry pracy turbosprężarki. Ubytek spalin lub powietrza przez nieszczelności prowadzi do spadku ciśnienia doładowania, a w konsekwencji do zmian parametrów pracy silnika. Badania takie przeprowadzono na silniku ZS – Renault G9T. Jest to silnik o pojemności skokowej V_{ss} = 2,188 dm^3 doładowany turbosprężarką firmy Garett, powszechnie stosowany w samochodach osobowych i dostawczych.

W prezentowanych badaniach zastosowano układ zasilający (wtryskiwacze, turbosprężarka, sterownik silnika) od silnika pojazdu dostawczego, osiągającego moc maksy-

were recorded using a vacuum chemiluminescent detector by EcoPhysics. The CO and CO_2 analyzers operated based on the principle of absorbing infrared radiation and for the analysis of the hydrocarbons emission, flame ionization detector was used, whose principle of operation is based on burning of the hydrocarbons.

The results of the measurements of the engine parameters were stored during the entire experiment to ensure on-going control of the engine condition or to determine a possible malfunction and oversee the course of subsequent stages of the cycle. The results of the measurements of the effective engine parameters were reduced to normal conditions as per Polish standards PN-ISO 15550:2009.

Figures 8–12 show the influence of the reduced value of the charging pressure, resulting from the leakage, on the effective parameters of the Renault G9T engine. The leakage of the charging system was simulated by two holes of the diameter of 3 and 12 mm (the cross-section area was 7 and 112 mm^2 respectively) located in the line between

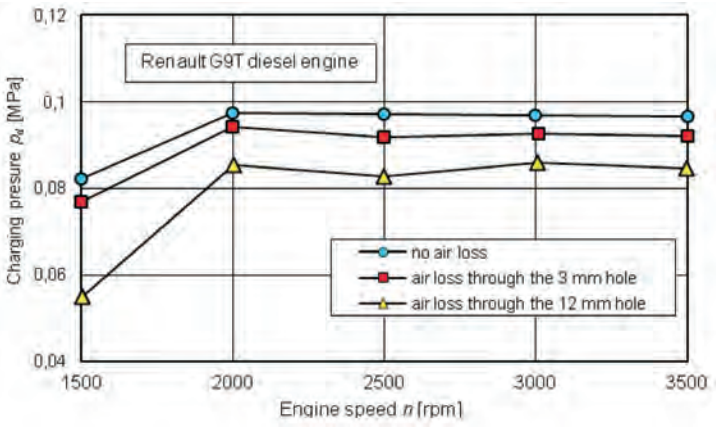

Fig. 8. The influence of the charging system leakage on the values of charging pressure p_d of a Renault G9T diesel engine [1]

Rys. 8. Wpływ nieszczelności układu doładowania na wartość ciśnienia doładowania p_d silnika ZS Renault G9T [1]

the turbocharger and the intercooler. The tests of the influence of each leakage on the full load engine characteristics were performed by developing a full load engine characteristics in the range of 1500–3500 rpm [1].

As the engine speed changes (Fig. 8) in the range 1500–2000 rpm a sudden increase in the charging pressure takes place. Above n = 2000 rpm the charging pressure remains on a constant level and for a fully functional turbocharger has a value of p_d = 0.097 MPa.

Irrespective of the engine speed during the operation of the turbocharger with a leakage caused by a hole of the diameter of 3 mm in the first case and 12 mm in the second case, an almost parallel shift of the engine charging pressure characteristics $p_d = f(n)$ towards lower values occurs. A drop in the charging pressure of a turbocharger during operation with the

malną 66 kW przy prędkości obrotowej 3000 obr/min oraz momencie 290 N·m przy 1750 obr/min.

Badania silnika wykonano na typowym stanowisku dynamometrycznym. Silnik był obciążany hamulcem typu Schenck W 230 o maksymalnej mocy 230 kW. Moment obrotowy wytwarzany przez silnik był mierzony przy użyciu przetwornika tensometrycznego. Prędkość obrotową rejestrowano za pomocą przetwornika impulsowego, który współpracował z wieńcem zębatym umieszczonym na przyłączu hamulca. Do pomiaru zużycia paliwa wykorzystano wagę paliwową AVL FuelBalance, która umożliwiała próbkowanie zużycia paliwa co 5 s. Przepływ powietrza przez chłodnicę powietrza doładowującego wywołano, stosując zespół dwóch wentylatorów. Temperaturę płynu chłodzącego w silniku utrzymywano na poziomie 80–85 °C z wykorzystaniem zewnętrznego wymiennika ciepła.

Do analizy składników spalin zastosowano zestaw analizatorów spalin CEBII – 2000. Jest to w pełni zautomatyzowany, sterowany komputerowo zestaw przyrządów pomiarowych. Udziały takich składników spalin, jak tlenki azotu NO i NO_x był rejestrowany przy użyciu próżniowego detektora chemiluminescencyjnego analizatora firmy EcoPhysics. Analizatory CO i CO_2 działały na zasadzie pochłaniania promieniowania podczerwonego, natomiast do rejestracji węglowodorów zastosowano analizator płomieniowo-jonizacyjny, którego zasada działania była oparta na spalaniu węglowodorów.

Wyniki pomiarów parametrów pracy silnika gromadzono w ciągu całego eksperymentu w celu bieżącej kontroli jego stanu technicznego lub określenia okoliczności ewentualnej awarii oraz kontroli przebiegu kolejnych faz cyklu badawczego. Wyniki pomiarów parametrów użytecznych silnika zredukowano do warunków normalnych zgodnie z normą PN-ISO 15550:2009.

Na rysunkach 8–12 pokazano wpływ zmniejszonej wartości ciśnienia doładowania, spowodowanej nieszczelnością układu doładowania, na parametry

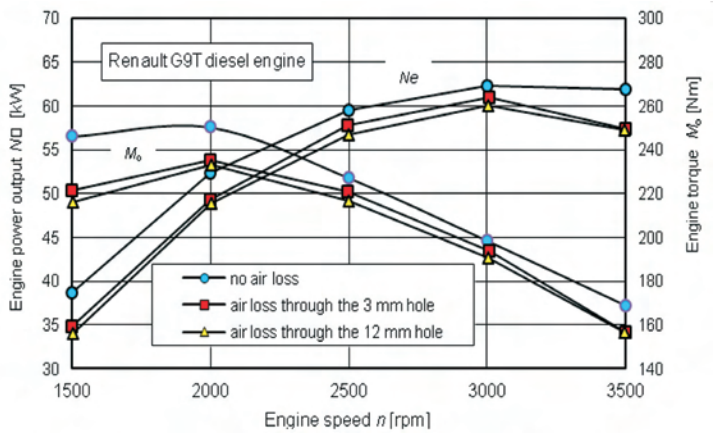

Fig. 9. The influence of the charging system leakage on power N_e and torque M_o of the Renault G9T diesel engine [1]

Rys. 9. Wpływ nieszczelności układu doładowania na moc N_e i moment M_o silnika o ZS Renault G9T [1]

3 mm hole is 0.004 MPa and the 12 mm hole – 0.014 MPa, as compared to a fully functional turbocharger.

From the full load characteristics of the Renault G9T engine it results that the greatest power N_e and torque M_o is produced by the engine when the charging system is airtight and fully functional, which confirms proper pairing of the engine and the turbocharger – Fig. 9.

A reduction of the charging pressure due to a leakage results in a drop of effective power in the entire range of engine speeds and torque with an almost parallel shift of characteristics $N_e = f(n)$ and $M_o = f(n)$ of the tested engine towards lower values.

A drop in the charging pressure by 0.004 MPa (escape of air by the 3 mm hole) results in a decrease of maximum effective power by 3.7% and torque by 3.9%. A further drop in the charging pressure following the escape of air through the 12 mm hole does not result in a significant drop of effective engine power and torque.

From the characteristics presented in Fig. 10 we know that the lowest unit fuel consumption is achieved by the engine when the turbocharger is fully functional. The loss of pressure through the leakage leads to an increased unit fuel consumption in the entire range of engine speeds and the most significant influence is seen when the engine speeds are extreme. The leakage in the charging system caused by the 3 mm hole at n = 1500 rpm leads to an increase in the fuel consumption by 13.6% as compared to a fully functional engine.

The influence of the charging system leakage (charging pressure) on the concentration of the exhaust components: nitrogen oxides (NO_x), carbon monoxide (CO) and hydrocarbons (HC) of the Renault G9T engine has been shown in Figures 11–13. The influence of the leakage on the concentration of NO_x and CO is significant in the range of engine speeds 1500–2500 rpm. A reduction of the charging pressure by 0.014 MPa (leakage caused by the 12 mm hole) results in a drop of the concentration of nitrogen oxides to the level of 550 ppm, i.e. 25%. This is due to the specificity of NO_x formation whose maximum concentration in the exhaust gas occurs when the engine produces maximum power at high temperatures.

użyteczne silnika Renault G9T. Nieszczelność układu doładowania silnika zamodelowana została dwoma otworami o średnicy 3 i 12 mm (pole przekroju poprzecznego odpowiednio 7 i 112 mm^2), znajdującymi się w przewodzie pomiędzy turbosprężarką a chłodnicą powietrza doładowującego, przez które następował ubytek powietrza doładowującego. Badania wpływu każdej nieszczelności na charakterystyki zewnętrzne silnika wykonano przez sporządzenie charakterystyki zewnętrznej silnika w zakresie prędkości obrotowych 1500–500 obr/min [1].

Wraz ze zmianą prędkości obrotowej silnika (rys. 8) w zakresie 1500–2000 obr/min następuje gwałtowny wzrost ciśnienia doładowania. Natomiast powyżej n = 2000 obr/min ciśnienie doładowania utrzymuje się na stałym poziomie i podczas pracy sprawnej (szczelnej) turbosprężarki ma wartość $p_d = 0{,}097$ MPa.

Niezależnie od prędkości obrotowej silnika, podczas pracy turbosprężarki z nieszczelnościami spowodowanymi w pierwszym przypadku otworem 3 mm, a w drugim otworem o średnicy 12 mm, następuje niemal równoległe przesunięcie charakterystyk ciśnienia doładowania $p_d = f(n)$ silnika w stronę mniejszych wartości. Spadek ciśnienia doładowania podczas pracy turbosprężarki z nieszczelnością w postaci otworu o średnicy 3 mm wynosi 0,004 MPa, a otworu o średnicy 12 mm –0,014 MPa w stosunku do ciśnienia doładowania sprężarki szczelnej.

Z charakterystyki zewnętrznej silnika Renault G9T wynika, że największą moc N_e i moment M_o uzyskuje silnik podczas pracy ze szczelnym układem doładowania, co świadczy o właściwym doborze sprężarki do silnika – rys. 9.

Zmniejszenie, w wyniku nieszczelności, ciśnienia doładowania powoduje w całym zakresie badanych prędkości obrotowych spadek mocy użytecznej, momentu obrotowego z jednoczesnym niemal równoległym przesunięciem charakterystyk $N_e = f(n)$ i $M_o = f(n)$ badanego silnika w stronę mniejszych wartości.

Spadek ciśnienia doładowania o 0,004 MPa (ucieczka powietrza przez otwór o średnicy 3 mm) powoduje zmniejszenie maksymalnej mocy użytecznej o 3,7% i momentu

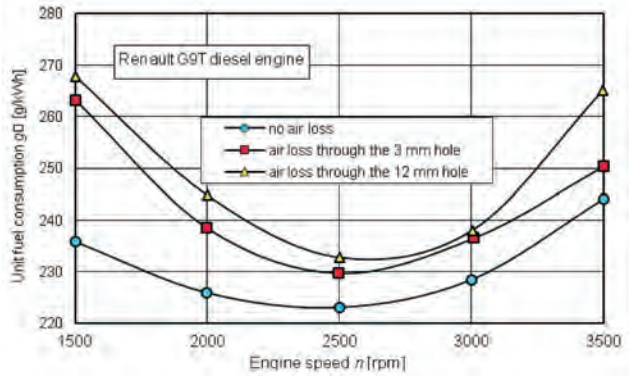

Fig. 10. The influence of the charging system leakage on specific fuel consumption g_e of the Renault G9T engine [1]

Rys. 10. Wpływ nieszczelności układu doładowania na jednostkowe zużycie paliwa g_e silnika Renault G9T [1]

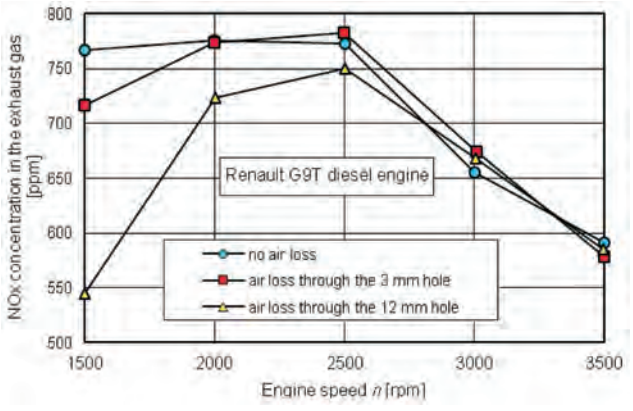

Fig. 11. The influence of the charging system leakage on the NO_x concentration in the exhaust gas of the Renault G9T engine [1]

Rys. 11. Wpływ nieszczelności układu doładowania na zawartość NO_x w spalinach silnika Renault G9T [1]

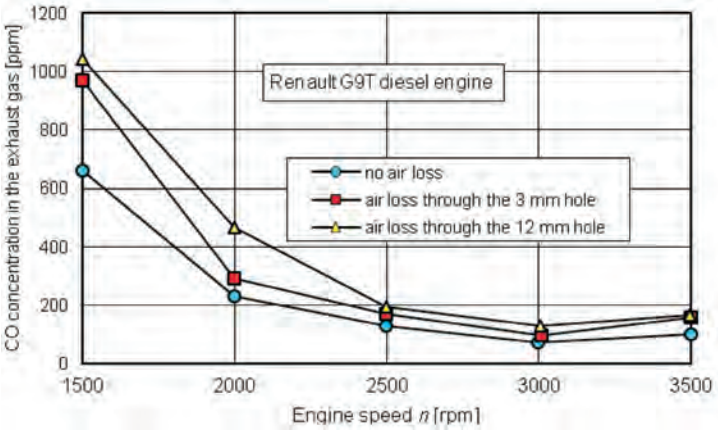

Fig. 12. The influence of the charging system leakage on the CO concentration in the exhaust gas of the Renault G9T engine [1]

Rys. 12. Wpływ nieszczelności układu doładowania na zawartość CO w spalinach silnika Renault G9T [1]

The leakage in the system results in a drop of the charging pressure and oxygen concentration in the cylinder charge, which is impactful on the NO_x level in the exhaust gas. The concentration of NO_x at the engine speeds of 1500 rpm is thus comparable with the concentration of NO_x at 3500 rpm.

The influence of the charging system leakage (charging pressure) on the concentration of CO in the exhaust gas of the Renault G9T engine has been shown in Fig. 12.

As the Renault G9T engine speed increases in the range 1500–2500 rpm a sudden drop in the concentration of CO in the exhaust gas occurs (irrespective of the system air-tightness). Above n = 2500 rpm the concentration of CO in the exhaust gas remains on a steady (low – 100 ppm) level, whether or not there is leakage in the turbocharging system. As the air loss in the charging system increases, a significant increase in the concentration of carbon monoxide occurs in the engine speed range of 1500–2500 rpm. This phenomenon is particularly environmentally disadvantageous.

The concentration of hydrocarbons in the exhaust gas of the tested engine is miniscule and at the engine speed of maximum power n_N = 3000 rpm it remains on the level

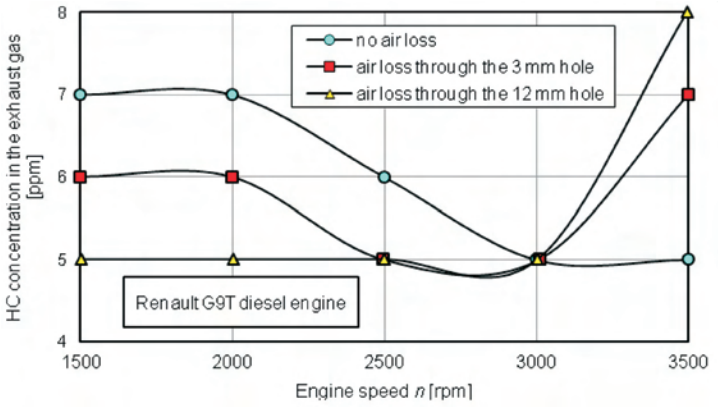

Fig. 13. The influence of the charging system leakage on the HC concentration in the exhaust gas of the Renault G9T engine [1]

Rys. 13. Wpływ nieszczelności układu doładowania na zawartość HC w spalinach silnika Renault G9T [1]

maksymalnego o 3,9%. Dalszy spadek ciśnienia doładowania w wyniku wypływu powietrza przez otwór 12 mm nie powoduje istotnego spadku mocy użytecznej i momentu obrotowego silnika.

Z przedstawionych na rysunku 10 charakterystyk wynika, że najmniejsze jednostkowe zużycie paliwa badany silnik osiąga podczas pracy turbosprężarki szczelnej. Ubytek powietrza przez nieszczelności powoduje zwiększenie jednostkowego zużycia paliwa w całym zakresie prędkości obrotowej silnika, największy jego wpływ zaznacza się podczas pracy silnika przy skrajnych prędkościach obrotowych. Nieszczelność układu doładowującego spowodowana otworem o średnicy 3 mm powoduje przy prędkości n = 1500 obr/min zwiększenie jednostkowego zużycia paliwa o 13,6% w stosunku do silnika w pełni sprawnego.

Wpływ nieszczelności układu doładowania (ciśnienia doładowania) na stężenie toksycznych składników spalin: tlenków azotu (NO_x), tlenku węgla (CO) oraz węglowodorów (HC) silnika Renault G9T pokazano na rys. 11–13. Wpływ nieszczelności na stężenie NO_x i CO jest znaczny

w zakresie prędkości obrotowej 1500–2500 obr/min. Zmniejszenie ciśnienia doładowania o 0,014 MPa (nieszczelność spowodowana otworem o średnicy 12 mm) powoduje spadek zawartości tlenków azotu do poziomu 550 ppm, a więc o 25%. Wynika to ze zjawiska tworzenia się NO_x, których maksymalne stężenie w spalinach występuje podczas pracy silnika w obszarze mocy maksymalnej i w wysokiej temperaturze.

Nieszczelność układu spowodowała spadek ciśnienia doładowania i zawartości tlenu w dostarczonym do cylindrów ładunku, co wpłynęło na zmniejszenie zawartości NO_x. Tym samym zawartość NO_x przy prędkości obrotowej 1500 obr/min jest porównywalna z zawartością tlenków azotu przy 3500 obr/min.

Wpływ nieszczelności układu doładowania (ciśnienia doładowania) na stężenie CO w spalinach silnika Renault G9T przedstawiono na rys. 12.

Wraz ze wzrostem prędkości obrotowej silnika Renault G9T w zakresie 1500–2500 obr/min następuje (niezależnie od szczelności układu) gwałtowne zmniejszenie zawartości CO w spalinach. Natomiast powyżej n = 2500 obr/min zawartość CO w spalinach utrzymuje się na stałym, niskim (około 100 ppm) poziomie, niezależnie czy silnik doładowywany jest turbosprężarką z nieszczelnością, czy też nie. Wraz ze wzrostem ubytku powietrza z układu doładowującego następuje znaczny wzrost zawartości tlenku węgla w spalinach w zakresie 1500–2500 obr/min. Jest to zjawisko szczególnie niekorzystne ze względu na ochronę środowiska.

Zawartość węglowodorów w spalinach badanego silnika jest nieznaczna i przy prędkości obrotowej mocy maksymalnej n_N = 3000 obr/min utrzymuje się na poziomie około 5 ppm niezależnie od nieszczel-

of approx. 5 ppm whether or not the system has a leakage (Fig. 13). If the system is airtight, the concentration of HC in the exhaust gas decreases in the entire range of engine speeds. A disadvantageous influence of the leakage on the HC concentration becomes visible when the engine exceeds the speed of maximum power n_N = 3000 rpm. The concentration of HC in the exhaust gas increases to 8 ppm with the leakage caused by the 12 mm hole.

6. Conclusions

The analysis of the literature and obtained research results allowed formulating the following conclusions:

1. The service life of a properly operated and maintained turbocharger can be very long. Only improper operation and maintenance me be the reason for premature wear or malfunctions. The efficiency of the turbocharger system of a diesel engine is decisive of the efficiency of the entire engine including its performance.
2. The loss of air from the charging system is a very disadvantageous phenomenon in terms of the operating parameters: reduced engine power, increased unit fuel consumption, increased exhaust emissions and reduction engine flexibility.
3. The loss of air from the charging system leads to an increase in the temperature of combustion, which leads to increased thermal loads of the piston-crankshaft assembly. This may lead to a reduced life of the mating parts.
4. It appears purposeful to continue research aiming at determination of the influence of the intake system leakage on the EURO emission standard compliance during reproduction of the unified driving cycle.

ności układu doładowującego (rys. 13). Przy szczelnym układzie doładowującym zawartość HC w spalinach maleje w całym zakresie prędkości obrotowej. Niekorzystny wpływ nieszczelności na stężenie HC zaznacza się po przekroczeniu przez silnik prędkości obrotowej mocy maksymalnej n_N = 3000 obr/min. Zawartość HC w spalinach wzrasta do 8 ppm przy nieszczelności spowodowanej upustem powietrza przez otwór 12 mm.

6. Wnioski

Przeprowadzona analiza literatury i uzyskanych wyników badań pozwoliła na sformułowanie następujących wniosków:

1. Prawidłowo użytkowana i obsługiwana turbosprężarka jest zdolna do niezawodnej pracy przez wiele lat. Tylko niewłaściwa eksploatacja może być przyczyną jej przedwczesnego zużycia lub awarii. Sprawność układu doładowania silnika ZS w dużym stopniu decyduje o sprawności całego silnika i jego osiągach.
2. Ubytek powietrza z układu doładowania jest zjawiskiem bardzo niekorzystnym ze względu na obniżenie parametrów użytecznych silnika: spadek mocy, zwiększenie jednostkowego zużycia paliwa, wzrost stężenia składników toksycznych w spalinach oraz zmniejszenie elastyczności silnika.
3. Ubytek powietrza z układu doładowania powoduje zwiększenie temperatury spalania, co w efekcie prowadzi do zwiększenia obciążeń cieplnych elementów układu tłokowo-korbowego silnika, co może mieć wpływ na zmniejszenia jego trwałości.
4. Celowe wydaje się wykonanie dalszych badań mających na celu określenie wpływu nieszczelności układu dolotowego na spełnienie wymagań zawartych w normach EURO podczas odtwarzania zunifikowanego cyklu jezdnego.

Bibliography/*Literatura*

[1] Adamczuk M., Ocena wpływu ciśnienia doładowania na osiągi silnika o zapłonie samoczynnym (ZS), praca dyplomowa. WAT, Warszawa 2013.

[2] Dziubak T., Szwedkowicz S. Experimental research on filtering fibers in a cyclone–porous barrier system, Combustion Engines, No. 3/2014 (158).

[3] Dziubak T. Filtracja powietrza wlotowego do silników spalinowych pojazdów mechanicznych. WAT, Warszawa 2012.

[4] Mysłowski J. Doładowanie silników. WKŁ, Warszawa 2011.

[5] www.naprawa-turbosprezarek.pl/turbosprezarki_uszkodzenia_usterki_turbin.html. [data dostępu: 12.08.2015].

[6] www.zssplus.pl/publikacje/publikacje49.htm. [Data dostępu: 25.08.2015].

[7] www.turbo-pro.pl/pl/przyczyny-awarii.html. [Data dostępu: 28.09.2015.]

[8] PN-ISO 15550:2009 – Silniki spalinowe tłokowe. Określanie i metoda pomiaru mocy silnika – Wymagania ogólne.

Tadeusz Dziubak, DSc., DEng. – Professor at the Faculty of Mechanics Military University of Technology, Warsaw, Poland.

Dr hab. inż. Tadeusz Dziubak – profesor na Wydziale Mechanicznym Wojskowej Akademii Technicznej w Warszawie.

e-mail: *tadeusz.dziubak@wat.edu.pl*

Miroslaw Karczewski, DEng. – doctor at the Faculty of Mechanics Military University of Technology, Warsaw, Poland.

Dr inż. Miroslaw Karczewski – adiunkt na Wydziale Mechanicznym Wojskowej Akademii Technicznej w Warszawie.

e-mail: *miroslaw.karczewski@wat.edu.pl*

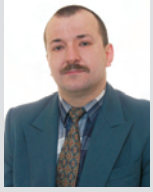

Article citation info:
VANHAELST, R., KHEIR, A., CZAJKA, J. A systematic analysis of the friction losses on bearings of modern turbocharger. *Combustion Engines*. 2016, 164(1), 22-31. ISSN 2300-9896

Robin VANHAELST
Alaa KHEIR
Jakub CZAJKA

PTNSS-2016-103

A systematic analysis of the friction losses on bearings of modern turbocharger

In the article, a novel test rig for determining the friction losses of modern turbocharger is presented. The friction torque of the bearing of turbocharger can be measured direct and stationary at any speed up to 100,000 min⁻1 by the friction test rig developed by the Ostfalia, University of Applied Science (UAS). Since 2010, over 50 turbochargers were measured on the test bench in extensive measurement series. The results give valuable and new insights of the influence of the next parameters on the bearing friction losses: oil temperature, oil pressure, thrust force and oil flow rate. Furthermore, a comparison between the different bearing types (semi-floating, full floating and ball bearings) was performed. The main observations and results are discussed in the scientific article.

Key words: *friction power, test rig, turbocharger, floating bearing, ball bearing, oil temperature, oil pressure, thrust force*

1. Introduction

One of the possibilities to improve the efficiency new combustion engines is to optimize the turbocharging systems. A turbocharger with high efficiency and excellent dynamic properties is essential for low fuel consumption combined with good driving performance. The overall efficiency is in this case composed of the response levels of the turbine, the compressor and the mechanical efficiency of bearing system. A CFD simulation can be used for a forecast of the turbine and compressor efficiencies. On a powerful hot gas test rig the simulated results can be confirmed [1].

Within the framework of research projects the simulation models have been established in order to calculate the lubricating properties of journal and thrust bearings. The direct measurement of friction losses of a bearing system under real conditions is up to date difficult to measure [2, 3].

Therefore, the research group for thermodynamics and alternative driving systems of the Ostfalia, UAS in Wolfsburg works, since 2010 on a friction test rig to determine with different measuring method the friction losses of turbocharger bearings.

2. Measurements of friction losses on bearings of turbochargers

The shaft of modern turbocharger rotates up to 300,000 rpm. In order to achieve these high speeds and realize a long life the mechanical demands on these bearings are a big challenge. On the shaft of modern turbochargers an axial thrust- and radial bearing are applied.

In order to quantify the most important properties of a bearing, a test rig was set up which can detect the friction power or the friction torque of a turbocharger shaft. Other important factors like the oil temperature and oil pressure can be varied by the test rig. Figure 1 shows the basic structure of the test rig.

The determination of the frictional power can be record direct or indirect. With the direct measurement method, the torque, which is caused by the friction in the bearing, is detected by a torque sensor. The shaft is driven by a high speed electric engine, which is controlled by a pulse width modulation. The engine is mounted on a micro positioning unit within the test bench adjustable in three directions.

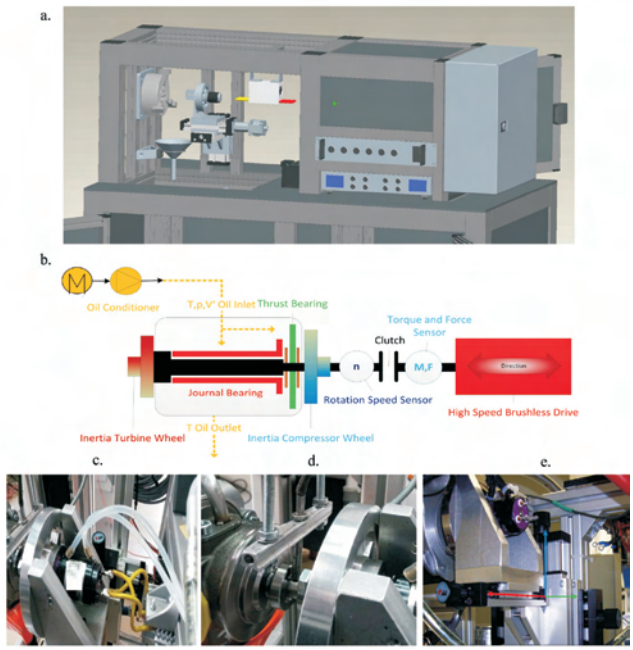

Fig. 1. The Ostfalia friction power test rig: a) CAD representation of test rig, b) schematic structure of test rig with measurements technique, c) drive engine with torque sensor, d) clutch with speed sensor e) drive engine with linear adjustment

The turbocharger can be mounted on the turbine or the compressor side of the bearing housing on the test bench. The construction of the test rig ensures an orthogonal alignment with negligible angular displacement (< 0.1°) between turbocharger and the shaft of electric engine. The connection between the shaft of the engine and the turbine shaft is made by a torx-clutch. This type of clutch allows certain angle resilience when the shaft during operation due to the lubrication film begins to "swim". With the micrometer positioning unit it is possible to set up the alignment exactly.

The torque of the shaft is measured by detecting the reaction force of the electric drive by means of a full Wheatstone bridge with strain gauges. The sensor is screwed to the electric drive and has in contrast to a torque – measuring shaft no speed limitation. The speed measurement is done by an inductive speed sensor.

To investigate the thrust force on the turbocharger (TC) bearings systems, the thrust bearing of the turbocharger is loaded by a force acting in the axial direction, so the thrust force can be measured with a special axial force sensor with strain gauges. The thrust force is set up by variation the direction of the linear actuator, which is mounted at the linear unit in the axial direction. By driving the electric drive against the turbocharger shaft, the clutch is closed and the thrust force can be applied. The torx-clutch can only push the TC shaft in direction of thrust bearing, but by changing the drive side for example on turbine side, it's possible to vary the thrust force. So it's possible to determine friction losses by positive or negative thrust force.

The lubricant supply of the bearing and the shaft is ensured by an oil conditioning unit. This consists of an oil pump, an oil pressure sensor and an oil heating and oil cooling system so the temperature can be vary between 0 °C – 120 °C and the pressure between 2-6 bar absolute. A flow sensor measured the oil volumetric flow.

The control and regulation and the visualization of all measured variables is carried out by the software "LabView". The software can set and read out the measurement data and control parameters via PXI system from National Instruments. Measurements can be performed with or without inertia masses for compressor and turbine wheels.

First, a measurement point is adjusted at a desired speed. After a short time, which is used for stabilization of the parameters like oil pressure, oil temperature, thrust force and speed, a measurement with a frequency of 25-100 Hz over a period of 10 s is recorded. This measurement results in a high number of measurement values, an arithmetic average is built for each parameter.

With the indirect method of the frictional power measurements inertia mass of turbine a compressor wheel is mounting on the shaft. The shaft is accelerated to a speed of 100,000 rpm, after a delay time, the electric drive stops and is disengaged, so the clutch is opened. This is realized by a rapid return of the linear actuator in the axial direction. The speed drop of the outgoing shaft is detected at high frequency. The drop of the speed and the known inertia mass the friction torque can be calculated.

3. Test results

This section describes the results and presented the different analyzed parameter.

3.1. Variation of the oil temperature

By determining the influence of the oil temperature on the friction of turbocharger shaft without applying an axial load to a speed range of 5,000 till 80,000 rpm was measured at a speed of 5,000 rpm increment. The oil supply temperature has been conditioned to 0 °C, 50 °C, 90 °C and 110 °C with a constant pressure of 3 bar (absolute).

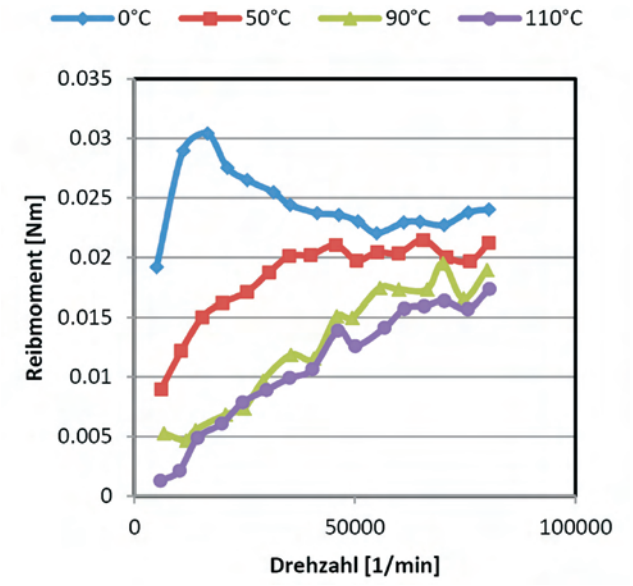

Fig. 2. The friction torque under the influence of oil temperature

Figure 2 shows the trend of the friction torque by different oil temperatures over the speed. The friction torque at 90 °C and 110 °C oil temperature has a progressive trend. Both friction types the adhesive and the mixed friction are already overcome in the initial rotational speed of 5000 rpm. An increase in the oil temperature results in a reduction of the friction torque of the plain bearing. The increase in the friction torque at low speed and oil temperature 0 °C and 50 °C can be observed.

An increased oil temperature leads to a decrease of the viscosity. This viscosity drop is explained by the cohesive forces of the molecules. It is caused by the lower shear stress τ during the rotation of the shaft.

Lower shear stress requires a lower force to apply the movement of the shaft relative to the bearing tin. So the friction torques in Fig. 2 decrease dependent the increase of oil temperature.

At higher speeds there is a higher friction loss inside the bearing. This increased friction power causes an increasing local temperature, which result in a decrease of the oil viscosity so the real oil temperature is much higher than the inlet temperature.

At higher speeds, due to the lower viscosity, lower shear forces occur and the friction decreases. At lower shaft speeds, the frictional power (the heat generation due to friction) within the bearing is too small to induce a high local fluid temperature. The high torque at 0 °C and 50 °C in lower speeds are justified by the fact that the real lubricating film temperature within the bearing approaches in this field of oil supply temperature and leads to a high viscosity. There is a higher friction loss inside the bearing, between the shaft and tin. This increased friction power obtained a local temperature increase, which leads to a decreased viscosity.

The Figure 3 shows the trend of the oil flow by variation of the oil temperature at constant oil pressure for different

speed. The oil flow increases with higher oil temperatures. The oil flow by 0 °C and 50 °C increased with a linear trend depend by the speed, while the oil volumetric flow decrease linearly at 90 °C and 110 °C with the speed. This is, as already explained, due to a throttle effect in dependence by the centrifugal force in the full-floating bearing.

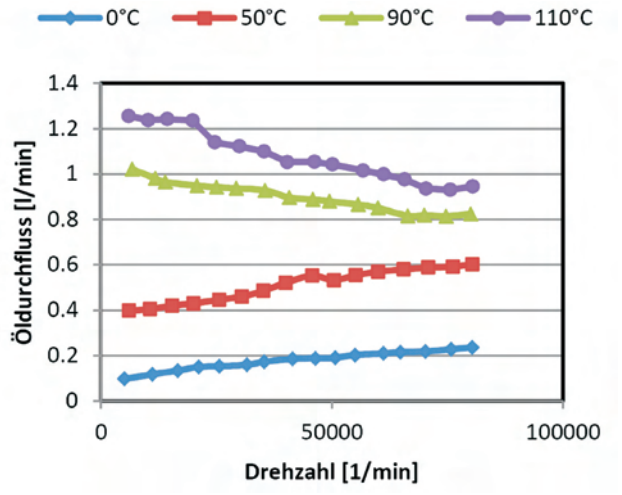

Fig. 3. The oil volumetric flow as a function of oil temperature

Figure 4 shows the trend of the friction losses for different oil temperatures in dependence of the speed. The friction loss increases with each setting of oil temperature proportionally with the speed.

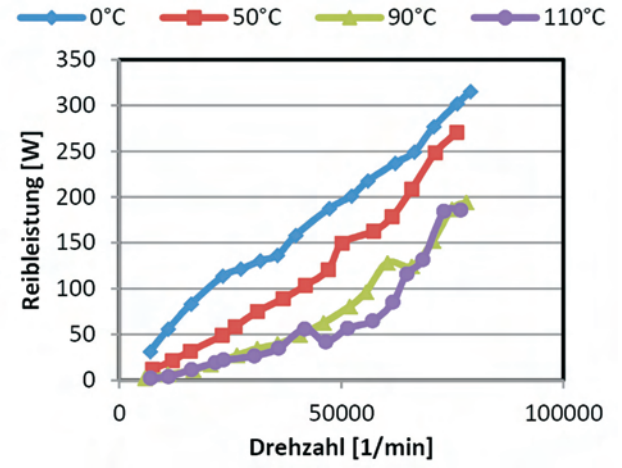

Fig. 4. Friction power as a function of oil temperature

3.2. Direct- and indirect measurement of friction power loss

The presented test rig in chapter 2 enables a direct or an indirect measurement of the friction loss in bearing systems of turbochargers. In the direct method every speed points is adjusted stationary and the torque on the electric drive is captured. With the indirect measurement method, which is popular in use, the TC shaft is accelerated to 100,000 rpm after a persist time the drive stops and a linear actuator disengages the clutch. The drop of speed changing by a known time can be measured, so the friction loss power can be calculated. To achieve the longest possible run of the shaft, it is important to mount an inertia mass fitted to the turbine and compressor wheels. The direct determination of friction power is carried out for reasons of comparability with inertia masses. Both measurement methods are carried out by an oil pressure of 3 bar and without thrust force. Figure 5 shows the friction torque at 90 °C and 30 °C oil temperature.

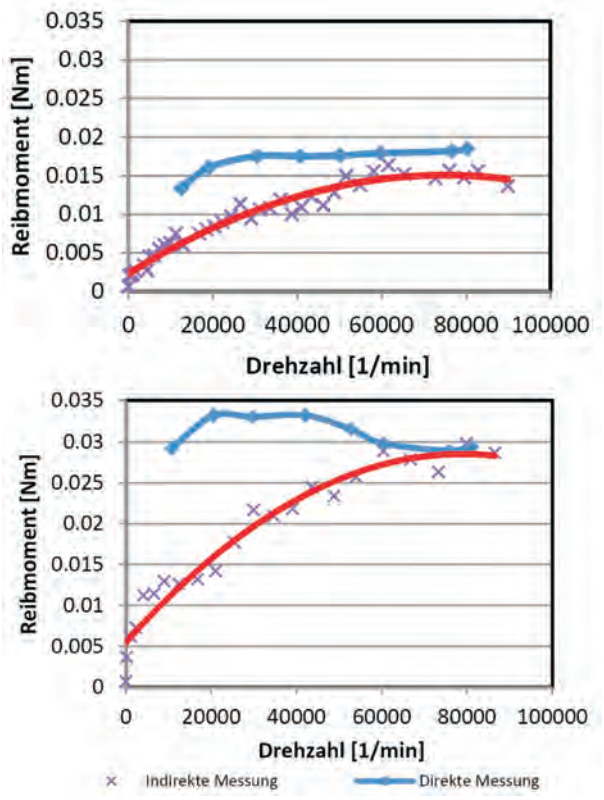

Fig. 5. The results of the direct- and indirect friction torque measurement with 3 bar oil pressure (top 90 °C inlet temperature and bottom 30 °C inlet temperature)

The results of the two measurement methods show that there are differences in both trends of the friction torque in all speed ranges. At 30 °C inlet oil temperature there are big differences between the two methods of measurement at speeds below 60,000 rpm and greater than 90 °C inlet oil temperature. At speeds above 60,000 rpm, the curves approach each other. At 90 °C inlet oil temperature, the difference between the friction torque with increasing speed decreases. For a more accurate interpretation of the measurement results, the oil supply and the oil outlet temperatures are depend on the shaft rotation – shown in Fig. 6.

It can be seen that the changes of oil temperature at 30 °C oil inlet temperature by the indirect measurement method is much higher than the direct method. There is a big temperature differences between inlet and outlet temperature at the two measurement methods. While the difference in temperature with increasing speed is gradually decreased greater in the stationary measurements (maximum of about 14 °C), the temperature difference increases linearly with the indirect measurement method (up to about 24 °C). The

main difference in the friction torque in the indirect dynamic roll-out measurement method is created by holding time of 30 s. Here the produced friction losses dissipated in the local lubricant and the components of the bearing system, so that the real local temperature is much higher than the supplied oil inlet temperature. So the viscosity of the oil which is in the bearing heats up, whereby the viscosity decreases exponentially with increasing temperature and decrease the shear stresses between the bearing tin and the shaft.

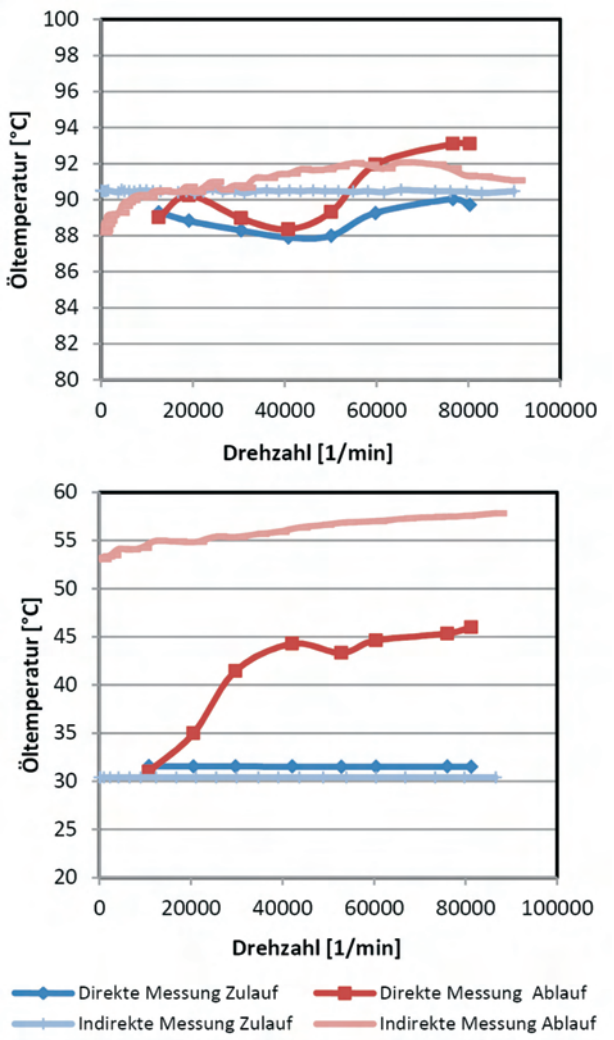

Fig. 6. The inlet and outlet oil temperatures by different measurement methods (top 90 °C inlet temperature and bottom 30 °C inlet temperature)

By rolling-out the shaft, the bearing assembly is cooled slowly. So at low speeds, the real temperature of the lubrication in the turbocharger by the indirect measurement method is significantly higher than the direct method. This effect results in a significantly lower friction torque. At 30 °C and 90 °C, the curves of friction torque between the two measurements variations are approaching at approx. 60,000 rpm. Above this speed, there is a good correlation between the two measurement methods. At lower speeds (below 60,000 rpm) the difference between the two measurement methods is significantly higher.

The difference is due to the aforementioned hypothesis significantly more pronounced than an oil temperature of 30 °C. At oil temperature of 110 °C there is almost a full agreement of the two measurements.

Because the information content of the direct measurement method is higher, in this article all other measurements were carried out by this way.

3.3. Variation of the oil pressure

In this experiment, the turbocharger shaft is measured without thrust force in a speed range of 10,000 rpm – 80,000 rpm. The oil pressure is varied in a range from 2 bar – 6 bar (absolute) by an oil temperature of 90 °C. To determine the frictional torque over the speed range are determined by the friction torque sensor.

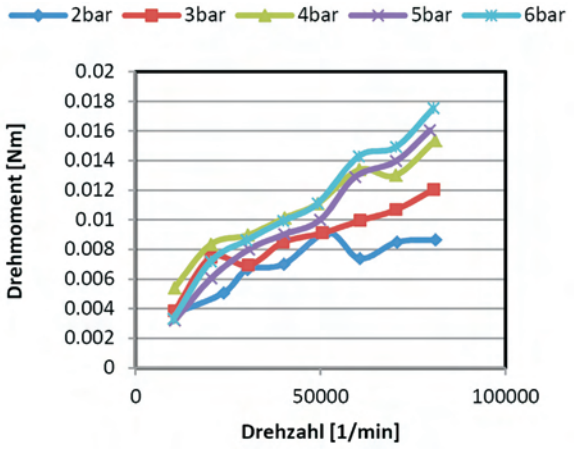

Fig. 7. The friction torque by variation the oil pressure at 90 °C

Figure 7 shows the trend of the friction torque by variation of the oil pressures over the speed. The friction torque increases with the speed. In the speed range below 50,000 rpm, the curves of the respective oil supply pressures do not show major differences. At speeds in excess of 50,000 rpm, the curves are drifting apart with increasing speed. It is striking that at 80,000 rpm and 2 bar absolute oil pressure is the lowest and the highest friction arises at 6bar absolute oil pressure. One explanation for this is shown the behavior of the oil flow. Figure 8 illustrates the trend of the oil flow at various the oil pressures on the speed.

An increase in the oil pressure causes an increase in the oil volumetric flow. A higher oil flow does not necessarily lead to a greater volume flow through the plain bearing. The most of the oil flows around the journal bearing and cools the bearing tin. Due to the higher heat output of the plain bearing of the lubricating film is cooled and the local viscosity increases resulting in increased friction torque and friction power. This is particularly noticeable at high speeds, because there, caused by the proportional dependence to the speed, generally higher friction losses. Higher oil flow rates lead to higher splash losses in plain bearings. Their impact is a higher friction torque and a higher friction power. Depending on the design of the plain bearing, the pressure dependence of the friction power is more or less pronounced.

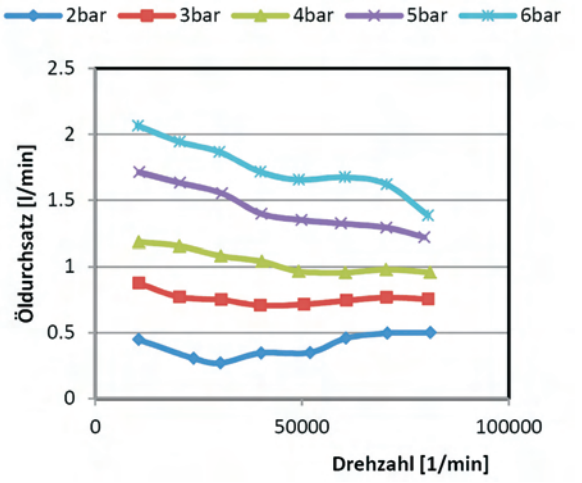

Fig. 8. The oil volumetric flow by variation the oil pressure at 90 °C

3.4. Variation of the shaft bearings

In the following variation three different bearing systems options are compared in terms of frictional power, friction torque and volumetric oil flow. In order to clarify the possible influence of the mounting, factors such as the oil temperature and oil pressure are constant (90 °C, 3 bar). The measurement is achieved without use a thrust force in a speed range from 5000 rpm to 80,000 rpm.

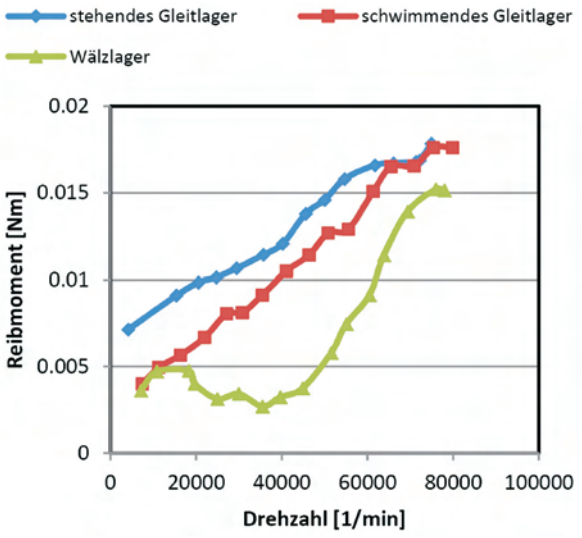

Fig. 9. The influence of different bearing types to the friction torque without thrust force at 90 °C

Figure 9 shows the trend of the friction torque at three different bearings types. As might be expected, the friction torque increases with the speed. The curves of the full- floating and semi-floating plain bearing show speed increases an approximately linear course of the friction torque. The highest friction torque in this bearing comparison is caused by the bearing tin of the hydrodynamic radial bearing. The examined ball bearing has the lowest friction torque trend. This is caused by the ball elements; the rolling friction type is less than plain friction type. At higher speeds, the advantage of the ball bearing against the plain bearing variants is lower.

The slightly increased friction or slightly increased friction losses of semi-floating or full-floating plain bearing is mainly because of the higher shear stresses caused by the higher speed difference of the bearing tin to the rotating shaft within the oil, which in turn leads to higher friction torques. Figure 10 illustrates the trend of the oil volumetric flow of the three investigated bearing types depend of the speed.

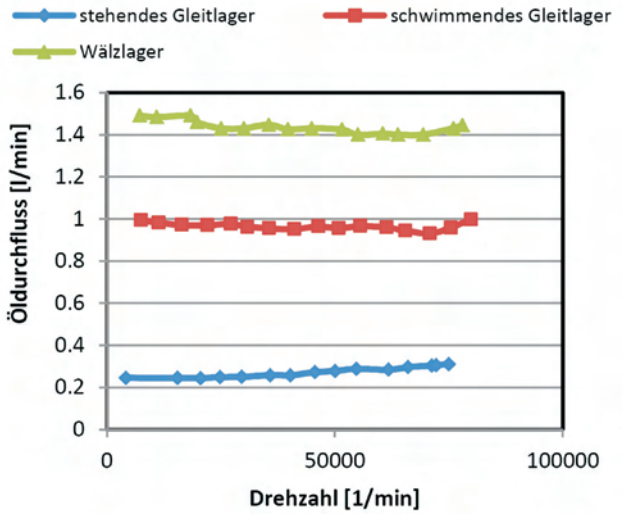

Fig. 10. The oil volumetric flow with influence of bearing types without thrust load at 90 °C

The oil flow has a nearly constant characteristic versus the speed at each examined bearing variant. The highest oil throughput caused by the ball bearings. This is approximately 1.4 l/min. This high oil flow is structurally designed to cool the rotor shaft and the bearing components can sufficiently. A large difference in the flow of oil between the bearings is striking. The also high oil flow of the floating plain bearing serves primarily to building the damping film between the bearing tin and housing. Figure 11 illustrates the trend of the friction power of the various radial bearing over the speed.

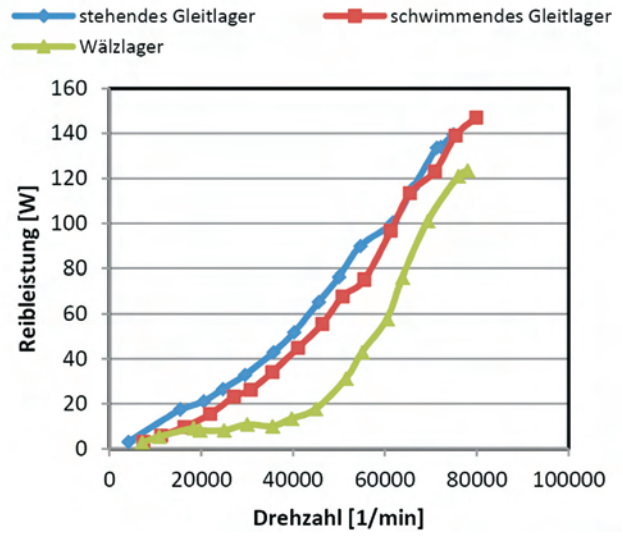

Fig. 11. The influence of bearing without friction power under axial force at 90 °C

The friction of ball bearings is considerably lower than for the plain bearing variants at low engine speeds, this leads to a significantly improved dynamic response during acceleration and an exhaust gas turbocharger. At speeds over 60,000 rpm, the friction performance of the different variants are lower.

3.5. Variation of the thrust force

In this variation, the three bearing types of the turbocharger shaft are varied from the previous section thrust force and measured in a speed range from 5000 rpm to 80,000 rpm by a thrust load of 20 N and 40 N. The oil pressure is kept constant at 3 bar absolute and the oil temperature adjusted to 90 °C. To determine the frictional losses torque and speed are determined by measurement.

3.5.1. Influence of thrust load on a full-floating plain bearing

Figure 12 illustrates the trend of the friction torque for various thrust forces in full-floating plain bearing depending on speed.

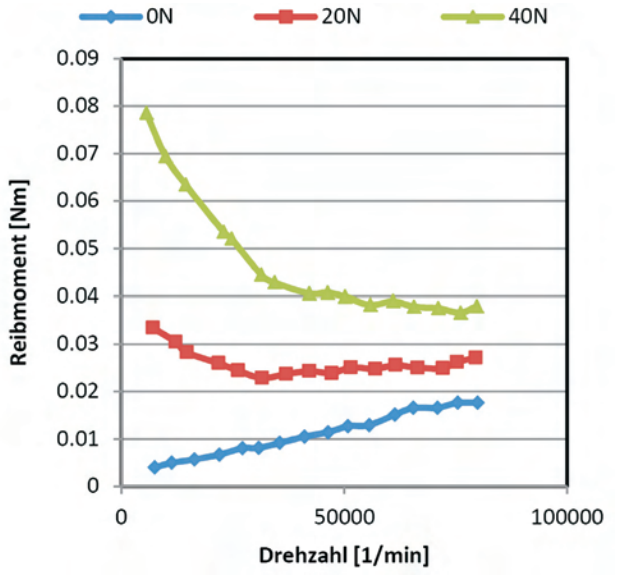

Fig. 12. The friction torque under the influence of the axial force, floating plain bearings at 90 °C

Figure 12 illustrates the trend of the friction torque at various thrust forces in a full-floating plain bearing depending on speed. The frictional torque increases with higher thrust forces. Especially in the low speed range a large difference in frictional torque between the various thrust forces can be seen.

The hydrodynamic thrust bearing is constructed that it enables the rotational movement between the disc and the distance tin. Through a supply channel, oil can flow into the oil chambers of the fixed thrust bearing. From these chambers, the oil between thrust bearing and the disc is flowing, between thrust bearing and distance disc. The next figure shows the basic structure of the thrust bearing.

If a one-sided thrust load is applied, the components can be brought in a rotary motion with a higher force, since they are pressed together. In addition, the oil which is between the disc and the thrust bearing can be abruptly displaced. This leads to an adhesive (n = 0 rpm) or a mixed friction (n > 0 rpm). The effect is higher at low speeds and at higher thrust load. Nearly fixed components of the axial and radial bearing (by n = 0 rpm) increases the relative speed difference between the radial bearing tin and the shaft, which reaches a speed of up to 80,000 rpm. Therefore the shear stress decreases within the oil film significantly and a high frictional torque is produced. This can be seen in Fig. 12, because the friction torque of the load by 40 N in the speed range from 5000 to 40,000 rpm is much higher than the friction torque of the load at 20 N.

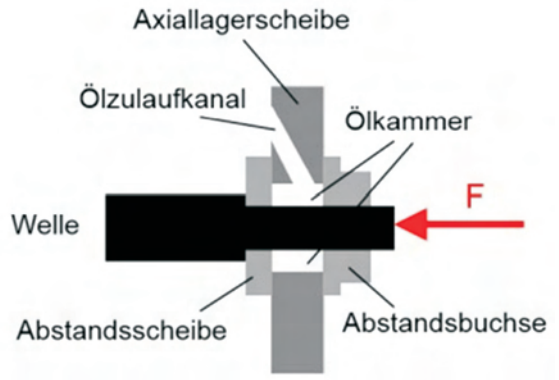

Fig. 13. The structure scheme of a hydrodynamic thrust bearing

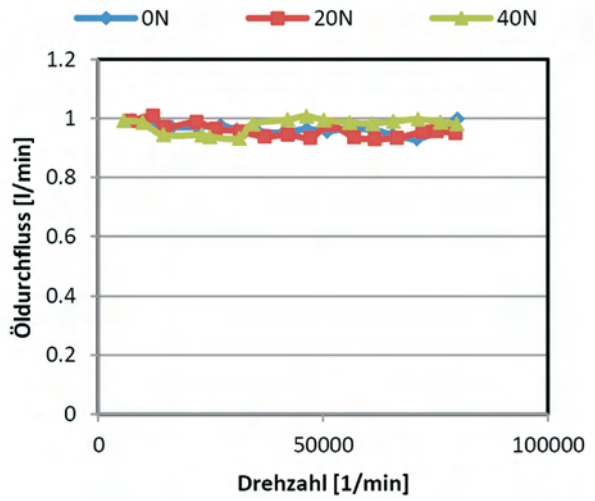

Fig. 14. The oil volumetric flow by influence of thrust force, in full-floating plain bearings at 90 °C

Only with increasing speeds a sufficiently large lubricating film could be reached between the surfaces to the compressed again to separate the components from each other and cause a sliding fluid contact. The oil film, which is separating the components, can re-rotate the bearing components take place, whereby the speed difference becomes smaller. By lower shear forces, the friction torque is reduced. From a speed by 40,000 rpm of separating oil film also ensures a constant trend of the friction torque.

Figure 14 illustrates the trend of the oil flow by different thrust forces in a full-floating plain bearing depending

of speed. The thrust load doesn't have an influence of the oil flow.

Figure 15 shows the results of friction power with different thrust load depending of speed.

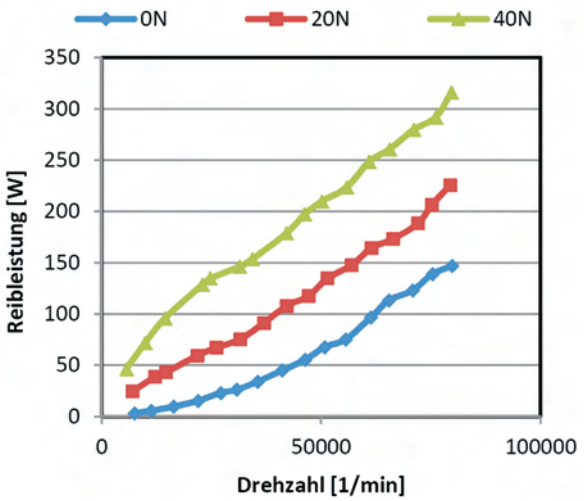

Fig. 15. The friction losses with influence of thrust load, in full-floating plain bearings at 90 °C

The friction losses increase with each loaded thrust force proportional to the speed. An increased thrust force causes higher friction losses. Here, the distance between the frictions is less than the performance data between 20 N and 40 N as well as between 0 N and 20 N. An explanation on this matter provides the construction of the hydrodynamic thrust bearing, which is described in Fig. 13.

3.5.2. Influence of thrust force on a semi-floating plain bearing

In the further experiment, the thrust force is increased in two steps in the semi-floating plain bearing.

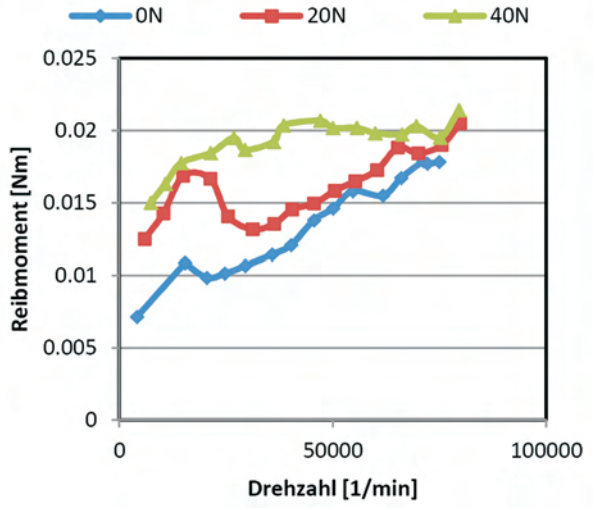

Fig. 16. The friction torque with influence of the thrust load in a semi-floating plain bearing at 90 °C

The friction torque increases slightly with higher thrust forces. The frictional torques with thrust load is only slightly above the frictional torque without thrust load. In the speed range between 10,000 rpm and 60,000 rpm by a load of 40 N and in the speed range between 5000 to 30,000 rpm by 20 N, the influence of thrust load is higher than at higher speeds, where a convergence of all curves takes place during thrust force.

Analog the explanation in chapter 3.5.1 the components of the thrust bearing are pressed together, by the thrust force of 20 N or 40 N. In a semi-floating plain bearing tin, the resulting impact is comparatively small, since even in the absence of a thrust force, the fixing of the tin has a high difference in speed between the shaft and the bearing tin. Only a small increase in friction torque is caused by the application of a thrust force. Figure 17 illustrates the trend of the oil flow by different thrust loaded in semi-floating plain bearing depending on speed.

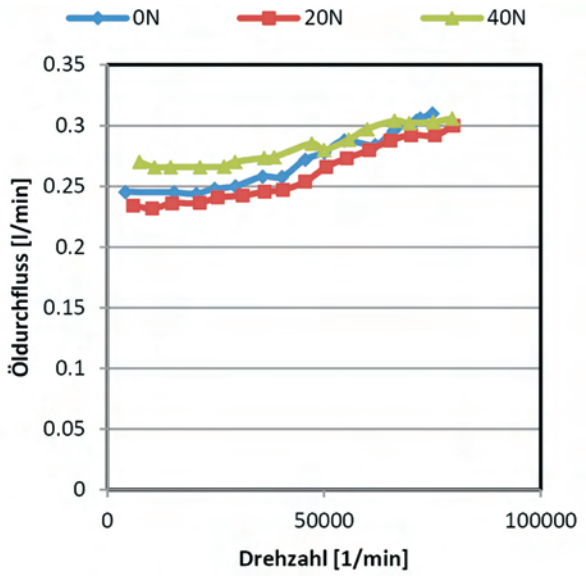

Fig. 17. The oil volumetric flow with influence of thrust force, in semi-floating plain bearing at 90 °C

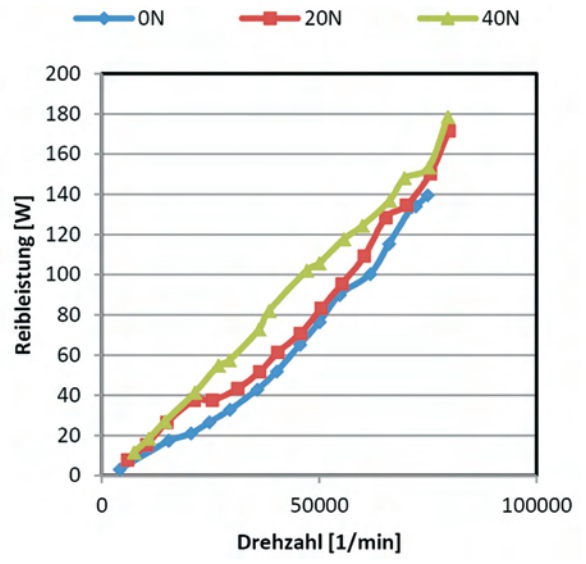

Fig. 18. Friction losses with influence of thrust load, in semi-floating plain bearings at 90 °C

The oil flow increases slightly by a load in the axial direction. It is thought that by displacing the thrust bearing the ratio of the inflow cross sections between plain bearing and bypass channel is changed and can flow more oil through the bypass channel.

Figure 18 represents the trend of the friction losses at various thrust forces in a semi-floating plain bearing depending on speed.

The curves of the friction losses with thrust load of 0 N, 20 N and 40 N have a small parallel shift in the curves on almost the same curve.

3.5.3. Influence of thrust force on a ball bearing

Figure 19 illustrates the trend of the frictional torque in a ball bearing by different thrust loaded depending on speed.

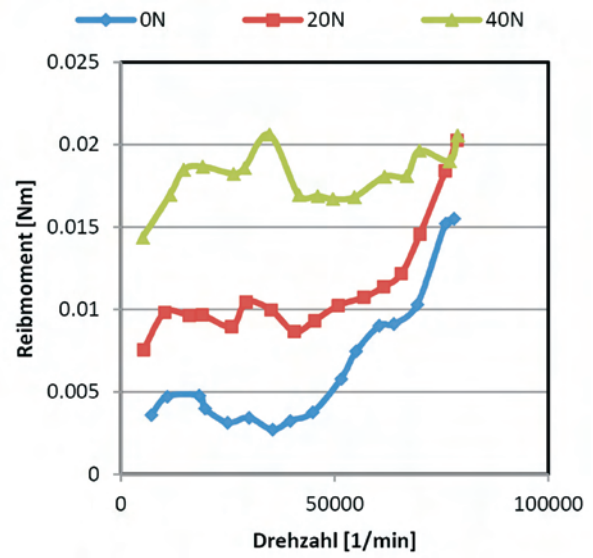

Fig. 19. The friction torque with influence of thrust load, in a ball bearing at 90 °C

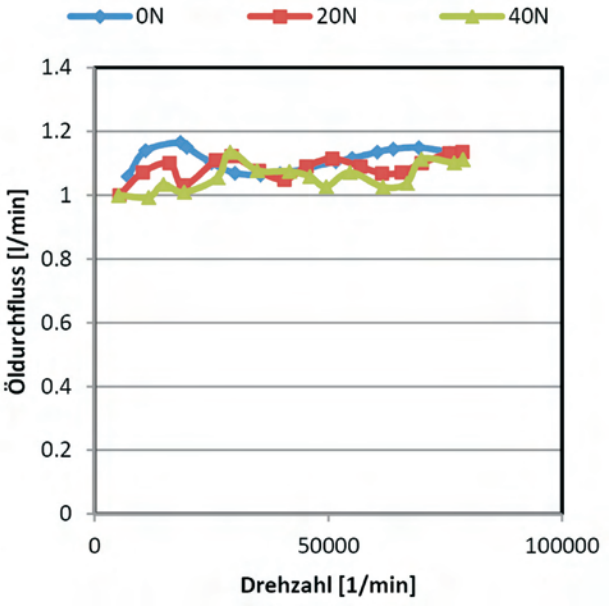

Fig. 20. The oil flow with the influence of thrust load, in ball bearing at 90 °C

The friction torque increases at higher thrust load. In contrast to the reaction of a plain bearing by a thrust load, in the ball bearing there is nearly no influence of the friction torque with increased thrust load, which was caused without this load. The design of the ball bearing, which is a diagonally ball bearing allows to absorb the radial load and the thrust load. Therefore, the friction increases are almost proportional to the thrust force. Figure 20 shows the oil flow of a ball bearing by changing the thrust load.

There is a clear increase, that the thrust load has no influence on the oil flow. A thrust load shifts the balls in the ball bearing insignificant, whereby the cross-section for the flow barely changes. Figure 21 illustrates the trend of the friction losses at various the thrust load of a ball bearing depending on speed.

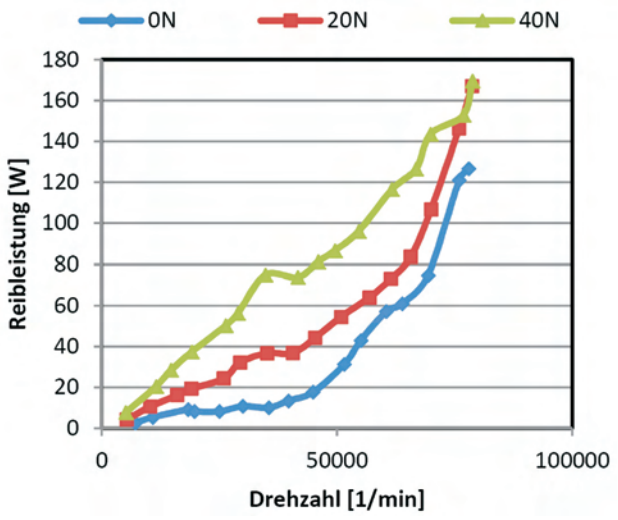

Fig. 21. The friction losses with influence of thrust load, in ball bearings at 90 °C

The friction losses increases with each applied thrust load proportional to the speed. The highest frictional power is thereby caused by a thrust load of 40 N. Similar to a full-floating and semi-floating plain bearing the friction of ball bearings is the lowest with influence of thrust load.

3.6. Influence of the load direction in a thrust bearing

In the following investigation, the axial bearing is charged with +20 N and –20 N and examined in a speed range from 10,000 rpm to 80,000 rpm. The oil pressure is thereby maintained constant at 3 bar and adjusted the oil temperature at 90 °C. The friction torque and speed are determined during this measurement. This test allows evaluating, whether the direction of the thrust force has an effect on the friction losses.

Figure 22 illustrates the trend of the friction torque by various the thrust forces when pulling or pushing the shaft. The curves of the friction torque show already discussed in chapter 3.5.1 the influence of thrust load. The need of oil film between the bearings surfaces of the thrust bearing occurs at increased starting torques at low speeds. With increasing speed, a sufficiently large lubricating film reaches these bearings and a fluid sliding film is built. The friction

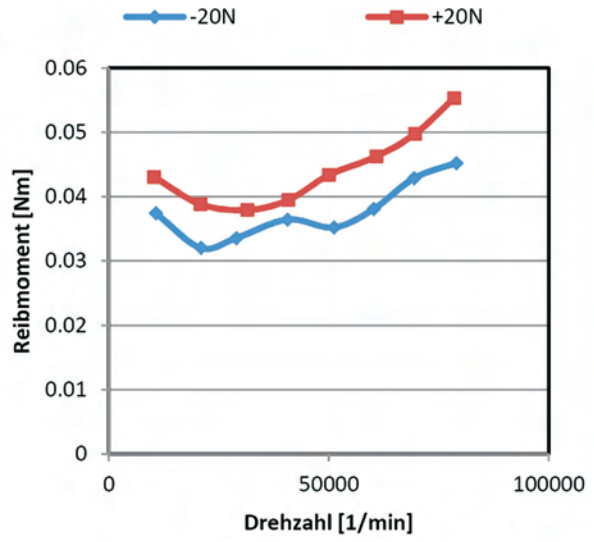

Fig. 22. The friction torque with the influence of the load direction in a thrust bearing at 90 °C

torque, which is caused by a forward (pushing) force differs from the torque of pulling force. The results clearly show that the thrust bearing caused by its asymmetrical bearing structure has a different friction torque depending on pulling or pushing shaft.

Figure 23 illustrates the trend of the friction losses at various thrust forces that are applied in pulling and pushing direction depending on speed. In a speed range from 10,000 rpm to 40,000 rpm the curves are nearly the same. From a rotation speed more than 40,000 rpm the friction increases more under the push load of +20 N compared to the pulling load by –20 N.

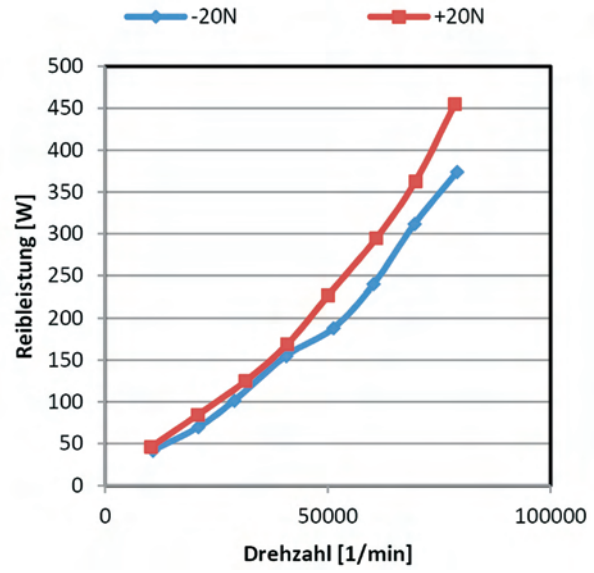

Fig. 23. The friction power influenced the direction of action of the axial force at 90 °C

4. Friction performance benchmark

As part of investigations on the Ostfalia friction test rig over 50 turbochargers were measured.

The extensive results allow putting up a map of friction power losses depending on speed. All turbochargers were measured at 3 bar oil pressure and 90 °C oil temperature without thrust load. Figure 24 shows the result of the benchmark friction losses map.

In the map in Fig. 24 there is a distinction between plain bearing (red and blue) and ball bearings (black). It is immediately apparent that there are in fact turbochargers with hydrodynamic radial bearing, which have lower friction losses than TC with ball bearings. This is due to special tribological measures in structure of bearing systems.

Furthermore, it was once again distinguished in the field of hydrodynamic radial bearings between applications for gasoline (in blue) and diesel engines (in red). It should be noted that there are bearings with a lower friction losses than turbocharger with ball bearings.

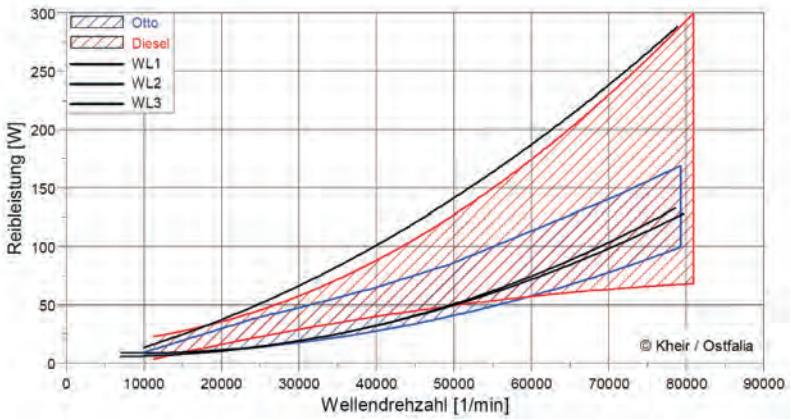

Fig. 24. The comparison of different bearing systems of turbochargers

The boost pressure of a diesel engine is much higher than that of a gasoline engine.

This results in higher thrust forces on the bearing; it must be absorbed by a larger thrust bearing. Although the measurements with unloaded thrust bearing was applied, the larger thrust bearing in diesel turbocharger cause a higher friction losses than turbocharger by gasoline engines.

The next Fig. 25 shows analogue to Fig. 24 the friction losses depending on the shaft diameter speed. So the constructional geometries of the shaft is includes the speed, so the maps shows the specific friction losses of more than 50 turbocharger were measured.

5. Summary

This article discusses the modern turbocharger bearings systems and its analysis. A specially developed and designed friction power test rig is introduced in this article. The friction of radial- and thrust bearings was discussed in detail. The resulting conclusions are briefly summarized here.

The oil temperature is a critical factor to minimize the friction losses, the friction losses decreases by increasing oil

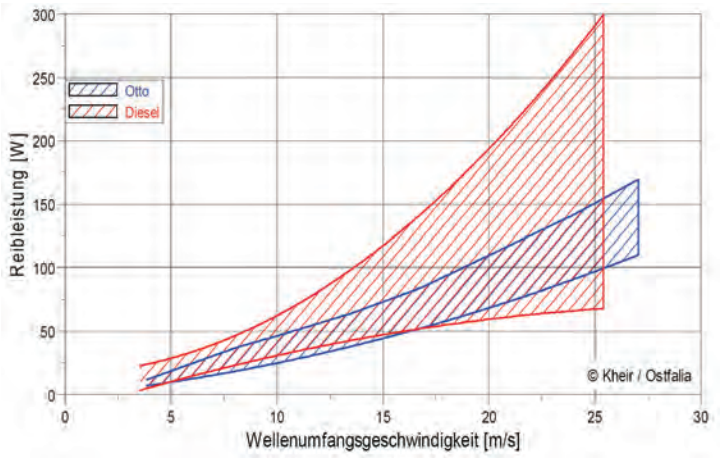

Fig. 25. The comparison of different application in plain bearings depend on shaft diameter speed

temperature. Here, the friction torque shows a clear downward trend with higher oil temperatures. This is especially noticeable at low speeds. The oil flow increases with an increase of the oil temperature. This results by increased splash losses and increased heat dissipation.

With respect to the oil pressure, an influence is recognizable only at higher speeds. The friction torque decreases at high speeds by a pressure reduction. The result is a lower friction performance compared to higher oil pressure values. The oil flow ratio is above the speed curve usually constant and increases with the increase of the oil pressure.

An axial force applied on a full-floating plain bearing causes a considerable increase in the friction torque. This is particularly evident at low engine speeds. With an increase of the rotation speed, the friction torque decreases. In semi-floating plain bearing the influence of the thrust force is smaller. In a fixed bearing tin there is a higher difference in speed between the tin and the shaft so it occurs when it is loaded by a thrust force; the difference in torque is lower than for a full-floating bearing tin. Consequently, the trends of the friction torque with thrust load have the same shape as the curve of the friction torque in the unloaded thrust bearing condition. In regard to the oil flow with an influence to a thrust load there isn't any affect by any bearing.

When comparing three different bearing types at 90 °C oil temperature and 3 bar oil pressure without thrust load, the trends of the friction torque for semi-floating and full-floating plain bearing shows nearly identical curves. The friction torque of the plain bearing is also higher than the friction torque of the tested ball bearing. The friction losses by a semi-floating bearing are a little bit higher than the friction in a full-floating bearing. The reason for this hypothesis is the different in the speed difference between shaft and bearing tin. There is also a big discrepancy in the oil flow between the bearing types. The greatest flow generates the ball bearing requires theses high flow for heat dissipation of the bearing components. The full-floating plain bearing also shows a high flow rate of about one liter per minute. This oil flow is needed to build the hydrodynamic oil film and to wash around the bearing tin to minimize any vibrations.

More friction losses were determined by an influence of the load direction in a thrust bearing, probably caused by the asymmetrical structure of the bearing oil flow.

The friction power test rig constructed by Ostfalia, University of Applied Sciences can make an important contribution, to evaluate the simulation results of bearings systems to match them with measurement results and to analyze different bearings options under realistic conditions.

Acknowledgement

The authors would like to thank the research and development department of Volkswagen AG for the support.

Bibliography

[1] Baar R., Porzig D., Rätz H.: Systemspezifische Schmierfilmdissipation in den radialen und axialen Lagerstellen von Abgasturboladern unter realen Betriebsbedingungen mit unterschiedlichen Ölzuführungsrandbedingungen Abschlussbericht über das Vorhaben Nr. 1020 (AIF-Nr. 16230).

[2] Smiljanovski V., Schorn N., Scharf J., Funken B., Pischinger S.: Messung des Turbinenwirkungsgrades bei niedrigen Turboladerdrehzahlen. 13. Aufladetechnische Konferenz Dresden, 2008.

[3] Schmitt S., Schmid W., Hertweck G., Schlegl M., Staudacher S.: High-Precision measurements of friction measurements of friction losses in turbochargers. 12. Aufladetechnische Konferenz Dresden, 2007.

Prof. Robin Vanhaelst, DSc., DEng. – Professor in the Faculty of Automotive Engineering Ostfalia University of Applied Sciences, Germany.
e-mail: *r.vanhaelst@ostfalia.de*

Alaa Kheir, MEng. – Faculty of Automotive Engineering Ostfalia University of Applied Sciences, Germany.
e-mail: *kheir.alaa@googlemail.com*

Jakub Czajka, DEng. – Volkswagen Poznań Sp. z o.o. Poznań, Poland.
e-mail: *jakub.czajka@vw-poznan.pl*

Article citation info:
JAWORSKI, P. et al. SCR systems for NO_x reduction in heavy and light duty vehicles. *Combustion Engines*. 2016, **164**(1), 32-36. ISSN 2300-9896.

Piotr JAWORSKI
Sebastian JAROSIŃSKI
Azael CORTES CAPETILLO
Łukasz Jan KAPUSTA
Adam ZIÓŁKOWSKI
Robert GRZYWNOWICZ

PTNSS-2016-104

SCR systems for NO_x reduction in heavy and light duty vehicles

Air pollution has become an important worldwide problem. The European Commission credits road and water transport as the major source of NO_x pollution, and of being responsible for around 50% of the total air pollution in urban areas. During the last decade, the use of SCR technologies have gained popularity as a method for NO_x reduction, the technology is widely considered as one of the solutions for road transport emissions. This paper presents a review of the different SCR system designs derived from the various factors and regulations in the automotive industry which have influenced the technology, along with a parametric study of a proprietary SCR system for heavy duty application.

Key words: *NO_x, SCR, urea, ammonia, exhaust, emissions, after treatment, heavy duty vehicle*

1. Introduction

Considering that catalytic emission control has been around for more than 40 years, and Selective Catalytic Reaction (SCR) been widely used on stationary plants for the abatement of NO_x [1], its introduction into the automotive market dating to the last decade (around 2005-2008) is relatively recent [2].

The main purpose of SCR catalytic converters is the abatement of NO_x contaminants, which are poisonous for humans and largely responsive for the catalytic destruction of ozone (O_3) in the atmosphere [3]. NO_x is the generic term for mono-nitrogen oxides primarily NO and NO_2 which are produced during combustions at high temperatures [3].

Diesel engines operate lean, and at lower temperatures than stoichiometry gasoline engines [4], thus preventing the complete reaction of NO_x species. As catalytic technology developed, it was evident that Hydrocarbon (HC) based catalyst were not sufficient for the reduction of NO_x agents on low temperature engines such as the diesel operated ones [1]. This problem popularized the use SCR systems using urea based solutions as a conduct of ammonia (NH_3) for the reduction NO_x contaminants to nitrogen (N_2) over a catalyst composed of base metals on diesel engines. The technology has proved a great success showing efficiencies of over 90% NO_x reduction in laboratory conditions [5].

According to the Regulation (EC) No 715/2007, the Euro 6 norm for heavy, medium and light duty engine demands for more than a 50% reduction of NO_x contaminants in comparison to Euro 5 (Tab. 1). Such demanding reductions on NO_x contaminates demand for further investigation and improvement on SCR reduction methods for light and heavy duty engines [6].

2. NO_x reduction – SCR methodology

The SCR method consist in a controlled injection of a water/urea solution, that turns into ammonia (NH_3), into the exhaust gasses to promote the reduction of NO_x contaminants at low temperatures over a based metal catalyst (Fig. 1). The process used to be located after the oxidation catalyst to avoid the oxidation of the injected solution before its catalytic reaction with NO_x contaminants [7].

The reduction of NO_x in the absence of an oxidizing catalyst can be achieved in a narrow range of temperature between 1075 to 1175 K and over 1200 K the ammonia (NH_3) oxidize to NO_x [8]. Due to that it is not possible to combine the ammonia as a reduction fluid in high temperature region. It is a reason why a technique commonly used on SCR systems is to locate the SCR process (including the

Table 1. Oxides of nitrogen emission limits comparison of Euro 5 vs Euro 6 according to EC No 715/2007

Vehicle		Reference mass (RM) [kg]	Limit values: Mass of oxides of nitrogen (NO_x) [mg/km]			
			Euro 5		Euro 6	
Category	Class		PI	CI	PI	CI
M	–	All	60	180	60	80
N1	I	RM ≤ 1305	60	180	60	80
	II	1305 < RM ≤ 1760	75	235	75	105
	III	1760 < RM	82	280	82	125
N2			82	280	82	125

PI = Positive ignition, CI = Compression ignition
M – 4 wheel vehicles for the carriage of passengers
N1 – 4 wheel vehicles for the carriage of goods (RM < 3 500)
N2 – 4 wheel vehicles for carriage of goods (3 500 < RM < 12 000)

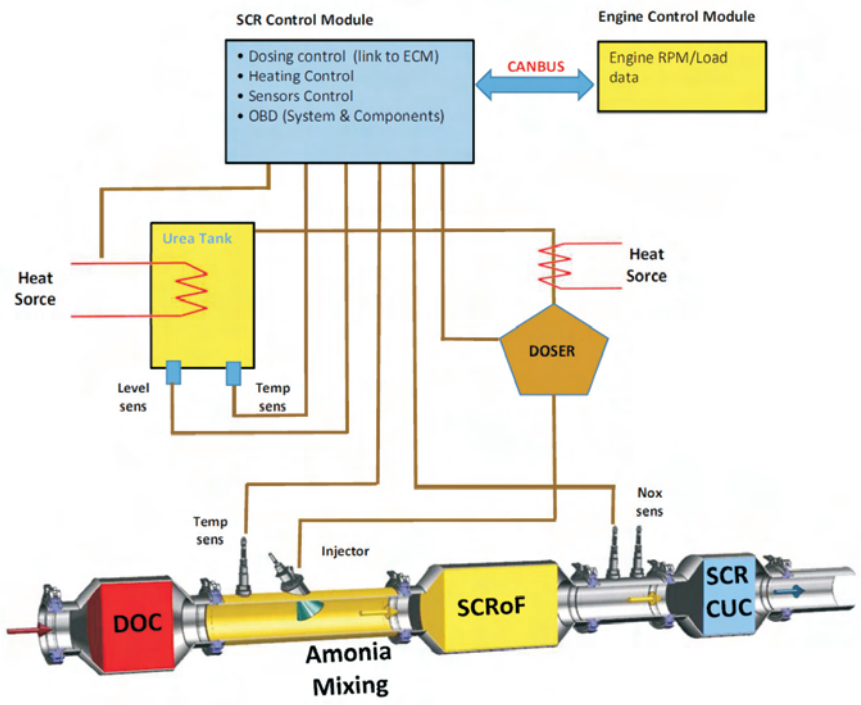

Fig. 1. After-treatment system

solution injection, mixing and catalytic converter) away from the engine to lower its temperature of operation.

NO is the most simple odd-electron molecule with a thermal stability and represents the major NO_x component in exhaust gases [9]. The catalytic decomposition of NO has been favored as the most desirable method for its removal [9].

NO releases oxygen during its decomposition, and in turn, this oxygen competes for adsorption sites over the catalyst surface, this is the reason why an additional liquid or gaseous reductant is required during the SCR process [6, 9]. SCR catalysts selectively decompose NO_x species by an hydrolysis process after adding urea as the source of ammonia (NH_3) into the exhaust mix, converting NO_x contaminants into N_2, NH_3, CO_2 and H_2O [7].

$$(NH_2)_2CO + H_2O \rightarrow 2NH_3 + CO_2 \quad (1)$$

$$4NH_3 + 4NO + O_2 \rightarrow 4N_2 + 6H_2O \quad (2)$$

$$4NH_3 + 2NO + 2NO_2 \rightarrow 4N_2 + 6H_2O \quad (3)$$

The effectiveness of SCR system depends on many factors including the type of catalysts, the injection pattern of ammonia (NH_3), the mixing efficiency, and temperature. Depending on the catalyst, the temperature of operation varies ranging from 300–800 K. There are three main groups of SCR catalysts [10]:

– Those supported by noble metals (Pt/Al_2O_3)
– Those with a base metal oxide (containing vanadium)
– Those of metal ion exchanged zeolites–crystalline silicate (Cu-ZSM-5).

The use of an external agent for the catalytic reaction of NO_x contaminants has always been considered the weak aspect of the SCR technology [1]. To start it is necessary the inclusion of a storage tank for the ammonia solution (NH_3) with all the complexities involved such as its maintenance and refilling [11]. Moreover, the injection system needs to be designed and adjusted for optimal operation to avoid overloading and crystallization [1, 12]. Finally the technology requires of an efficient ammonia distribution to ensure optimal efficiency [1].

Future advances on the technology needs to focus on compact designs that ensure a complete mixture of the ammonia solution in the air flow. In parallel the catalytic converters need to be develop to fulfill the need of simultaneously reduction of soot and NO_x contaminants.

3. SCR construction

Taking the above into account a clear design path for the SCR technology points toward an in-line SCR catalysts solution, able to provide a full emission reduction of HC, CO, NO_x and Soot at low temperatures under a single packaging (Fig. 2). An example of these designs is the SCRT® catalyst from Johnson Matthey which incorporates an SCR catalytic system as well as a CRT® (Continuous Regenerating Trap) to deal with NO_x and Soot at the same time [13].

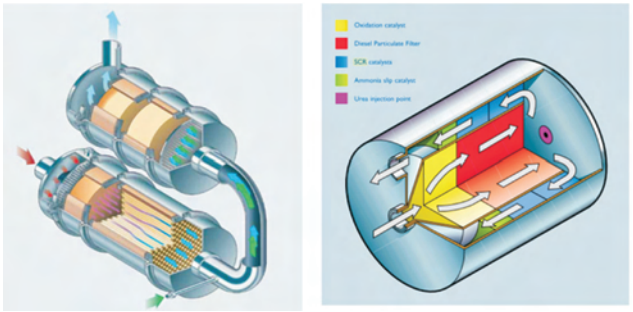

Fig. 2. First generation in-line SCRT system (left) and Compact SCRT system (right) by Johnson Matthey [13]

Initial SCRT development focused on 'linear' configurations where the CRT was followed by an in-line SCR unit, and further iteration lead to the compact SCRT design (Fig. 2).

Currently in the market, there are catalyst designs with incorporated reduction functions for CO, HC, NO_x and Soot into a single component or a single housing, capable of working at a range of temperatures, from 300–700 °C, and with a mixture of catalytic material.

To achieve this four-way function, it is necessary to have a coherent substrate arrangement, sufficient SCR catalytic loading and low levels of backpressure produced by the substrate.

Exhaust gases must pass first through the SCR catalyst and then through the oxidation catalyst. If exhaust gases bypass the SCR catalyst, and are exposed in first instance to the oxidation catalysts, the reductant, in this case ammonia, will be oxidise to NO_x contaminants, compromising the effectiveness of NO_x reduction [5].

It is necessary to account for certain parameters during the design process including:

– Packaging, which defines possible constructions solutions, like inline (Fig. 3, 4) or compact (Fig. 5)
– Boundary conditions such as mass flow and temperature
– Demand of emission limits (NH_3 distribution and NO_x conversion efficiency)
– Demand on pressure drop (pressure drop for each included elements)
– Cost.

Fig. 3. Concept of Close Coupled SCR system in HD application

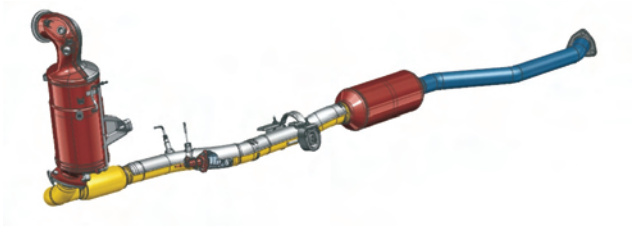

Fig. 4. Inline concept of SCR system in LD application

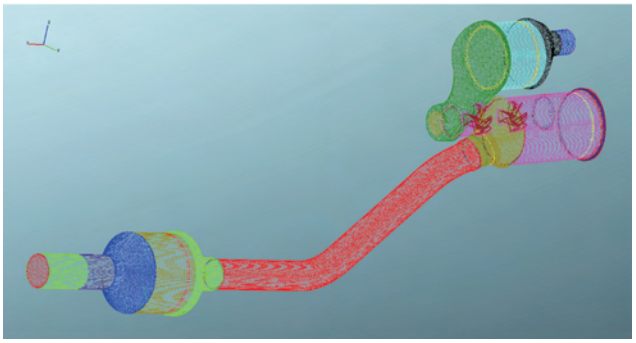

Fig. 5. Compact concept of SCR system in MD application

4. LD state of the ART

The design process of a compact LD SCR system such as the one in Fig. 4 involves various iterations in order to find the optimal solution that meets packaging, emissions and boundary condition limits. The different flow conditions state in relation to real drive conditions need to be considered. Two important parameters that also need to be validated during the design process are pressure drop (Tab. 2) and velocity uniformity (Fig. 6). It is of major importance to limit the pressure drop of the SCR design, which in many cases is mainly generated by the mixer.

Table 2. Pressure drop results for different flow conditions

Operating points	Mass flow	Back pressure	Press drop mixer only	Press drop mixer + pipe	Temperature @ mixer	
	kg/h	Pa	Pa	Pa	K	°C
1	300	7710	623	1121	571	298
2	125	2567	110	192	520	247
3	50	755	17	29	443	170
max	620	15910	2821	5021	815	542

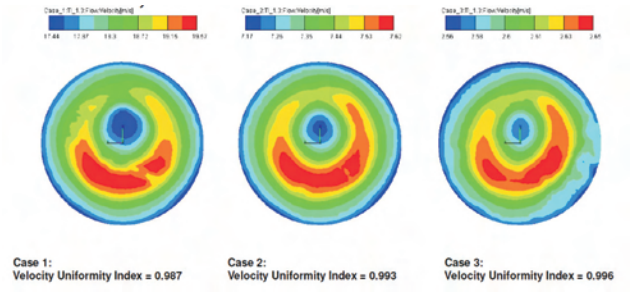

Fig. 6. Velocity uniformity at 25 mm of SCR for different flow conditions

The optimization of urea mixing process is the most challenging one, especially due the different flow conditions such as idle, medium and full load. Even if the uniformity of NH_3 can be achieve the conversion parameter can be still low (Fig. 7).

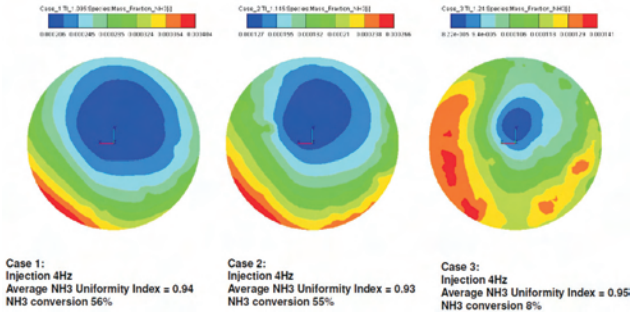

Fig. 7. NH_3 uniformity at 25 mm of SCR for different flow conditions

The reason for that is limited mixing and evaporation efficiency due to the low flow conditions. The droplets of urea water solution are to heavy to be drag by the flow and are deposed on pipe wall generating the wall film (Fig. 8). The vaporistion is limited in such flow conditions which will afftect the maximum conversion parameter. For presented LD application the conversion parameter is not a critical one, but it becomes critical for close coupled solutions.

Table 3. Velocity uniformity results for developed design

Bricks	I CFD Flow Uniformity	II CFD Flow Uniformity	III CFD Flow Uniformity	IV CFD Flow Uniformity	Flow Uniformity
DOC	83%	78%	87.5% 92.5% – S (swirl)	92.6% – S	> 90%
SCRoF	95.3%	96.4%	94.9%	95.0%	> 95%
SCR+CUC	93.6%	93.9%	98.4% – PP (perforated plate)	92.9%	> 92%

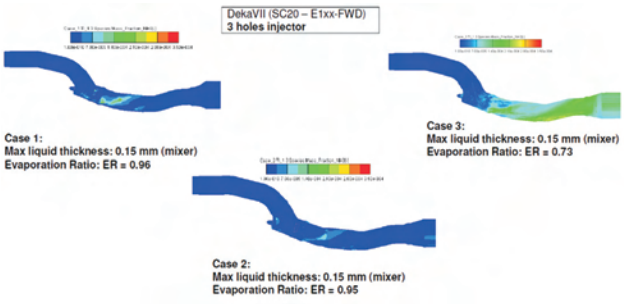

Fig. 8. Wall film generation in the exhaust pipe for different flow conditions

5. HD state of the ART

The design process of a HD or MD compact SCR system such as the one in Fig. 5 also involves various iterations in order to find the optimal solution that meets packaging, emissions and boundary condition limits. Two important parameters that also need to be validated during the design process are pressure drop and velocity uniformity (Tab. 3).

Table 4 shows the velocity uniformity percentages of the compact SCR design here presented. It can be seen how as iteration advanced, the velocity grew more uniform within the design.

Table 4 presents the results of pressure drop created by each component in each of the design iterations. For the computational fluid dynamic (CFD) analysis of the SCR system, it is crucial to accurately define the boundary conditions such as the inlet flow pattern, which is located directly after the turbine and results in the swirl flow (S). It is important to highlight how difficult it is to achieve a reliable uniformity on the SCR+CUC element due to different diameter of pipe and catalyst in-cone. The use of a perforated plate (PP) could be a solution to improve the flow uniformity, however, the addition of this component will be a source of pressure drop.

Table 4. Pressure drop results for developed design

Pressure drop @1050 kg/h 580°C	Concept 1 (one mixer) [mbar]	Concept 2 (two mixers) [mbar]	Concept 2 (two mixers + pp) [mbar]	Concept 3 (two mixers) [mbar]
Inlet cone	25.8	11.4	11.4	11.4
DOC	49.0	42.4	42.4	43.0
Injector cone	75.9	33.8	33.8	18.1
Mixer pipe	20.9	30.4	30.4	33.1
Midcone	24.7	37.8	37.8	37.4
SCRoF	151.0	151.1	152.1	153.2
Outlet cone	6.3	2.3	2.0	2.3
Tube	4.5	8.0	6.2	5.4
Inlet SCR's Cone	7.8	7.6	21.1	8.7
SCR+CUC	54.4	52.4	50.6	51.9
Outlet SCR's Cone	14.5	14.1	10.7	10.1
Overall	435.0	392.2	398.4	374.7

At the final stage of the design of the SCR system, the injection characteristics of the water/urea solution, commercially known as ad-blue, and the distribution of ammonia (NH_3) need to be validated numerically and experimentally. Typically this stage include the testing of one or double mixer solutions (Fig. 9). As shown by Table 5, the influence of the mixer position has a significant impact. By redesigning the mixer into a single stage design it was possible to obtain improved results as presented in Table 6.

Table 5. Gamma NH_3 distribution in double mixer concept

Operating Point [350 kg/h, 380 °C, 0.3 kg/h DEF]	
Cases	Gamma NH_3 (two mixers)
Case 1	94.57%
Case 2 (–10 mm)	91.97%
Case 3 (+10 mm)	94.12%
Case 4 (+20 mm)	92.63%

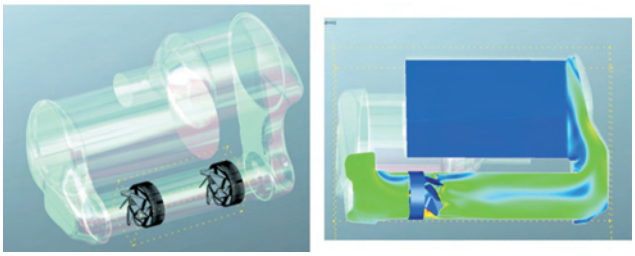

Fig. 9. Mixer models for CFD tests, on the left the double mixer, on the right one stage mixer concept

Table 6. Gamma NH_3 distribution in one stage mixer concept

Operating Point [350 kg/h, 380°C, 0.3 kg/h DEF]	
Cases	Gamma NH_3
Case 1	82.3%
Case 2	82.83%
Case 3	84.69%
Case 4	86.68%
Case 5	94.60%

6. Conclusions

Tightening emission regulations are expected to continue but not only for emission levels. For future Euro 7 regulations emissions levels will not change, changes in test methodology will continue to push depollution efforts on 2 levels:
– NO_x reduction level independent from driving conditions (urban, extra urban, uphill, highway),
– Optimization of fuel efficiency impact caused by AFT devices,
– Optimization of thermal management to minimize cold phase duration independent form driving conditions.

Such trend will demand for a continuous development of exhaust gas after treatment systems. The design of an SCR concept that meets the envisaged regulations will required a significant research process, nevertheless, if the task is followed employing the right analytical tools such as CFD and optimization techniques a solution which meets the required emission limits, design limitations and at an affordable production cost could be achieved.

Bibliography

[1] Kaspar J., Fornasiero P., Hickey N., Kašpar J. Automotive catalytic converters: current status and some perspectives, Catal. Today, vol. 77, no. 4, pp. 419–449, 2003.
[2] Furore, FUTURE ROAD VEHICLE RESEARCH R&D Technology Roadmap, Technology.
[3] S. Roy M.S., Hegde and Madras G. Catalysis for NOx abatement, Appl. Energy, vol. 86, no. 11, pp. 2283–2297, 2009.
[4] Farrauto R.J., Heck R.M. Catalytic converters: state of the art and perspectives, Catal. Today, vol. 51, no. 3–4, pp. 351–360, 1999.
[5] Boorse R.S., Dieterle M. Four-way diesel catalysts and method of use, US 8,246,922 B2, 2012.
[6] Koebel M., Elsener M., Kleemann M. Urea-SCR: a promising technique to reduce NOx emissions from automotive diesel engines, Catal. today, vol. 59, no. 3, pp. 335–345, 2000.
[7] Twigg M.V. Catalytic control of emissions from cars, Catal. Today, vol. 163, no. 1, pp. 33–41, 2011.
[8] Pârvulescu V.I., Grange P., Delmon B. Catalytic removal of NO, Catal. Today, vol. 46, no. 4, pp. 233–316, 1998.
[9] Garin F. Environmental catalysis, Catal. Today, vol. 89, no. 3, pp. 255–268, 2004.
[10] Skalska K., Miller J.S., Ledakowicz S. Trends in NOx abatement: A review, Sci. Total Environ., vol. 408, no. 19, pp. 3976–3989, 2010.
[11] Heck R.M., Farrauto R.J. Automobile exhaust catalysts, Appl. Catal. A Gen., vol. 221, no. 1–2, pp. 443–457, 2001.
[12] Schaub G., Unruh D., Wang J.,Turek T. Kinetic analysis of selective catalytic NOx reduction (SCR) in a catalytic filter, Chem. Eng. Process. Process Intensif., vol. 42, no. 5, pp. 365–371, 2003.
[13] Johnson Matthey Global Emissions Management: Focus on Selective Catalytic Reduction (SCR) Technology, 2012.

Piotr Jaworski, MSc. Eng. – research fellow, The Faculty of Power and Aeronautical Engineering at Warsaw University of Technology, Poland.
e-mail: *piotr.jaworski@itc.pw.edu.pl*

Sebastian Jarosiński, MSc. Eng. – Product Engineer, KATCON.
e-mail: *sebastian.jarosinski@katcon.com*

Azael Cortes Capetillo, DEng. – R&D and Innovation, KATCON.
e-mail: *azael.capetillo@katcon.com*

Łukasz Jan Kapusta, DEng. – Assistant Professor in the Faculty of Power and Aeronautical Engineering at Warsaw University of Technology, Poland.
e-mail: *lukasz.kapusta@itc.pw.edu.pl*

Adam Ziółkowski, MSc. Eng. – Design Engineer, KATCON.
e-mail: *adam.ziolkowski@katcon.com*

Robert Grzywnowicz, MSc. Eng. – Chief Engineer, KATCON.
e-mail: *robert.grzywnowicz@katcon.com*

Article citation info:
MITIANIEC, W. Combustion process of direct injected water-coal mixture in diesel engine. *Combustion Engines*. 2016, **164**(1), 37-43. ISSN 2300-9896.

Władysław MITIANIEC

PTNSS-2016-105

Combustion process of direct injected water-coal mixture in diesel engine

The paper describes the problem of coal-water mixture combustion process in heavy duty diesel engines in the energetic sector application. In the future due to depletion of crude oil resources we have to foreseen another fuel for application in power plants. Large deposits of coal and lignite in the world enable to utilize these fuels in different thermal machines, especially in internal combustion engines. A carbon powder containing small molecules about 10–20 micrometers dissolved in water is good fuel for applying in large capacity engines in electrical plants. Aqueous emulsion of coal has possibility of good cooling of injectors cooling and has also good lubricity. Initial experimental tests done in the world indicate a higher thermal efficiency of engine fuelled by water coal emulsion than engine fuelled by diesel oil and also gas turbine driven by gas from coal gasification technology. The increased emission of CO_2 can be reduced in the plants simply by chemical reduction. The paper explains thermochemical processes taking place in the engines during combustion process. The work parameters results obtained from calculations were compared with those obtained from CI engine fuelled by diesel oil. The paper is a certain challenge for finding a new fuel sources as a competition for crude oil and allows to get acquainted with new engine fuelling technology.

Key words: *transport, diesel engines, fuelling, water-coal emulsion, combustion*

1. Introduction

Numerous countries in the world are depended on petroleum in energetic sector and in order to be independent in the case of a crude oil crisis many works have been done on heavy duty diesel engines fuelled by coal or water-coal emulsion. The engines are mainly designated for production of electricity working at lower rotational speed (below 1000 rpm). The works done by General Electric on two cylinder test engine fuelled by micronized coal-water-slurry (CWS) with very small diameter of pulverized coal (d < 5 μm) was very successful, but the engine required a new injection system. An application of such engines is possible when a good fuel atomization with good penetration of coal molecules will be assured. The process should enable repeatability and durability of engine parts particularly of injectors. Many problems appear with applying of CWS concerning exploitation and wear of the engine parts. Due to predominant of coal atoms in the fuel such engines emit also higher amount of carbon dioxide to atmosphere in comparison to engines working on diesel oil at the same power. The main benefits is cheaper fuel and high enough caloric value of coal in comparison to gaseous fuels or alcohols. Coal occurring in large quantity in the world enables delivering of energy for centuries. For that reason research works should be done for preparation such engines working with coal-liquid emulsions and applying them in future. Several industrial applications were done in Australia at CSIRO [1, 2]. Also many research and theoretical studies were done with diesel engine fuelled directly by coal or by coal-water mixture [3–5]. Combustion process of CWS was considered by Mochalov et al. [6] and Redkina et al. [7]. The First stage of early work with coal fuel was led by Diesel and then by his co-worker Pawlikowski [8], with engines running for many years on dry solid fuels (dust firing) ranging from lignite to coke. A big study on fuelling of diesel engines with coal fuels was done by Wilson [9] and team for U.S. Department of Energy National Energy Technology Laboratory. By adding the water with fuel by injection into the combustion chamber we can decrease temperature of combustion process and thus decrease nitrogen oxides formation. Water evaporation process contributes to increasing of the charge mass in the cylinder, which influences on the change of indicated pressure.

Figure 1 presents possibility of applying of different sort driving systems in dependence of power and their influence on green gas emission (GGE). Nowadays the DICE are proposed in the range of power 0–200 MW. These heavy duty engines designated for energetic sector work with lower rotational speed. Their CO_2 emission is lower than for the system IGCC (integrated gasification combined cycle).

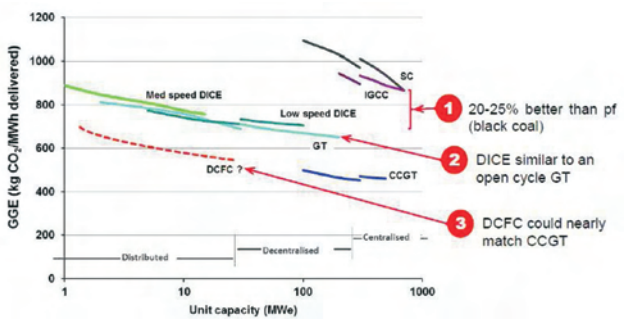

Fig. 1. Application of coal technologies in different thermal machines

The Australian research company CSIRO proposed a whole system of preparing coal-water mixture and injection system for DICE engine with respect to limitation of pollutants coming from combustion process. A proposed technological way for energy plants is shown in Fig. 2.

American company TIAX LLC tested two-cylinder engine with direct coal-water fuel (CWF) and presented many results of their work. In respect to injection system very important is injection timing. Figure 3 shows the period of CWF injection at maximum pressure 75 MPa and at 17% of engine load. The engine was equipped with two injectors (main and pilot). The main injection of CWS begins at 340 deg CA and finished at 376 deg CA.

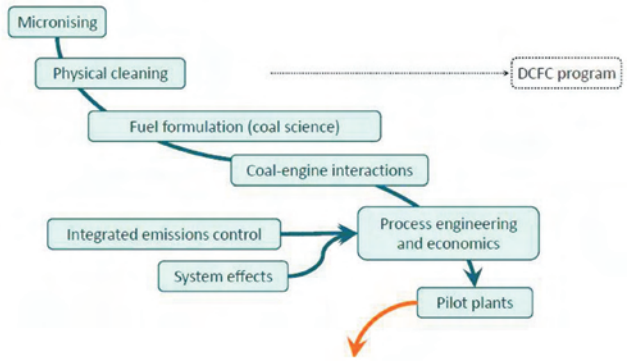

Fig. 2. CSIRO technology for DICEngines [2]

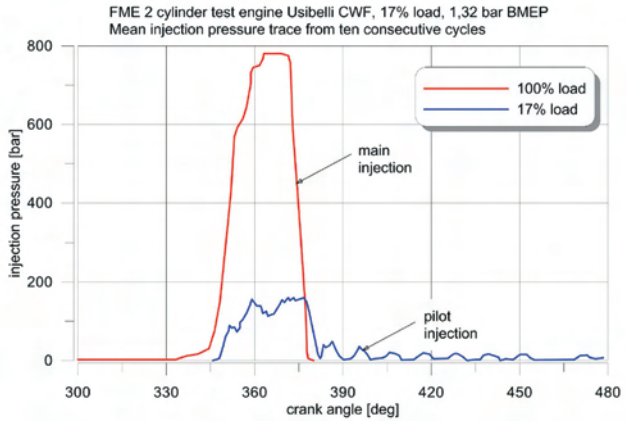

Fig. 3. Injection pressure trace for CWF in test engine [9]

2. Aim and scope of work

There are only few scientific works concerning the problem of coal-water slurry combustion in piston engines, however, many experimental tests were done in the world. Most of them were carried out in Australia and United States. The most important problem is finding dependencies between air fuel ratio and coal water ratio and variations of pressure and temperature of the charge during combustion process. One of the principal problems is determination of beginning of coal-water slurry injection and its duration as in classical diesel engines. The other task is determination of exhaust gas emission in dependence on water ratio in the slurry during injection process. The main task of the work is finding such dependencies and presentation of chosen results obtained from simulation process in CFD program. The work scope is limited to mathematical model of combustion of coal-water slurry and simulation of such process in diesel engine by using of CFD Ansys Fluent program. Naturally simulation of thermodynamic processes in piston engine requires applying of dynamic meshes caused by motion of the piston. The work shows also influences of controlling of water-coal ratio on temperature, pressure and mean indicated pressure in the cylinder. These dependencies were found by using 1-D simulation program written by the author.

3. Coal-water slurry combustion

Combustion of coal in piston engines differs from that in the boilers. The injected pulverized coal with water forms a mixture flowing into the cylinder through the injector nozzles. The nozzles should have higher diameter than for diesel oil. For that reason usually the DICE engines have higher cylinder capacity. The injection of the mixture occurs at high temperature of the compressed air. When a CWS drop gets in a hot combustion chamber there is immediate warm-up of the drop surface and water evaporation from the drop surface. Inside the drop there is gradual warming and as the temperature is increasing the moisture evaporates from the interior of the drop [6]. The process of water evaporation can be described by the following equation:

$$H_2O = \{H_2O\} \tag{1}$$

At high temperature, which still increases there is the process of thermal destruction (pyrolysis) of organic matter on the surface of CWS drop, accompanied by release of volatile substances. The molecules of coal quickly are destroyed and go into volatile as CO, CO_2, CH_4, H_2 and N_2, because bituminous coal and lignite contain those substances. The following equations describe the release of volatile substances:

$$CO + 0.5O_2 \rightarrow CO_2 \tag{2}$$

$$CH_4 + 2O_2 \rightarrow CO_2 + 2H_2O \tag{3}$$

$$H_2 + 0.5O_2 \rightarrow H_2O \tag{4}$$

Combustion of coal molecules in existence of water occurs in another way due to heat evaporation of water, which decreases gas temperature. Coal undergoes the gasification process and direct oxidation. The processes can be written as follows:

$$C + 0.5O_2 \rightarrow CO \tag{5}$$

$$C + H_2O \rightarrow CO + H_2 \tag{6}$$

$$C + O_2 \rightarrow CO_2 \tag{7}$$

Combustion of surfaces of coal molecules takes place together with water evaporation. The water injection is modelled by different approaches but the most often technique is uses the procedure of Taylor Analogy of Breakup [10] which was used in this work. On the other hand for water evaporation the Spalding model was used, which requires determination of Nusselt and Sherwood numbers. Evaporation is strictly dependent on temperature. Because the injection of water occurs near TDC when the charge temperature reaches value near 900 K and water droplets of small diameter very quick evaporate.

4. Pulverized coal particle combustion

Coal combustion can be calculated by taking into account a particle transport and eddy dissipation calculation for volatile gases contained in the coal particle. Two separate gases are considered in the calculation process: volatiles and char products that form during burning of carbon within the

particle. Volatiles can be only either a pure substance or can be a composition of many substances and for each substance a separate chemical reaction is considered. The combustion of the coal particle is a two stage process: the devolatilization of the raw particle of coal and oxidation of the residual char. The devolatilization and char oxidation processes occur very fast. The combustion process of coal-water slurry can be treated as normal combustion process of coal particle as mentioned above with taking into account water evaporation that decreases the charge temperature. Water vapours increase total mass of the gaseous charge. It was assumed that a coal particle consists of mass fraction of raw coal C_O, residual char after devolatilization C_{har} and ash C_A.

Devolatilization was described by Badzioch and Hawksley [11] in a single reaction model:

$$\frac{dC_O}{dt} = -k_v C_O \tag{8}$$

The rate of volatiles production in the gas phase is defined by:

$$\frac{dV}{dt} = Y k_v C_O \tag{9}$$

where: Y – actual yield of volatiles.

The rate of char formation is given by following formula:

$$\frac{dC_{char}}{dt} = (1 - Y) k_v C_O \tag{10}$$

The rate constant in Arrhenius form is obtained from formula:

$$k_v = A_v \exp\left(-\frac{E_v}{R T_p}\right) \tag{11}$$

where: T_p – temperature of coal particles, K, R – gas constant, J/(kmol K), A_v – kinetic reaction constant (from experiment), E_v – activation energy (from experiment), J/kmol.

Coal particle swells due to release of the gas during the devolatilization process. It was assumed that diameter of the coal particle changes in proportion to the volatiles released. After complete devolatilization the particle has increased diameter and this value is an input for burning of the char. The change of the particle diameter during devolatilization is calculated from the relation:

$$\frac{d}{dt} d_p = C_s d_{0,p} \frac{\dot{m}_{ref}}{m_{ref,0}} \tag{12}$$

where: d_p – current particle diameter, m, C_s – swelling coefficient, $d_{0,p}$ – particle diameter at the start of devolitalization, m, $\dot{m}_{ref}$ – rate of mass change of the reference material, $m_{ref,0}$ – mass of the reference material at the start of devolatilization.

5. Simulation of coal-water slurry combustion in diesel engine

Direct injection of coal-water slurry in CFD is defined as multiphase flow, because there is one gaseous phase consisting with many simple gases such as oxygen, nitrogen, carbon dioxide and water vapours. On the other hand the injection of micronized refine coal as a solid fuel (second phase) and water in the liquid form (third phase) determines evaporation of water, diffusion and volatilization of coal. Interaction between three phases can be solved by CFD computer program with taking into account dynamic motion of the piston (dynamic meshing). The author applied Ansys-Fluent program [12] for determination of thermodynamic parameters of the diesel engine with direct coal-water slurry (CWS). In the simulation of combustion process the simple geometry of engine was used. Main engine parameters are given in Table 1.

Table 1. Main geometrical parameters

Parameter	Value
Cylinder diameter	79.5 mm
Stroke	94.2 mm
Compression ratio	15.5
Engine rotational speed speed	1000 rpm

The mesh of engine model contains 85920 hexahedral cells at BDC. The amount of cells decreases during piston motion by applying of layering method in dynamic mesh option. Simulation of injection and combustion processes in naturally aspirated DICE engine with vertical and central position of the injector was carried out at following assumptions:

– start of injection CWS – 330 deg CA,
– duration of injection – 30 deg CA,
– amount of injector nozzles – 4,
– coal mass rate in each nozzle – 0.007 kg/s,
– water mass rate in each nozzle – 0.005 kg/s,
– diameter of pulverized coal – 5 μm.

Heat exchange between gas and cylinder walls was modelled by assumption of real values of walls temperature. Combustion process of coal takes place when it is a volatile form and then the kinetic chemical reaction has the following form:

$$C_{vol} + O_2 \rightarrow CO_2 \tag{13}$$

The precise combustion model will be published in future. Gasification process of coal occurs in high temperature (endothermic reaction between coal and water). The coal with high volatile species described as C_{vol} from Fluent library was taking for calculations. It was assumed the following oxidation reaction of coal with high amount of volatile gases:

$$C_{vol} + 1.598O_2 \rightarrow CO_2 + 1.417H_2O \tag{14}$$

From this equation results that C_{vol} contains 0.654 of C, 0.192 of O_2 and 0.154 of H_2. The rate constant and activation energy in Arrhenius kinetic form was assumed as follows:
– A_v = 2.119e+11
– E_v = 2.027e+8 J/kmol

The charge was treated as ideal gas containing the following species: oxygen, nitrogen, carbon dioxide, water (vapours) and coal volatiles after devolatilization. The calculation model took into account also the injection process of coal-water slurry through the injector with four symmetrical nozzles. It was assumed that the injection of water took place in the same time as injection of the coal at the same nozzle. The injection parameters of the coal-water slurry are presented in Table 2 for engine rotational speed equal 1000 rpm.

Table 2. Injection parameters of coal-water slurry

Parameter	Value
Start of injection BTDC	20 deg CA
End of injection ATDC	5 deg CA
Number of nozzles	4
Coal mass flow rate	0.005 kg/s
Water mass flow rate	0.003 kg/s
Temperature of slurry	310 K
Location of the injector	cylinder centre
Initial slurry velocity	140 m/s

6. Results of simulation

Coal injection parameters determine an excess air ration in the cylinder. During injection process the coal molecules transfer into volatile form due to high temperature and small diameter. Technical problems of CWS were not considered (flow through the nozzles). Engine work is assesses on the base of pressure course in the cylinder. In DICE engine at assumed injection parameters maximum of pressure reaches value 120 bars at 7 deg CA ATDC (Fig. 4). Such high pressure induces also a high mean indicated pressure. Simulation of engine work was carried out at air excess ratio λ = 1.5.

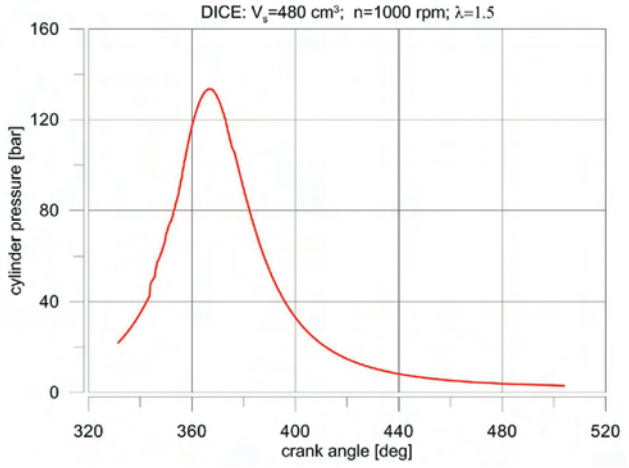

Fig. 4. Cylinder pressure trace

Temperature inside the cylinder is not so high in comparison to engine fuelled by diesel oil. Figure 5 shows course of mean temperature during compression combustion and expansion processes. The initial period of coal combustion characterizes fluctuation of temperature due to coal volatilization and water evaporation, which decreases temperature. Highest mean temperature reaches value 1500 K at 12 deg CA ATDC.

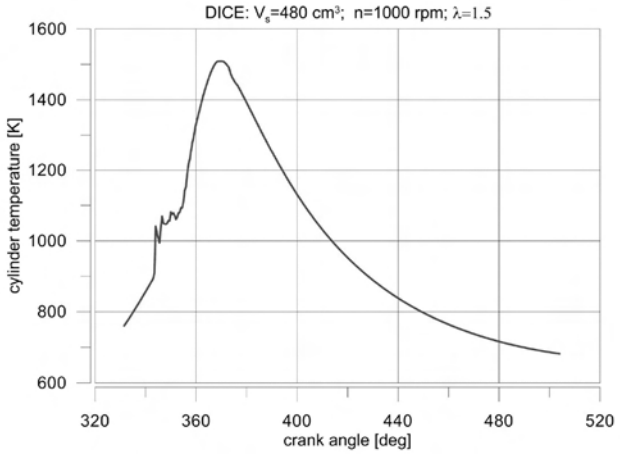

Fig. 5. Course of mean cylinder temperature

Combustion process of the coal injected together with water is observed by an increase of carbon dioxide. Figure 6 presents the change of CO_2 mass fraction. Beginning of fuel combustion occurs already at 13 deg CA BTDC and for assumed air excess ratio λ = 1.5 the maximum of CO_2 mass fraction reaches value about 0.1. It should be indicated that total charge mass of gas increases in respect to water evaporation.

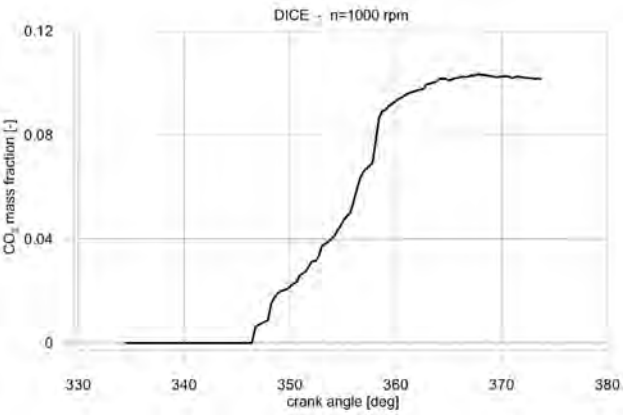

Fig. 6. Variation of mass fraction of carbon dioxide during combustion process

Temperature of the charge during combustion process of water-coal mixture is lower than in the case of burning of diesel oil in the same self-ignition engine. It is caused mainly by water evaporation, when the gas transfers the heat to the water droplets. The lower gas temperature during burning of the coal influences on lower value of mass fraction of nitrogen oxides, particularly on NO. It is confirmed by CFD

simulation and Fig. 6 shows very small value of NO mass fraction below 60 ppm, where in classical diesel engine NO_x molar fraction reaches value even 3000 ppm without the catalytic converter.

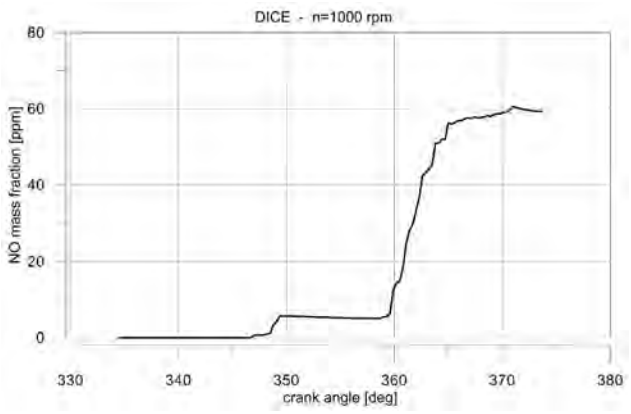

Fig. 7. Variation of mass fraction of nitrogen oxide during combustion process

The simulation of water-coal mixture in diesel engine gives many thermodynamic data, but only a few can be presented in the paper. The most essential factor is start of burning of the fuel, when kinetic reactions occur. In this case only one kinetic reaction of burning of the coal with high amount of volatile components (see eq. 7) was considered. The computer program calculates combustion reaction rate every adaptive calculation step (lower than 0.3 deg CA). The burning of fuel begins on the outer side of the injection streams, where is better contact with oxygen. Figure 8 presents contours of reaction rate (kmol/(m^3 s)) at 13 deg CA BTDC. Maximum of this parameter reaches value 0.0687 kmol/(m^3 s). Unsymmetrical development of the flame is caused by swirl of the charge. Because of evaporation of the injected water droplets the temperature inside the water-coal stream decreases significantly and is about 300 K lower than that on the outside of the slurry stream (Fig. 9). Temperature of the gas amounts about 1000 K and is enough high for beginning of burning of the coal and evaporation of water.

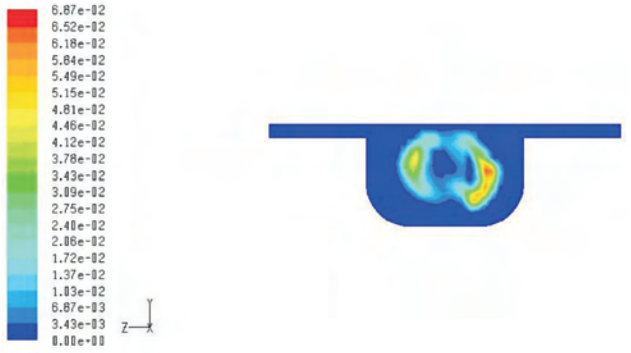

Fig. 8. Contours of combustion reaction rate [kmol/(m^3 s)] at 13 deg CA BTDC

After full injection of water-coal mixture almost whole fuel is burned and temperature of the charge in the piston cavity differs slightly. Contours of temperature at piston position 18 deg CA ATDC are shown in Fig. 10. The highest temperature value is reached on bottom of the piston because there are gathered a lot of carbon particles. Outside of the squish volume temperature of the gas is smallest.

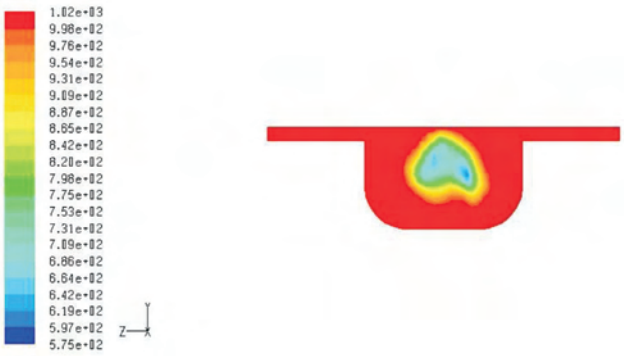

Fig. 9. Contours of temperature [K] at 13 deg CA BTDC

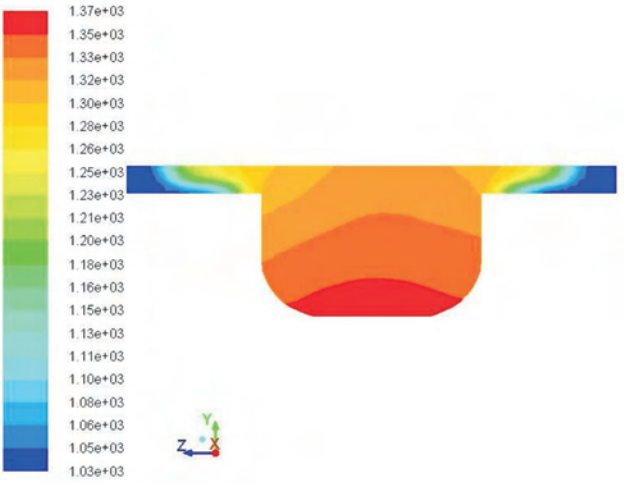

Fig. 10. Contours of temperature [K] at 18 deg CA ATDC

The end of the combustion process has lower activity, which is shown in Fig. 11 at piston position 18 deg CA ATDC. In comparison to reaction rate at piston position 13 deg CA BTDC (Fig. 8) in this case this parameter is many

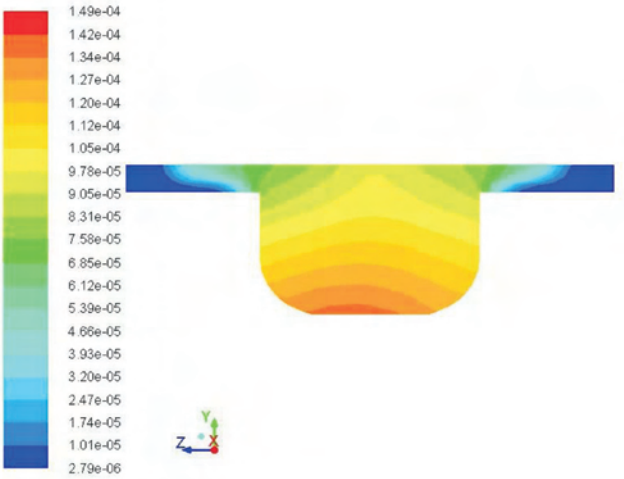

Fig. 11. Kinetic reaction rate [kmol/(m^3 s)] at 18 deg CA ATDC

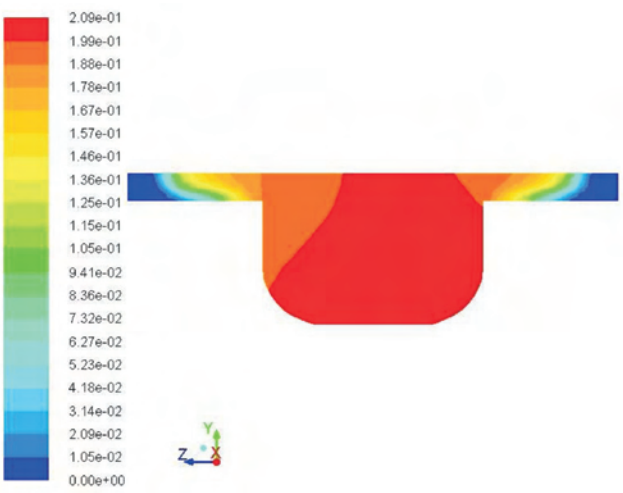

Fig. 12. Contours of mass fraction of CO_2 at 18 deg CA ATDC

times smaller, but still chemical reactions occurred on bottom of the cavity. This phenomenon influences on almost uniform distribution of carbon dioxide in the piston cavity, which was presented in Fig. 12. Mass fraction of CO_2 in the piston cavity reaches value 0.20 which indicates a complete coal oxidation. Like in diesel oil engine the combustion process does not occur in the squish region.

7. Water dose and engine parameters

Injection of coal particles together with water at high pressure influences on pressure and temperature traces in the diesel engine cylinder. It was developed the 0-D mathematical model for calculations of thermodynamic parameters in diesel engine with direct water-coal mixture. The computer simulation program was prepared which was based on this model with taking into account non-steady gas flow in the ducts and pipes. This complex model and computer program are outside of the scope of this paper. After the adoption of different values of water dose in the range of 0 to 0.015 g/cycle for the same engine geometry as in CFD simulation, many thermodynamic parameters were achieved such as pressure, temperature, indicated pressure, fuel consumption, engine efficiency etc. The most important is the change of pressure and temperature in the cylinder. Figure 13 presents the change of pressure in the engine with different water doses per one work cycle. The increase of water dose influences on decreasing of maximum of pressure a few percent, but in particular it should be noted a significant reduction of pressure before TDC. This phenomenon affects on reducing of negative work during compression stroke. Less negative work gives a higher total work and obviously higher engine power. Simulations were carried out for the same rotational speed 1000 rpm.

Evaporation of more water in the cylinder requires delivering of higher amount of heat from the gaseous charge. It was assumed that whole evaporation process takes place during combustion process and specific evaporation heat of water amounts 2263 kJ/kg. For the coal with high volatile species which has to be enriched the caloric value was assumed with value 28 MJ/kg. At such conditions one achieves a variation of temperature of the charge in the range of whole engine working cycle. Figure 14 presents curves of temperature for four different water doses per one cycle. Diesel engine working without adding the water indicates maximum of temperature about 2100 K, but adding small dose of water equal 0.005 g/cycle causes decreasing this parameter to value 1650 K. By increase of water dose to 0.015 g/cycle there is a reduction of temperature to value 1050 K.

By adding higher amount of water in the injected slurry the mass of the charge increases because the water vapours come into the gaseous charge.

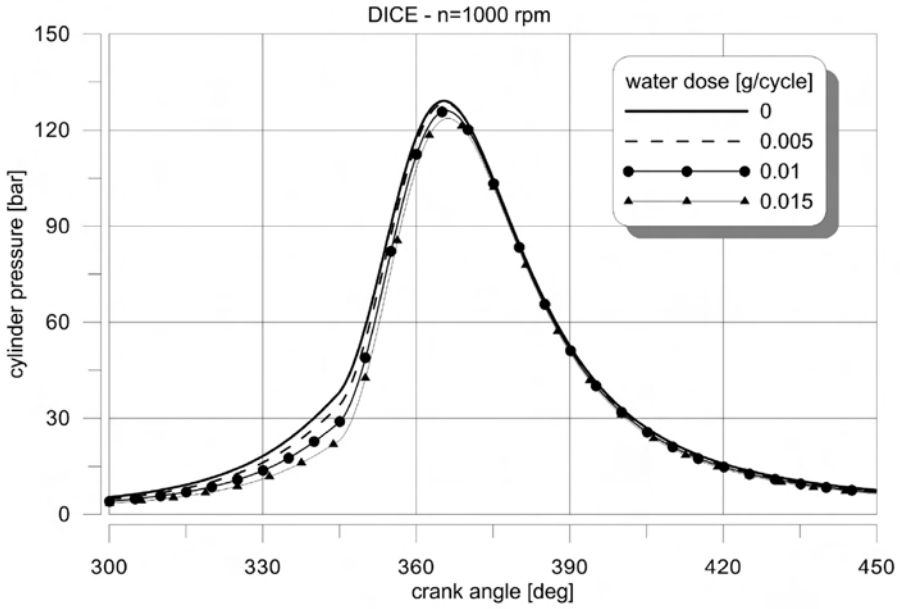

Fig. 13. Variation of cylinder pressure for different water doses at 1000 rpm with constant coal dose

8. Summary

Review of till now designed engine with direct coal-water slurry injection system and own input in a form of simulation results give certain remarks:

1. Heavy duty diesel engines with MRC (Micronised Refined Coal) injection system are designated for energetic plants. They enable efficient work with higher efficiency than diesel engine fuelled by diesel oil.
2. Combustion of coal takes place together with water evaporation and at high temperature a gasification process is observed.

3. Combustion of CWS in diesel engine is more efficient and ecologic (lower GGE) than for other energetic thermal machines (steam and gas turbine).
4. In the era of future fuel crisis replacement of diesel oil by coal fuel is a promising solution due to large coal deposits in the world.
5. The pressure and temperature of the charge in diesel engine fuelled by water-coal slurry is dependent on water dose per cycle. Higher water-coal ratio decreases the negative engine work and thus obtaining a higher value of total work.
6. The CWS diesel engine should be equipped with new resistive on corrosion and friction injection system and valve system.
7. Fuel injection process should be optimized in respect to obtaining maximum of pressure and temperature as in classical diesel engine.
8. Simulation process carried out at rotational speed 1000 rpm and start of injection process at 20 deg CA BTDC indicated that whole injected coal mass is fully burned. Emission of NO_x is quite low in comparison to the classic diesel engine.
9. Combustion process begins in the fuel jet shortly after beginning of fuel injection. From exploitation point of view the proportion of carbon mass to liquid water mass should be higher as possible but enough for lubrication of injector.

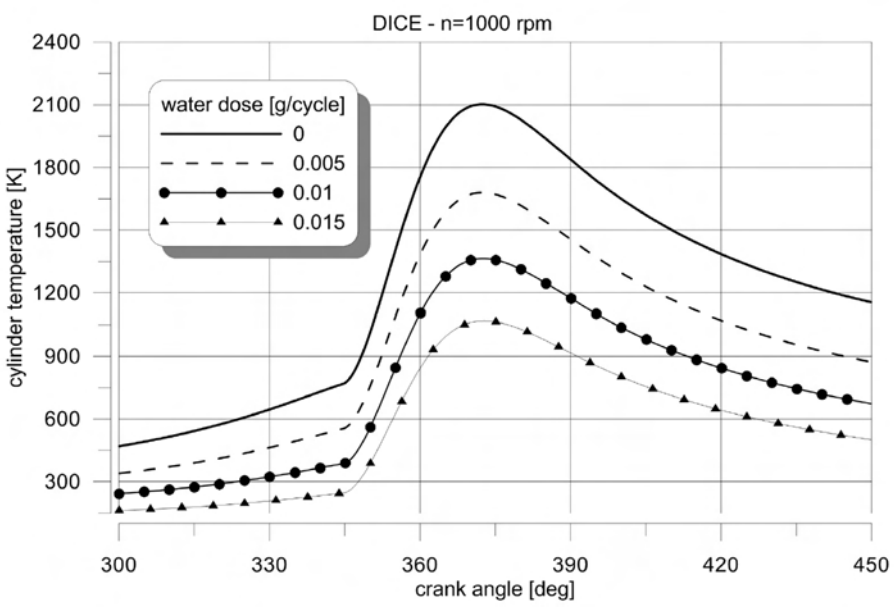

Fig. 14. Variation of cylinder temperature for different water doses at 1000 rpm with constant coal dose

References

[1] Wibberley L. J. DICE-the best option for coal? DICEnet, www.dice-net.org, May 2014.
[2] Wibberley L. J. MRC-DICE – a game changer for electricity generation, CSIRO Energy Technology, APEC EGCFE, 22 Feb. 2012.
[3] Caton J.A., RosegayK. H. A Review and Comparison of Reciprocating Engine Operation Using Solid Fuels, SAE Transactions, SAE Paper 831362, Vol. 92, 1984.
[4] Nelson L.P., Seeker W.R., Zimperman R.A. The Atomization, Ignition and Combustion Characteristics of Coal Slurry Fuels in Medium-Speed Diesel Engines, Joint Central and Western States Sections, Combustion Institute, Paper No 3-1A, April 1985.
[5] Kalpesh V., Shyam D. Review of charcoal-diesel slurry: an alternative fuel for compression ignition engine, International Journal of Advanced Engineering Research and Studies, E-ISSN2249–8974, IJAERS/Vol. I/ Issue III, pp. 143-147, April-June, 2012.
[6] Mochalov S.P., Rybenko I.A., Ermakowa L.A. Mechanism and Mathematical Modeling of Coal-Water Slurry Combustion in Swirl Adiabatic Combustion Chamber, World Applied Sciences Journal 19 (1): 20-25, 2012.
[7] Redkina N. I., Khodakov G. S., Gorlov E. G.: Coal Fuel Slurry for Internal Combustion Engines, Solid Fuel Chemistry, 2013, Vol. 47, No. 5, pp. 306–314. © Allerton Press, Inc., 2013.
[8] Used of powdered Fuel in the Diesel Engines, Power House, Vol. XIII, London, 5.02.1929.
[9] Wilson R. Clean Coal Diesel Demonstration Project, Final report DE-FC21-94MC31260, TIAX LLC Acorn Park Cambridge, Massachusetts, USA, March 2007.
[10] Han Z., Fan L., Reitz R.D., Multidimensional Modeling of Spray Atomization and Air-Fuel Mixing in a Direct Injection Spark Ignition Engine, SAE Paper 970884, SAE International Congress & Exposition, Detroit, 1997.
[11] Badzioch S., Hawksley P.G.W., Kinetics of Thermal Decomposition of Pulverized Coal Particle, Ind. Eng. Chem 9, 521, 1970.
[12] Ansys Fluent Theory Guide, Release 13, Canonsburg, PA, USA, 2010.

Władysław Mitianiec, DSc., DEng. – Professor of Cracow University of Technology in the Faculty of Mechanical Engineering at CUT, Poland.
e-mail: *wmitanie@usk.pk.edu.pl*

Article citation info:
ŻMUDKA, Z., POSTRZEDNIK, S., PRZYBYŁA, G. Throttleless control of SI engine load by fully flexible inlet valve actuation system. *Combustion Engines*. 2016, **164**(1), 44-48. ISSN 2300-9896.

Zbigniew ŻMUDKA
Stefan POSTRZEDNIK
Grzegorz PRZYBYŁA

PTNSS-2016-106

Throttleless control of SI engine load by fully flexible inlet valve actuation system

A system with independent, early inlet valve closure (EIVC) has been analysed. The open, theoretical cycle has been assumed as a model of processes proceeding in the engine with variable inlet valve actuation. The system has been analysed individually and comparatively with open Seiliger-Sabathe cycle which is theoretical cycle for the classic throttle governing of engine load. The influence of EIVC on fuel economy, cycle work, relative charge exchange work and cycle efficiency has been theoretically investigated. The use of the analysed system to governing of an engine load will enable to eliminate a throttling valve from inlet system and reduce the charge exchange work, especially within the range of partial load. The decrease of the charge exchange work leads to an increase of the internal and effective works, which results in an increase of the effective efficiency of the spark ignition engine.

Key words: *spark-ignition engine, variable valve actuation, early inlet valve closure, theoretical cycle, charge exchange process, cycle efficiency*

1. Introduction

Realization of a charge exchange process in a combustion engine requires surmounting flow resistances in inlet and exhaust systems so execution of an adequate work co-called the charge exchange work. A charge exchange system have an essential impact on effectiveness of the engine work. Each element installed in the charge exchange system generates flow resistance of a fresh charge in a intake system and combustion products in a exhaust system. These resistances bring about an increase of the charge exchange work which contributes to a decrease of the internal and the effective work of an engine. Increase of the charge exchange work for partial load in the spark-ignition engine is connected with a method of load control. Quantity governing with the aid of a throttle, installed in an intake system, is disadvantageous especially from thermodynamic point of view because throttling generates exergy losses [1].

Increasing the energy efficiency of an internal combustion engine with spark ignition is possible by eliminating the throttle. This may be accomplished by using fully independent control of intake or/and exhaust valves [3–5]. The most flexible solution for independent control of the valves is to use electromagnetic actuators but they are still under construction and are not in mass production because of electro-mechanical problems [6, 7]. However, currently the most advanced solution is an electro-hydraulic system [8–10].

Fully independent valve drive enables engine load control according to different, the following strategies [2, 3]
– late inlet valve closure (the open Atkinson-Miller cycle) [4, 11–13],
– early inlet valve closure [5],
– early exhaust valve closure ,
– fully-independent both valves control.

The system with early exhaust valve closure also allows the implementation of internal exhaust gas recirculation.

Variable valve train system also allows the realization of engine operation with low inlet valve lift at partial load. The impact of the low inlet valve lift on fuel consumption and other parameters of the gasoline engine was studied by Begg et al. [14] and Clenci et al. [15].

The use of early inlet valve closure (EIVC) in the diesel engine was investigated by Zammit et al. [16]. They studied the influence of EIVC on emissions, fuel economy and exhaust gas temperature of a turbocharged, 4 cylinder common rail direct injection diesel engine. At all conditions, the effect of EIVC on fuel economy was negligible or a fuel economy penalty.

Benefits in terms of fuel economy resulting from the application of EIVC in the SI engine are significant especially under light load operating conditions because EIVC eliminates throttle from an intake system which reduces the charge exchange work.

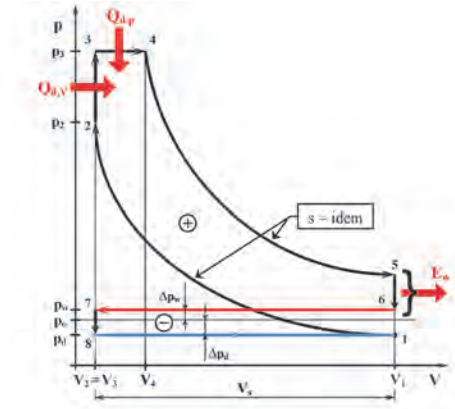

Fig. 1. Open Seiliger-Sabathe cycle, i.e. ideal cycle taking resistances in the inlet and exhaust systems into consideration

In the present study, the use of the independent inlet valve actuation has been proposed in order to increase of efficiency of the open, ideal cycle and effective efficiency of the spark-ignition engine [2]. Theoretical research of the system with early inlet valve closure (EIVC) has been carried out. The open Seiliger-Sabathe cycle (presented in Fig. 1) is the reference cycle for an assessment of advantages and effectiveness of work gaining in consequence of application of the early inlet valve closure [4, 5].

2. The system with early inlet valve closure

2.1. Basic characteristics of the cycle

The open, theoretical cycle, presented in Fig. 2, has been assumed as the model of the processes proceeding in an engine with early inlet valve closure. The open cycle has been obtained by modification of the ideal cycle by addition of the processes characterizing the charge exchange.

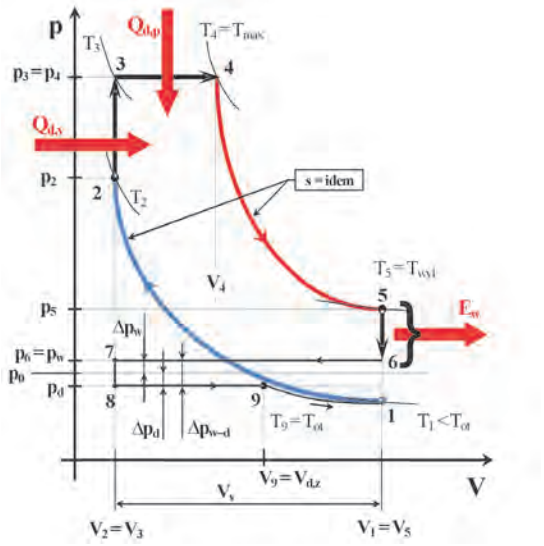

Fig. 2. The open, theoretical cycle of the system with early inlet valve closure

The volume V_9 ($V_{d,z}$) of a cylinder, at which an inlet valve closure occurs during filling stroke, is the control parameter of a load (the filling). Simultaneously, this is parameter adjusting the mass of a fresh air-fuel mixture fed into a cylinder. The volume $V_{d,z}$ can be expressed in relation to the minimum volume of the cylinder:

$$\varepsilon_d = \frac{V_{d,z}}{V_2}, \qquad 1 < \varepsilon_d \le \varepsilon \tag{1}$$

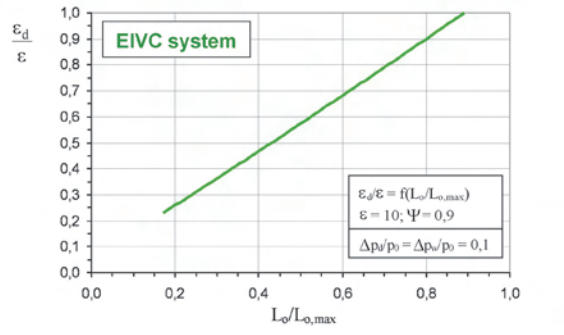

Fig. 3. Control parameter $\varepsilon_d/\varepsilon$ of the EIVC cycle versus cycle work

The relative values of the control parameter ε_d (in relation to the total compression ratio ε) depending on the cycle work are presented in Fig. 3. Near-linear interdependence between the control parameter and the cycle work is favourable in respect of load governing.

The pressure drop Δp_w determines the flow resistance in the exhaust system and the pressure drop Δp_d determines the flow resistances in the intake system. In the cycle analysis, the assumption was made that the filling process finishes in the point „9" at (Fig. 2):

the volume $V_{d,z} \equiv V_9 \le V_1$, the pressure $p_d = p_0 - \Delta p_d$ and the temperature $T_9 = T_0$.

2.2. Fuel dose

The maximum mass m_0 of the fresh charge is fed into a cylinder when intake valve closing occurs at bottom death centre, then:

$$V_{d,z} = V_1, \text{ that is } \varepsilon_d = \varepsilon,$$

and for simultaneous absence of the flow resistance in the inlet and exhaust systems:

$$\Delta p_w = 0, \Delta p_d = 0, \text{ then } p_9 = p_1 = p_0.$$

The maximum mass of the fresh mixture can be described by the formula [2, 3]:

$$m_0 = \frac{p_0 V_1}{(MR) T_0} M_m, \quad p_0 \approx p_{ot}, \quad T_0 \approx T_{ot} \tag{2}$$

where: M_m – molar mass of the fresh mixture.

For the made assumptions, the basic fuel dose amounts to:

$$m_{p,0} = \frac{p_0 V_1}{(MR) T_0} \frac{M_m}{[1 + \lambda_0 n'_{a,min} M_a (1 + X_a)]}. \tag{3}$$

The fuel dose m_p depends on an engine load. The basic parameters influencing the fuel dose are the following:

$V_{d,z}$ – cylinder volume at the moment of the inlet valve closure,

T_0 – temperature of the fresh charge,

Δp_d – pressure drop in the inlet system, during filling,

Λ – excess air ratio.

For partial load, the cylinder volume $V_{d,z}$ ranges:

$$V_2 < V_{d,z} \le V_1 \text{ hence } 1 < \varepsilon_d \le \varepsilon$$

The flow resistances in the inlet and exhaust systems are taken into consideration:

$$\Delta p_w \ge 0 \text{ and } \Delta p_d \ge 0 \text{ so } p_d \le p0$$

and an assumption is made that the temperature of the fresh charge is equal to the ambient temperature T_0. Then, the fuel mass m_p amounts to:

$$m_p = \frac{p_d V_{d,z}}{(MR) T_0} \frac{M_m}{[1 + \lambda n'_{a,min} M_a (1 + X_a)]} \tag{4}$$

Relative fuel dose for the partial loads of an engine results from the formulas (3) and (4). For the assumption that λ = idem, the following relation is obtained:

$$m_p = m_{p,0} \frac{p_d V_{d,z}}{p_0 V_1} \tag{5}$$

that can also be noted as:

$$m_p = m_{p,0}\left(1-\frac{\Delta p_d}{p_0}\right)\frac{\varepsilon_d}{\varepsilon} \qquad (6)$$

Change of the engine load is achieved by the change of the fuel dose m_p and the ratio ε_d is the principal control parameter. The relative fuel dose $m_p/m_{p,0}$ depending on the cycle work for the EIVC cycle is presented in Fig. 4.

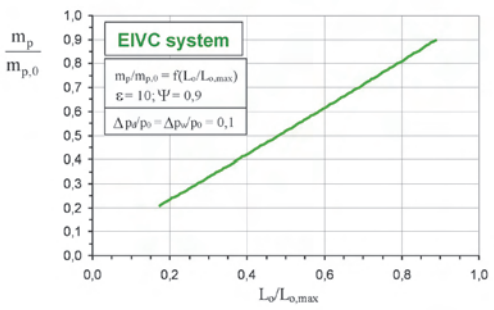

Fig. 4. Relative fuel dose $m_p/m_{p,0}$ versus work for the EIVC system

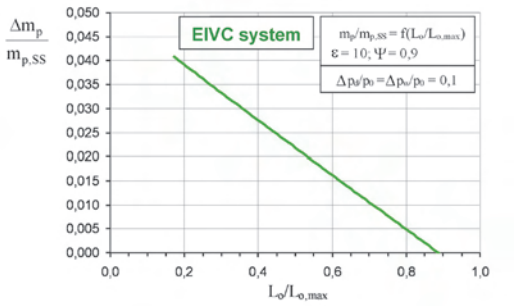

Fig. 5. Relative reduction of the fuel dose for the EIVC cycle compared to the open Seiliger-Sabathe cycle

Relative reduction of the fuel dose $\Delta m_p/m_{p,SS}$ for the EIVC system, in comparison with the system with the classic, throttle governing (the open Seiliger-Sabathe cycle) is illustrated in Fig. 5. Using the EIVC system results in the fuel economy of up to about 4% for the lowest value of the cycle work (engine load).

2.3. Work of the cycle

The work of the EIVC cycle (Fig. 2) can be expressed as the sum of the absolute works of the individual processes:

$$L_o = L_{1\text{-}2} + L_{2\text{-}3} + L_{3\text{-}4} + L_{4\text{-}5} + L_{5\text{-}6} + L_{6\text{-}7} + L_{7\text{-}8} + L_{8\text{-}9} + L_{9\text{-}1} \qquad (7)$$

Substituting relations expressing the absolute works of the individual processes to the equation (7) the relative cycle work is obtained:

$$\frac{L_o}{p_0 V_1} = \frac{1}{\kappa-1}\left\{\gamma\varphi\left[\varepsilon^{(\kappa-1)} - \varphi^{(\kappa-1)}\right] + \left(\frac{\varepsilon}{\varepsilon_d}\right)^{(\kappa-1)} - \varepsilon^{(\kappa-1)}\right\} + \varepsilon^{(\kappa-1)}\gamma(\varphi-1) + \left(\frac{\varepsilon}{\varepsilon_d}\right)^{\kappa}\left[\frac{\varepsilon_d-1}{\varepsilon} - \frac{1+\dfrac{\Delta p_w}{p_0}}{1-\dfrac{\Delta p_d}{p_0}}\left(\frac{\varepsilon-1}{\varepsilon}\right)\right] \qquad (8)$$

where γ and φ are the load parameters: $\gamma = \dfrac{p_3}{p_2}$, $\varphi = \dfrac{V_4}{V_3}$.

The specific work $L_o/(p_0V_1)$ of the EIVC cycle versus control parameter $\varepsilon_d/\varepsilon$ is presented in Fig. 6 and the cycle work in relation to the maximum work of the ideal Seiliger-Sabathe cycle is illustrated in Fig. 7. Characteristic curves in the both figures are near-linear which is beneficial for governing reasons.

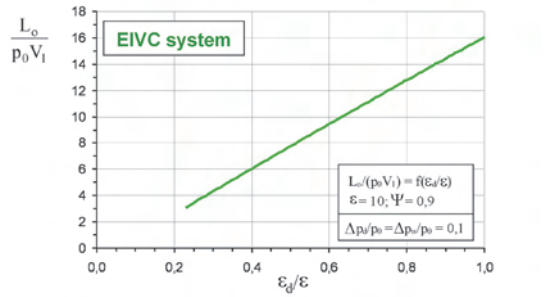

Fig. 6. Specific work $L_o/(p_0V_1)$ of the EIVC cycle versus control parameter $\varepsilon_d/\varepsilon$

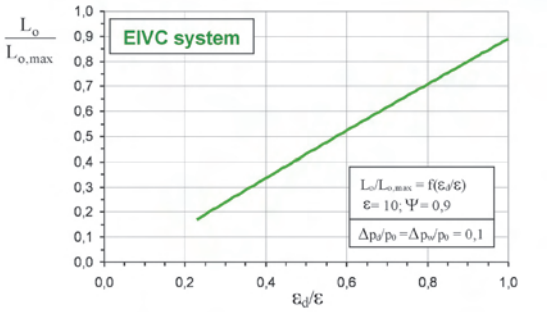

Fig. 7. Ratio of work of the EIVC cycle to the maximal work of the Seiliger-Sabathe cycle versus control parameter $\varepsilon_d/\varepsilon$

2.4. Charge exchange work

The charge exchange work L_w of the EIVC cycle (Fig. 2) can be expressed as the sum of the useful works of the individual processes:

$$L_w = L_{u,6\text{-}7} + L_{u,7\text{-}8} + L_{u,8\text{-}9} \qquad (9)$$

Then specific charge exchange work L_w in relation to the product (p_1V_1) is obtained

$$\frac{L_w}{p_1 V_1} = -\frac{\dfrac{\Delta p_w}{p_0}(\varepsilon-1) + \dfrac{\Delta p_d}{p_0}(\varepsilon_d-1)}{\varepsilon\left(1-\dfrac{\Delta p_d}{p_0}\right)}\left(\frac{\varepsilon}{\varepsilon_d}\right)^{\kappa} \qquad (10)$$

The index μ of the relative charge exchange work is calculated by definition:

$$\mu = \frac{|L_w|}{L_o}, \qquad (11)$$

as a ratio of the charge exchange work (10) to the cycle work (8).

The theoretical Seiliger-Sabathe cycle with classic throttle governing of the SI engine load is the reference cycle for assessing the benefits of using the system with early inlet valve closure. Therefore for comparison, characteristics of

the specific charge exchange work $L_w/(p_0V_1)$ and the relative charge exchange work μ both for the open Seiliger-Sabathe cycle and EIVC cycle are presented in Figs 8 and 9. These works for EIVC cycle are much smaller in the entire load range except for full load.

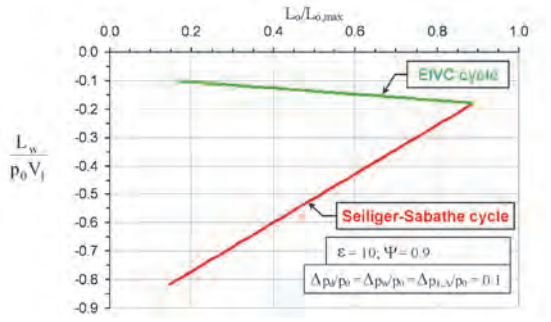

Fig. 8. Comparison of the specific charge exchange works $L_w/(p_0V_1)$ for the EIVC cycle and Seiliger-Sabathe cycle versus work of the cycle

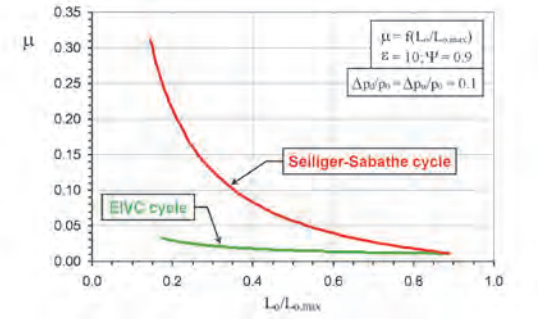

Fig. 9. Comparison of the relative charge exchange works μ for the EIVC cycle and Seiliger-Sabathe cycle versus work of the cycle

An important advantage of the EIVC system is reduction of the absolute value of the charge exchange work with the decrease of the engine load. For this reason, the relative charge exchange work μ for the EIVC system does not reach significant values (Fig. 9). Its maximum value does not exceed 3.5% for the lowest load. The reverse, unfavorable situation is observed for Seiliger-Sabathe cycle – the absolute value of the charge exchange work significantly increases with a decrease of the load and the value of the relative charge exchange work exceeds 30%.

2.5. Efficiency of the cycle

Efficiency of an ideal cycle is defined as a ratio of the cycle work L_o to the supplied heat Q_d:

$$\eta_o = \frac{L_o}{Q_d}, \tag{12}$$

which can also be formulated using the relative quantities:

$$\eta_o = \frac{\frac{L_o}{p_{1,A}V_{1,A}}}{\frac{Q_d}{p_{1,A}V_{1,A}}} = \frac{\frac{L_o}{p_{1,A}V_{1,A}}}{E_0} \tag{13}$$

Next, inserting the energy-stoichiometric parameter E_0 [2, 3] and (9) to (13), the following formula is obtained:

$$\eta_o = \frac{\kappa-1}{\varepsilon_A^{(\kappa-1)}\left[\gamma-1+\kappa\gamma(\varphi-1)\right]}\left\{-\frac{\varepsilon_A^{(\kappa-1)}-1}{\kappa-1}+\gamma(\varphi-1)\varepsilon+\frac{\gamma\varphi}{\kappa-1}\left(\frac{\varepsilon_A}{\varepsilon}\right)^{(\kappa-1)}\left[\varepsilon^{(\kappa-1)}-\right.\right.$$
$$\left.\left.-\left(\frac{\frac{\Delta p_d}{p_0}+\frac{\Delta p_w}{p_0}}{1+\frac{\Delta p_{1,A}}{p_0}}\right)\left(\frac{\varepsilon-1}{\varepsilon_A}\right)\right. \tag{14}$$

The efficiency η_o is significant parameter which enables assessment of the cycle in the energy aspect. Comparison of the cycle efficiencies for the system with early inlet valve closure and the open Seiliger-Sabathe cycle depending on the cycle works is presented in Fig. 10.

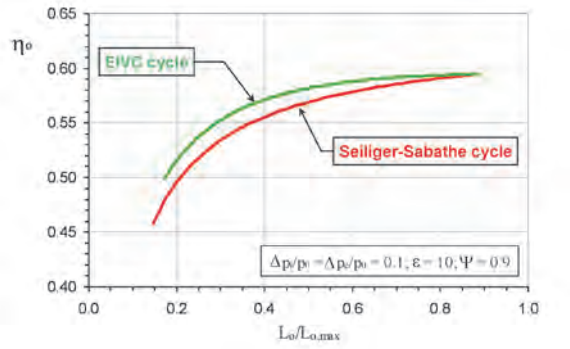

Fig. 10. Comparison of the efficiencies ηo of the EIVC cycle and Seiliger-Sabathe cycle versus work of the cycle

The energy efficiency of the EIVC cycle is higher by 2 percentage points than the efficiency of the open Seiliger-Sabathe cycle almost in the entire load range.

3. Conclusion

The theoretical research on the system with independent, early inlet valve closure has been conducted. The open, ideal cycle has been assumed as a model of the processes proceeding in a combustion engine working according to the analysed system. The theoretical Seiliger-Sabathe cycle with classic throttle governing of an engine load is the reference cycle for evaluation of benefits and the work effectiveness of EIVC. The effects of use of the investigated system can be expressed best of all by the energy efficiency of the cycle. At all conditions except full load, this efficiency for EIVC is higher than the Seiliger-Sabathe cycle. The consequence of increased efficiency is reduction of fuel consumption. Fuel economy can reach up to 4% under light load operating conditions. These benefits are due to a significant reduction in the charge exchange work because early inlet valve closure allows the elimination of the throttle from intake system of SI engine. Thus, the SI engine load control by EIVC strategy gives the desired effects.

Investigations on variable valve actuation are conducted by many scientific as well as research and development centres. This testifies topicality of the presented problems.

Acknowledgements

This scientific work was supported by Faculty of Power and Environmental Engineering of the Silesian University of Technology within the statutory research.

Nomenclature

E_0 – energy-stoichiometric parameter
E_w – waste energy, J
EIVC – early inlet valve closure
L_o – cycle work, J
M – molecular weight, kg/kmol
$m_{p,0}$ – basic fuel dose, kg
$m_{p,SS}$ – fuel dose for Seiliger-Sabathe cycle, kg
m_0 – maximum mass of the fresh combustion mixture, kg
$n_{a,min}$ – minimal specific amount of air for complete combustion, kmol/kg fuel
p – pressure, Pa
Δp_d – pressure drop in the inlet system during filling, Pa
Δp_w – pressure drop in the exhaust system, Pa
Q – heat, J
(MR) – universal gas constant, J/(kmol K)
SI – spark ignition
T – temperature, K
T_0 – temperature of the fresh charge, K
V – volume, m^3
$V_{d,z}$ – cylinder volume at the moment of the inlet valve closure, m^3
X – humidity, kmol H_2O/kmol d.g.

Greek symbols

γ, φ – load parameters
ε – compression ratio
ε_d – load control parameter for EIVC system
η_o – thermal efficiency of a cycle
κ – isentropic exponent
λ – excess air number
λ_0 – excess air number for maximal mass of the fresh charge
μ – relative charge exchange work
Ψ – heat distribution number

Bibliography

[1] Żmudka Z., Postrzednik S. Flow resistance in the engine inlet-exhaust system as affected by the engine parameters. Combustion Engines 2009 1(136).
[2] Żmudka Z. Energy and ecological aspects of the charge exchange process improvement in an internal combustion engine. Silesian University of Technology Publishing House, Gliwice 2010.
[3] Postrzednik S., Żmudka Z. Application research on procedures for independent control of the internal combustion engine valves. Project nr N502 026 32/2190. PBU-30/RIE-6/07, Report, Gliwice 2009.
[4] Żmudka Z., Postrzednik S., Przybyła G. Late intake valve closing as a way of the throttleless control of SI engine load. Journal of KONES – Powertrain and Transport, 2012 19(1) 491-499.
[5] Żmudka Z., Postrzenik S., Przybyła G. Realization of the Atkinson-Miller cycle in spark-ignition engine by means of the fully variable inlet valve control system. Archives of Thermodynamics, 2014 35(3) 191-205.
[6] Cope D., Wright A., Corcoran C., Pasch K. Fully flexible electromagnetic valve actuator: design, modeling, and measurements. SAE Technical Paper, No. 2008-01-1350, 2008.
[7] Picron V., Postel Y., Nicot E., Durrieu D. Electro-magnetic valve actuation system: first steps toward mass production. SAE Technical Paper No. 2008-01-1360, 2008.
[8] Bernard L., Ferrari A., Micelli D., Perotto A., Rinolfi R., Vattaneo F. Elektrohydraulische Ventilsteuerung mit dem „MultiAir"-Verfahren. MTZ, 12, 2009.
[9] Bernard L., Ferrari A., Rinolfi R., Vafidis C. Fuel economy improvement potential of UniAir throttle-less technology. ATA International Symposium on "SIE: the CO2 challenge", paper 02A5012, Venice 2002.
[10] Haas M., Rauch M. Electro-hydraulic fully variable valve train system. ATZ autotechnology, 2010, 10(02).
[11] Franca O.M. Impact of the Miller cycle in the efficiency of an FVVT engine during part load operation. SAE Tech. Paper, No 2009-36-0081, 2009.
[12] Jia M., Li Y., Xie M., Wang T. Numerical evaluation of the potential of late intake valve closing strategy for diesel PCCI (premixed charge compression ignition) engine in a wide speed and load range. Energy 2013, 51, 203-215.
[13] Gonca G., Sahin B., Ust Y. Performance maps for an air-standard irreversible Dual-Miller cycle (DMC) with late inlet valve closing (LIVC) version. Energy 2013, 54, 285-290.
[14] Begg S.M., Hindle M.P., Cowell T., Heikal M.R. Low intake valve lift in a port fuel-injected engine. Energy 2009, 34, 2042–2050.
[15] Clenci A.C., Iorga-Siman V., Deligant M., Podevin P., Descombes G., Niculescu R. A CFD (computational fluid dynamics) study on the effects of operating an engine with low intake valve lift at idle corresponding speed. Energy 2014, 71, 202-217.
[16] Zammit J.P., McGhee M.J., Shayler P.J., Lawa T., Pegg I. The effects of early inlet valve closing and cylinder disablement on fuel economy and emissions of a direct injection diesel engine. Energy 2015, 79, 100-110.

Zbigniew Żmudka, DSc., DEng. – Faculty of Power and Environmental Engineering, Silesian University of Technology, Gliwice, Poland.
e-mail: *zbigniew.zmudka@polsl.pl*

Prof. Stefan Postrzednik, DSc., DEng. – Faculty of Power and Environmental Engineering, Silesian University of Technology, Gliwice, Poland.
e-mail: *stefan.postrzednik@polsl.pl*

Grzegorz Przybyła, DEng. – Faculty of Power and Environmental Engineering, Silesian University of Technology, Gliwice, Poland.
e-mail: *grzegorz.przybyla@polsl.pl*

Article citation info:
PIELECHA, I. Analysis of the repeatability of fuel spray indexes in a spray-guided spark-ignited direct-injection engine. *Combustion Engines*. 2016, **164**(1), 49-55. ISSN 2300-9896.

Ireneusz PIELECHA

PTNSS-2016-107

Analysis of the repeatability of fuel spray indexes in a spray-guided spark-ignited direct-injection engine

The development and research works on liquid fuel injection in spark-ignited direct injection (SIDI) engines, apart from so common in recent years simulation methods, still have a significant cognitive substrate. This is related to experimental research on repeatability of combustion process using multi- and mono-cylinder test engines and Rapid Compression Machines. The repeatability of preparation and delivery processes has immediate impact on repeatability of combustion process. Except for the necessity of obtaining the repeatability of fuel amounts, the repeatability of injected fuel spray is required. The penetration range and spray area in combustion chamber have direct impact on mixture creation and formation. The optical research on fuel injection has been made in order to determinate its repeatability. The research on unrepeatability of fuel spray propagation has been conducted using piezoelectric injectors of outward-opening type, being primary elements of the spray-guided combustion systems. The results of research were presented in the form of index of variation of the selected parameters. The evaluation of the results of the optical research concerns radial spray penetration and fuel spray velocity. Unrepeatability has been presented with coefficient of variation of radial penetration in relation to the time of injection duration. It has been observed that the coefficients of various parameters are lower with longer times of fuel injection.

Key words: *spray atomization, optical research, image analysis, fuel penetration*

1. Introduction

Combustion systems of SI (spark ignition) engines with direct injection at the time of mixture ignition require very precise synchronization of time of fuel spray penetration in the direction of the spark plug. For combustion systems with fuel amount split into several parts such requirements are even more stringent. Ignition dose should be delivered at a specified time before spark plug discharge, as in its immediate surrounding is required a mixture enabling a reliable ignition. Research carried out by Waltner et al. [17] emphasizes the importance of this issue, especially in the aspect of a fuel injection control system and mixture formation in the combustion chamber.

The research by Waltner et al. [17] proves that the range of correct ignitability of the mixture with a three-part injection applied is much wider than that for the two-part injection. It is so due to a better distribution of the mass of fuel injected during injection of a dose split into three parts compared to that split into two parts. It can be therefore concluded, that an increase of the fuel amount (an increase of the engine load) forces the use of a multi-part fuel injection. Multi-part injection enables a better control of the quality of the composition of a mixture formed around the spark plug. The central location of the injector close to the spark plug makes it possible to obtain the value of the combustion air factor λ guarantying appropriate ignitability of the mixture.

For the high-speed flow of fuel from the injector (of about 100 m/s) a proper fuel atomization occurs. In the piezoelectric injectors (direct injection) of gasoline atomized under pressure higher than 5 MPa (in the tests the pressure of 20 MPa was applied) the loss of spray stability does not involve the formation of a membrane. Due to the waves of short lengths it has not enough time to break up into rings [2]. This means an increase of the Weber number and allows determination of the impact of external factors on the drops formation. The secondary breakup of drops ensues from aerodynamic force in the area of increased dynamic pressure of the gas when the aerodynamic force is greater than the forces of surface tension. The greater the Weber number is, the smaller the dimensions of drops after the secondary break-up are [2]. Secondary breakup of drops is a very complex and insufficiently studied phenomenon; for this reason, the values of Weber number are specified in quite a wide range.

In paper [13], it was found that in the spark ignition engines with direct injection (utilizing multi-orifice injector), Weber number ranges from 1 to 250, however for the largest number of drops this value ranges from 1 to 30.

Secondary breakup of drops is divided into number intervals [4]. When the drops of D diameter are characterized by a low Weber number ($We < 12$), most often their deformation, and not their breakup, takes place. Taking into consideration the liquid viscosity during breakup causes the increase of the value of Weber number required for breakup. Liquid viscosity μ_c is related to its density ρ_c and surface stresses σ_c with the use of Ohnesorge number [4]:

$$Oh = \mu_c/(\rho_c D \sigma_c)^{0.5} \quad (1)$$

Division of the secondary atomization into five areas considering the Weber number and Ohnesorge number ranges for gasoline and diesel are given in the papers [4, 5]. These papers indicate a relationship between the type of the secondary breakdown and the Weber number. It was shown that the Ohnesorge number has an impact on the breakdown of drops only if its value is greater than 1 (Fig. 1).

Thus, obtaining proper fuel atomization is closely related to the uniformity and repeatability of its atomization. Any change to atomization leads to different spray penetration and

this generates different fuel speed. This leads to a variable breakup and non-uniform formation of drops.

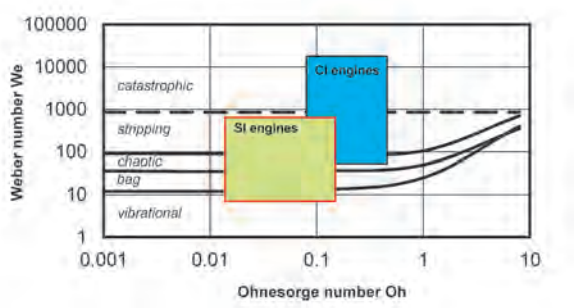

Fig. 1. Map of secondary atomization regimes as functions of Ohnesorge and Weber numbers [4, 5]

Previous research on non-uniformity of fuel injection from injectors of outward-opening type involves mainly issues of the linear analysis of fuel spray penetration. Paper by Peterson [11] concerning the ignitability of the mixture formed in the spray-guided systems (SG) focuses on linear distribution of the spray speed and its ignitability in the surrounding of the spark plug. Oh and Bae [10] conducting tests with the use of a constant-volume chamber determined only the linear penetration of the fuel spray. Studies of the radial propagation of the fuel spray were conducted by El-Asrag et al. [6]; however, they involved the issue of simulation of the flow of fuel from the injector in a micro-scale. The focus was on radiational issues caused by the dynamics of the fuel spray flow.

2. The reasons for undertaking the subject

The above-presented aspects concerning the ignitability of the mixture are closely related to the quality of its formation. Obtaining an effective ignitability of the mixture (with high probability of ignition) requires a uniform distribution of the injected fuel spray and also its proper breakup. Non-uniformity might be mainly caused by variations in the regulations of the injector (for new injectors) or non-uniform wear (exploited injectors).

Due to the expected non-uniformity in fuel spray penetration the analyses were undertaken to identify the subsequent fuel spray penetrations on the basis of optical tests. Such studies are possible during the simulation analysis; however, the conducted experiments show some imperfections of the optical tests.

The studies presented below were designed to obtain answers to the question of uniformity of the fuel spray penetration during high-pressure injection of fuel from the system of outward-opening type. This uniformity was determined on the basis of:

a) the radial penetration of the fuel spray P obtained for the injector; these tests were carried out for the round angle of fuel spray atomization with resolution of 2 degrees; as a criterion for the maximum permissible value of non-uniformity was assumed the 5% coefficient of variation of the radial penetration in relation to the circular profile of such a flow.
b) radial penetration averaged from the measuring cycles; these studies were carried out in range up to 1 ms; the criterion of maximum permissible non-uniformity was also established at 5% variation from the mean of such radial penetration;
c) radial speed (V) of spray of injected fuel; this parameter was specified indirectly using the penetration calculated previously for subsequently recorded images and analyzing the time of subsequent records; the criterion of maximum permissible non-uniformity was also established at 5% of coefficient of variation – CoV(V).

3. The research object and apparatus

The study was carried out using a piezoelectric injector with outward opening of the needle. The new Siemens injector was used to eliminate the influence of operating conditions (wear) on the assessment of uniformity of fuel atomization. In the tests was used an injector with static fuel flow of 35 g/s at 10 MPa, and the value of the maximum fuel pressure of up to 30 MPa. The angle of the spray atomization was 90 degrees and the minimum dose was 2 mg/inj. The needle stroke was ranging in different sources from 30 μm [18] to 36 μm [9]. The injector was controlled by a voltage of 190 V and minimum time of its opening was about 0.15 ms [1]. In the tests was used petrol fuel with a density of 720-775 kg/m^3 (at temperature of 15 ^{o}C) with a sulphur content of up to 10 ppm and the octane number of 95.

Optical tests of fuel atomization and determination of geometric indexes of the fuel spray were conducted with the injector mounted in the constant-volume chamber with fuel at a pressure of 20 MPa (measured by AVL sensor SL31D-2000 with a resolution of 0.001 MPa and accuracy of 1% FS – full scale). The back-pressure of the air in the test chamber was 2 MPa (as measured by the Keller PA21 SR sensor with a resolution of 0.001 MPa and reading accuracy of 2% FS). The injection duration was established at 0.3 and 0.7 ms (controlled by an external system – a sequencer). The tests were carried out with 20 repetitions of fuel spray atomization at each injection.

The test chamber was lit with two 500 W halogen lamps each, placed in opposition in order to obtain the maximum value fuel spray luminance. The diameter of the quartz

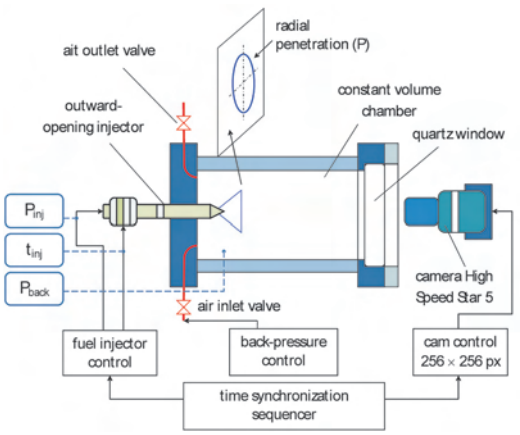

Fig. 2. The test bench for testing the repeatability of fuel injection

window enabling optical access was 90 mm. The view of the testing bench is presented in Fig. 2.

The optical observations were conducted using the High Speed Star 5 camera by LaVision with CMOS converter. The camera was equipped with a Nikon Nikkor lens, 50 mm 1:1.4 (D) with the shutter set to 8. Images were recorded with a frequency of 20 kHz at a resolution of 256 x 256 pixels. The characteristics of the electrical signal (5V, TTL) for controlling the forced start of fuel injection, the time of its duration as well as the start time of images recording was provided by the sequencer with time resolution of 2 ns [12].

4. Optical tests of repeatability of fuel atomization

4.1. Optical tests of fuel atomization

The flat exposition of the recorded images was analyzed. As might be observed in Fig. 2, the radial propagation of injected fuel spray was recorded, which means the camera was parallel to the axis of the injector. Such parallel placement of the injector and the camera enables to get most information on non-uniformity of radial propagation of fuel spray. Exemplary results of the tests of atomization at injection pressure of 20 MPa, the back-pressure in the test chamber of 2 MPa and two different injection durations are shown in Fig. 3.

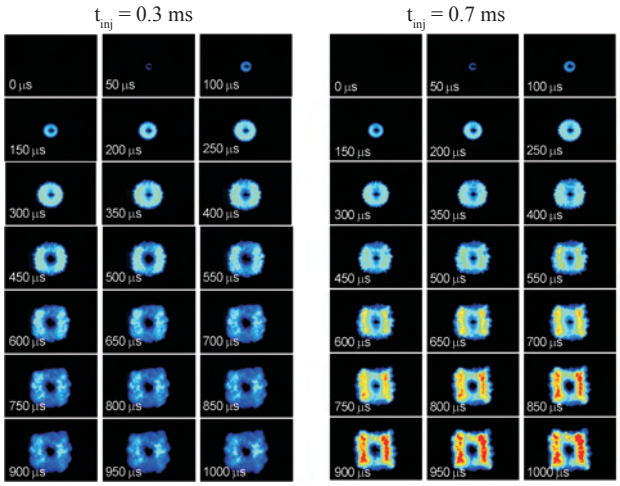

Fig. 3. The recorded images (sample) of fuel atomization at a pressure of injected fuel P_{inj} = 20 MPa, P_{air} = 2 MPa and the injection duration: a) 0.3 ms, b) 0.7 ms

The change in the intensity of the light indicates a change in the concentration of fuel in the spray. Distinctive, close to square, shape of the fuel spray is the result of the injector design presented, among others, in publications [3, 7].

The paper [7] in a numerical way specifies speed of fuel flow from the injector with the outward opening of the injector needle. The calculations confirmed not only the influence of the shape of the injector hole, but also the influence of the geometry of the needle on the flow of liquid spray. Similarly to the current tests, the right sections of the injected fuel spray close to square were obtained (radial range). This shape is clearly seen for longer injection durations and for long time of fuel atomization recording.

4.2. Evaluation of specific indexes of fuel atomization

The photos presented above are the basis for the analysis of the radial penetration of fuel spray in relation to particular value of the round angle. The analysis was conducted for angle increments of $\Delta\alpha = 2^{o}$ for the analyzed subsequent penetrations of fuel spray with time interval of 0.05 ms. An example of such penetration for two different injection durations is shown in Fig. 4. This figure shows 20 consecutive radial penetrations of fuel spray from 0.05 ms to 1 ms.

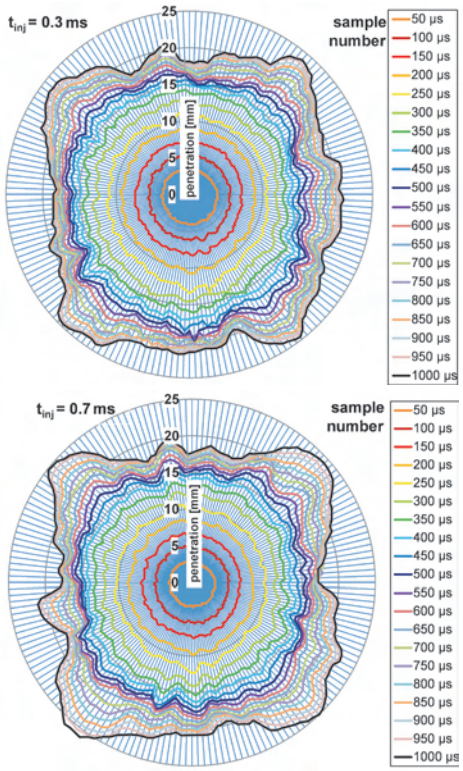

Fig. 4. Analysis of the fuel penetration for two different injection durations with the filming speed of 20 kHz

Significant deviations from the mean value are observed for the atomization time of t = 0.35 ms and for further atomization of the fuel spray. These deviations are more significant for longer time of fuel injection. However, the change in shape of the spray from round to square takes place at the same time of atomization t = 0.6 ms.

A detailed analysis of the index of fuel penetration non-uniformity indicates the presence of high value of CoV (P) at minimum atomization time (t = 0.05 ms) – Fig. 5a. For the injection duration of t = 0.3 ms the CoV(P) value ranged from 7% to 10%. During atomization in the time ranging from 0.1 to 0.2 ms the value of deviations is reduced to approximately 5%. Later the non-uniformity of the radial spray penetration increases, which is indicated by increasing value of the CoV factor. It obtains the maximum value of approximately 10% for atomization time of t = 1 ms. The analysis of this non-uniformity for the injection duration t_{inj} = 0.7 ms indicates smaller radial deviation of the fuel spray penetration – Fig. 5b. Smaller values of these disper-

sions are observed only for the initial and middle phases of the atomization time. The CoV(P) obtains values below 5% for the atomization time ranging from t = 0.1 ms to 0.5 ms for the selected characteristics. However, it should be noted that for all analyzed fuel atomization processes for the time ranging from 0.1 to 0.4 ms all repetitions have met the limit of 5% non-uniformity of the CoV index.

It follows from the above that, during the injection of small amounts (t_{inj} = 0.3 ms) the penetration of the fuel spray is uniform only up to 0.2 ms (CoV(P) < 5%) (Fig. 5), while for large injected amounts (t_{inj} = 0.7 ms) the radial penetration is uniform even up to 0.5 ms (CoV(P) < 5%). This means that for the injector of outward-opening type the ignition of small amounts at short intervals is required, and the intervals can be extended (almost twice) during injection of large amounts. The presented injection duration (t = 0.3 ms and t = 0.7 ms) ensure the uniformity of distribution of the fuel spray penetration, and thus can increase the probability of ignition as the variations in the radial penetrations are insignificant.

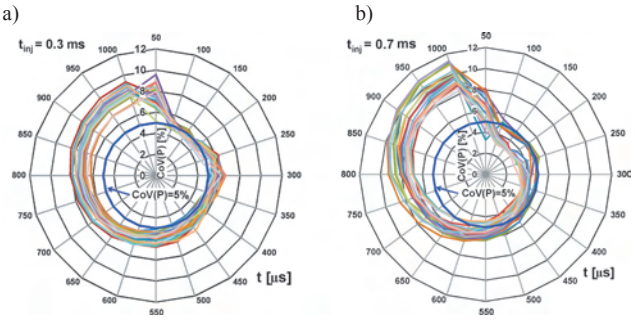

Fig. 5. Specific coefficients of variation of the radial penetration related to the subsequent times of fuel atomization: a) a small fuel amount of t_{inj} = 0.3 ms; b) a large fuel amount t_{inj} = 0.7 ms

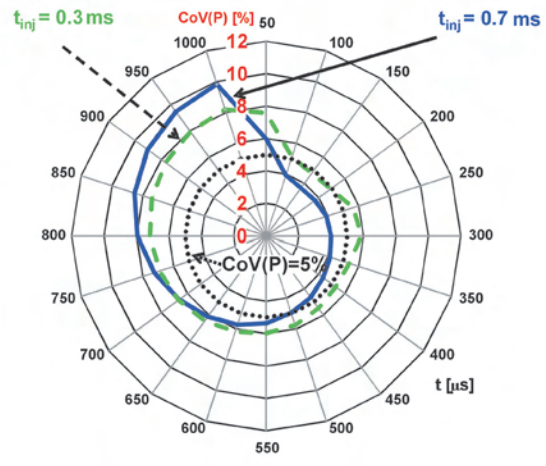

Fig. 6. The average values of the non-uniformity of the radial distribution on circular profile of the fuel spray for different amounts of fuel injected

Later in the article the average values of the geometric indexes of injected fuel spray are analyzed: the average radial penetration of fuel spray and the average value of speed of the fuel spray front.

5. The evaluation of average values of indexes of fuel atomization

5.1. Evaluation of the uniformity of the average radial fuel penetration

Evaluation of uniformity of the average radial fuel spray penetration was conducted for 20 subsequent repetitions of fuel injections. The analysis was carried out for the time range from 0.05 ms to 0.3 ms for the same fuel amounts as previously. The values of the radial penetration of fuel spray are shown in Fig. 7. The most significant changes in the radial penetration of fuel spray were observed during the start of injection. With the time of injection, the reduction in the dispersion of this index was observed.

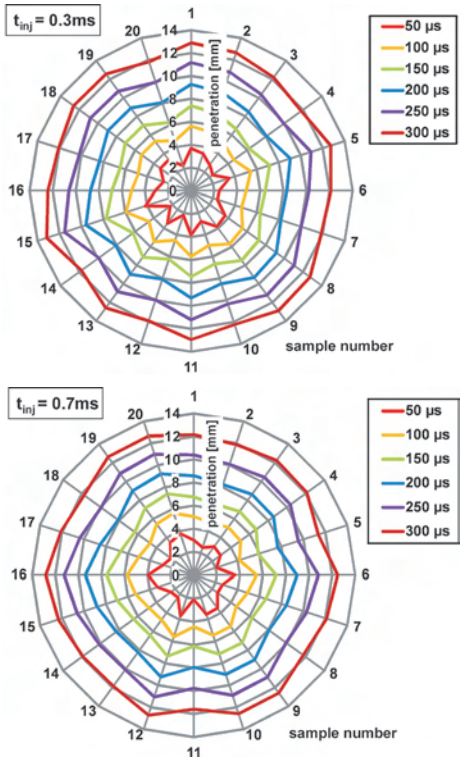

Fig. 7. The results of the radial penetration test of 20 consecutive amounts of injected fuel in the time range from 0.05 to 0.3 ms (for two amounts with injection durations t = 0.3 ms and t = 0.7 ms)

The analysis of the results presented in Fig. 7 indicates the existence of significant values of non-uniformity in the radial penetration amounting to 20% during injection initiation (regardless of the amount). The full analysis of the non-uniformity of the radial penetration of fuel amount indicates the existence of a critical time, after which the values of the non-uniformity of the radial penetration are smaller than 5%. This critical time falls at approximately 0.2 ms (Fig. 8). After this time, the dispersions of the values are below 5%, which is acceptable. It should be noted that the obtained time of t = 0.2 ms, after which the non-uniformity of the penetration reaches the value below 5% does not depend on the injection duration or on the fuel amount.

The optical analysis of the geometric indexes of fuel spray is possible when on the basis of the subsequent images, the fuel spray penetration might be determined unequivo-

cally. This penetration depends on a number of factors the most important of which are the fuel pressure and the density of the medium into which the fuel is injected. This density is closely related to the back-pressure of this medium. In the tests presented, the fuel pressure to medium back-pressure ratio was 10:1. For such values the analysis of unequivocally determined fuel spray penetration was conducted. Such tests are possible if the spray penetrates into the analyzed space without increasing the vortex of the front of the fuel spray. The conducted analysis shows that for smaller amounts (t = 0.2 ms) the fuel spray penetrates into the chamber for up to about 0.4 ms (Fig. 9). After this time there is an increased intensity of radial vortex of the fuel spray which makes it impossible to unequivocally determine the increase of its penetration. Larger values of injection durations (higher amounts) increase this time up to 0.5 ms.

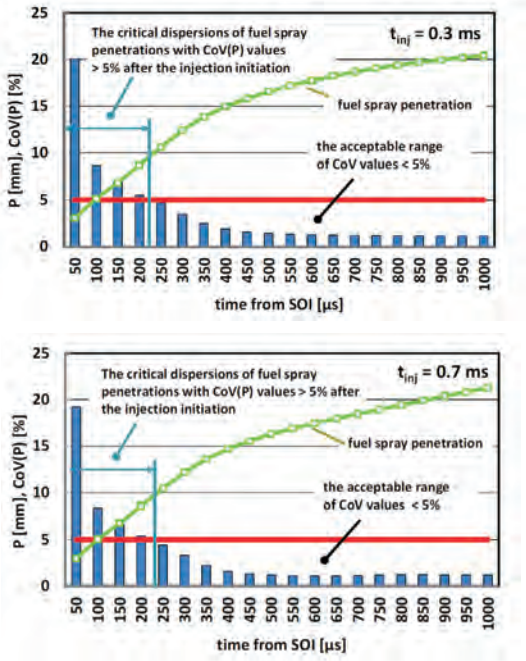

Fig. 8. The analysis of the non-uniformity of the average radial penetration of fuel injected at different injection durations

A confirmation of that analysis is, among others, the paper [15], in which the Authors utilizing the Mie method determined the directions of movement of the atomized fuel. In the initial phase of the injection the air is "displaced" by the atomized fuel. Due to a high relative density of the air, under the influence of resisting forces acting on the atomized fuel a vortex is created which directs the fuel spray outwards. As the spray has the shape of a hollow cone, the air is carried up, which was also shown in the papers [14, 16]. Then, in conjunction with air resistance forces, another rotating whirl is created (of vortex type). These whirls, depending on the back-pressure, effectively reduce the penetration of the spray.

Complementary to these studies can be studies by Kim et al. [8], in which the velocity of mixture vortex during fuel spray injection was determined. The tests were carried out at the pressure of injection into the constant-volume chamber of 20 MPa. From the distribution of the velocity field it ensues that the spray velocity is not greater than 50 m/s (after the injection duration t = 0.5 ms). The recirculation zone is formed at the bottom part of the spray, where the vortex of the mixture is dominant. The air flowing out from the inside of an empty cone carries the charge up and outward into the direction of the injector.

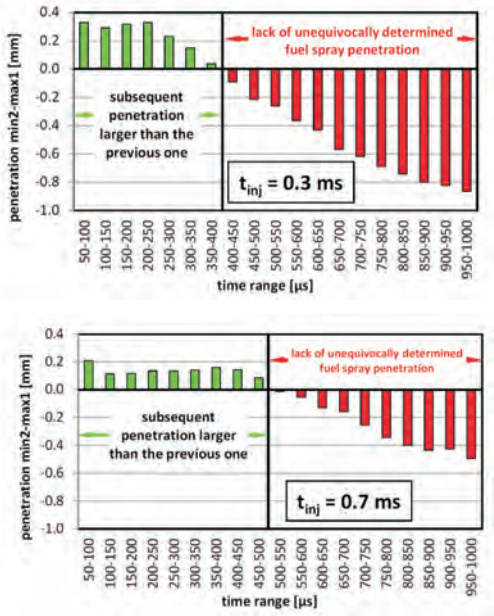

Fig. 9. The analysis of the possibility of determining the fuel spray penetration on the basis of optical analysis

5.2. The assessment of average values of fuel spray velocity

The velocity of fuel flowing out in proximity of the injector needle ranges from about 150 m/s (on the basis of own tests [19, 20]) to 200 m/s [8] depending on the pressure of the fuel injected and the back-pressure of the medium. The velocity of the air movement causing swirling of the atomized fuel spray (the end of its cone) is approximately 5-10 m/s.

In static tests (without mixture movement) with the use of a constant volume chamber the velocity tests were conducted taking into consideration the specified time after the start of the fuel injection. The test results were correlated with the fuel spray penetration as the spray velocity was determined on the basis of the difference of spray penetration in relation to the time of filming. The values contained in Fig. 10 show that the highest spray velocity is obtained after the fuel starts to flow from the atomizer. The value of the velocity obtained ranges from 45 to 75 m/s. With the propagation of fuel spray this velocity decreases. What is also characteristic is that the non-uniformity of this velocity decreases rapidly. After 0.1 ms from the start of the injection the spray velocity is variable within a minor range. The analysis shown in Fig. 11 indicates existence of significant non-uniformity of velocity n the initial phase of fuel injection. For the time up to 0.7 ms the values of the non-uniformity oscillate within the range of about 5%. Although the fuel spray velocity decreases, the

non-uniformity of the velocity in the final measuring range increases. This is caused by deeper radial penetration of fuel and reduced possibilities of determining the spray penetration (and the spray velocity).

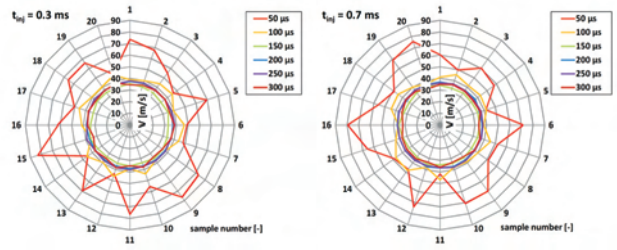

Fig. 10. The variation of fuel spray velocity at two injection durations for 20 consecutive repetitions

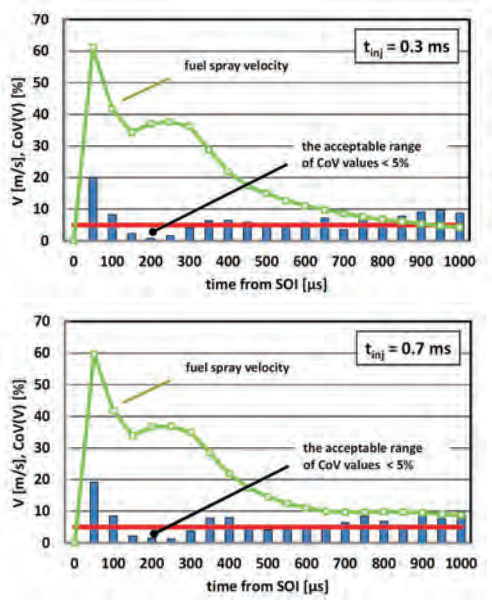

Fig. 11. The analysis of the fuel spray velocity and its non-uniformity at two amounts of injected fuel (t = 0.3 ms and t = 0.7 ms)

As the presented tests on fuel spray penetration show, the most significant non-uniformities occur during the start of the fuel injection. Therefore, in the further part of this paper is presented the detailed analysis of the phase of fuel flow from the injector.

6. The assessment of the conditions at the start of the fuel injection

The assessment was carried out during the injection, at t = 0.05 ms after the injection start. The fuel spray penetration was analyzed for 20 consecutive doses of fuel injected. The results of this analysis are shown in Fig. 12. It shows that at the time of injection t = 0.3 ms the maximum variation between the penetrations obtained can range from 2.2 mm to 4.1 mm. For the increased dose of injected fuel the initial average spray penetration after time t = 0.05 ms is also 3 mm.

The detailed radial analysis of such penetration is presented in Fig. 13. It shows quite considerable variation in the spray penetration even during one fuel injection. Taking into consideration such significant variations in spray penetration, it is impossible to place the injector and the spark plug in too close a proximity. There is no certainty if the fuel in such a short time reaches a specific point in space in order to ensure the ignitability of the mixture.

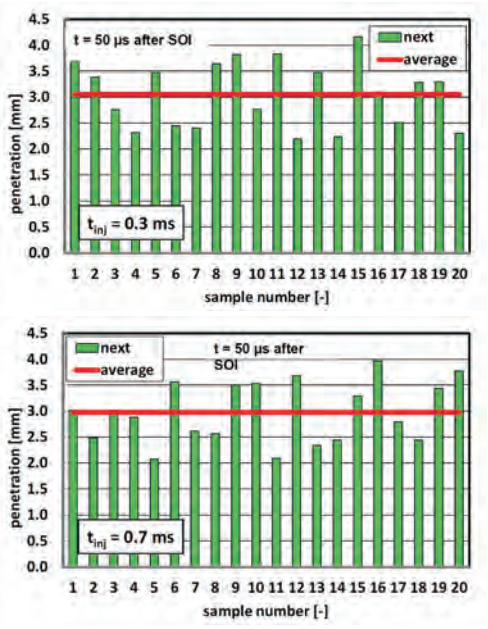

Fig. 12. The instantaneous and average value of the fuel spray penetration during injection for 20 subsequent measurements

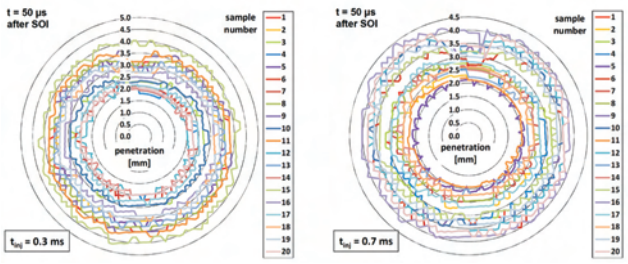

Fig. 13. The analysis of the radial fuel spray penetration after time t = 0.05 ms at two fuel injection durations (t = 0.3 ms and 0.7 ms)

Summary

The presented analysis of the non-uniformity of fuel spray penetration and non-uniformity of its velocity makes it possible to draw several conclusions:

1. The fuel injection from injectors of outward-opening type is characterized by a high repeatability of the radial spray penetration (deviation from the circular profile) for the time range from t = 0.1 to 0.5 ms during injection of small doses, and for the time range from t = 0.1 to 0.2 ms for large doses of fuel injected (based on Fig. 5). This means that during the injection of small doses, it is necessary to shorten the time between the start of injection and the ignition. Injection of large doses at fuel pressure to air pressure ratio of 10:1 increases this non-uniformity (the critical value of which is estimated at 5%).
2. Assessment of the average fuel spray penetration (based on Fig. 8) indicates the existence of a time, after which the value of non-uniformity of spray penetration falls below

5%. This time, irrespective of the injected fuel amount, was determined at approximately 0.2 ms.

3. The average value of the radial fuel spray penetration from the beginning of fuel injection is identified within the range of up to 0.4 ms (based on Fig. 9). This means that for the back-pressure the radial spray penetration is unequivocally increased up to the time pointed out above. In the subsequent time intervals it is impossible to determine unequivocally the spray penetration, which might be caused by high rate of petrol fuel evaporation as well as by the occurrence of swirling resulting from the air cone inside the atomized liquid.
4. Due to the high initial velocity of fuel spray (for time up to t = 0.05 ms) and the lack of a clear determination of its velocity it is not possible to obtain high efficiency of ignition in so short a time after the commencement of the injection. Significant deviations in determining the fuel spray velocity also ensues from significant non-uniformity of the spray penetration obtained after such time. It can also be caused by variations at the initiation of fuel flow from the injector. This may involve the need to increase the speed of recording in order to determine the exact beginning of fuel flow from the injector.

Acknowledgements

The author wishes to thank Prof. K. Wisłocki and MEng. P. Borowski, MEng. W. Cieslik, MEng. M. Skowron, MEng W. Bueschke from Poznań University of Technology for their participation in the research and critical, yet invaluable remarks on the analysis of optical investigations into fuel injection.

Bibliography

[1] Achleitner E., Bäcker H., Funaioli A. Direct injection systems for Otto engines. SAE Technical Paper 2007-01-1416, 2007, doi:10.4271/2007-01-1416.

[2] Aleiferis P.G., Serras-Pereira J., van Romunde Z., Caine J., Wirth M. Mechanisms of spray formation and combustion from a multi-hole injector with E85 and gasoline. Combustion and Flame. 2010, **157**, 735-756.

[3] Arcoumanis C., Kamimoto T. Flow and combustion in reciprocating engines. Springer, Berlin – Heidelberg, Germany, 2008.

[4] Ashgriz N. Handbook of atomization and sprays. Theory and applications. Springer, New York 2011.

[5] Chen H., Reuss D.L., Sick V. Analysis of misfires in a direct injection engine using proper orthogonal decomposition. Experiments in Fluids. 2011, **51**. doi:10.1007/s00348-011-1133-z.

[6] El-Asrag H.A., Iannetti A.C., Apte S.V. Large eddy simulations for radiation-spray coupling for a lean direct injector combustor. Combustion and Flame. 2014, **161**, 510-524.

[7] Gavaises M., Tonini S., Marchi A., Theodorakakos A., Bouris D., Matteucci L. Modelling of internal and near-nozzle flow of a pintle-type outwards-opening gasoline piezo-injector. International Journal of Engine Research. 2006, **7**, doi:10.1243/14680874JER00306.

[8] Kim S., Kim Y., Lee J. Analysis of the in-cylinder flow, mixture formation and combustion processes in a spray-guided GDI engine. SAE Technical Paper 2008-01-0142, 2008, doi:10.4271/2008-01-0142.

[9] Marchi A., Nouri J., Yan Y., Arcoumanis C. Spray stability of outwards opening pintle injectors for stratified direct injection spark ignition engine operation. International Journal of Engine Research. 2010, **11**. doi:10.1243/14680874JER605.

[10] Oh H., Bae C. Effects of the injection timing on spray and combustion characteristics in a spray-guided DISI engine under lean-stratified operation. Fuel. 2013, **107**, 225-235. doi:10.1016/j.fuel.2013.01.019.

[11] Peterson B., Reuss D.L., Sick V. On the ignition and flame development in a spray-guided direct-injection spark-ignition engine. Combustion and Flame. 2014, **161**, 240-255. doi:10.1016/j.combustflame.2013.08.019.

[12] Pielecha I. Modelling of gasoline fuel spray penetration in SIDI engines. International Journal of Automotive Technology. 2014, **15**(1), 47-55. doi:10.1007/s12239-014-0005-y.

[13] Rotondi R., Hélie J., Leger C., Mojtabi M., Wigley G. Multihole gasoline direct injection spray plumes. 23rd Annual Conference on Liquid Atomization and Spray Systems, Brno, Czech Republic, 2010.

[14] Sauter W., Pfeil J., Velji A., Spicher U., Laudenbach N., Altenschmidt F., Schaupp U. Application of particle image velocimetry for investigation of spray characteristics of an outward opening nozzle for gasoline direct injection. SAE Technical Paper 2006-01-3377, 2006. doi:10.4271/2006-01-3377.

[15] Skogsberg M., Dahlander P., Denbratt I. Spray shape and atomization quality of an outward-opening piezo gasoline DI injector. SAE Technical Paper 2007-01-1409, 2007. doi:10.4271/2007-01-1409.

[16] VanDerWege B., Han Z., Iyer C., Muñoz R., Yi J. Development and analysis of a spray-guided DISI combustion system concept. SAE Technical Paper 2003-01-3105, 2003. doi:10.4271/2003-01-3105.

[17] Waltner A., Lückert P., Schaupp U., Rau E., Kemmler R., Weller R. Future technology of the spark-ignition engine: spray-guided direct injection with piezo injector. The potential of synthetic fuels to meet future emission regulations, 27st International Vienna Engine Symposium 2006, Wien, Austria, 2006.

[18] Warnecke V., Achleitner E., Bäcker H. Development status of the Siemens VDO piezo injection system for spray-guided combustion. 27th International Vienna Motor Symposium, Wien Austria, 2006.

[19] Wisłocki K., Pielecha I., Czajka J., Maslennikov D. The influence of fuel injection parameters on the indexes of fuel atomization quality for a high pressure injection. SAE Technical Paper 2010-01-1499, 2010. doi:10.4271/2010-01-1499.

[20] Wisłocki K., Pielecha I., Czajka J., Maslennikov D. The qualitative spray characteristics of high-pressure gasoline injection system. 23rd European Conference on Liquid Atomization and Spray Systems – ILASS – Europe 2010, Brno 2010.

Ireneusz Pielecha, DSc., DEng. – professor at the Faculty of Machines and Transport of Poznan University of Technology.

e-mail: *ireneusz.pielecha@put.poznan.pl*

Article citation info:
CHŁOPEK, Z. et al. Comparative examination of pollutant emission from an automotive internal combustion engine with the use of vehicle driving tests. *Combustion Engines*. 2016, **164**(1), 56-64. ISSN 2300-9896.

Zdzisław CHŁOPEK
Jacek BIEDRZYCKI
Jakub LASOCKI
Piotr WÓJCIK

PTNSS-2016-108

Comparative examination of pollutant emission from an automotive internal combustion engine with the use of vehicle driving tests

The pollutant emission from automotive internal combustion (IC) engines is highly susceptible to engine operation states determined by vehicle velocity processes. The article presents results of comparative examinations of specific distance pollutant emission characteristics determined from various vehicle driving tests. The specific distance pollutant emission was determined using vehicle type-approval and special tests as well as tests developed at the Automotive Industry Institute (PIMOT), treated as realizations of the stochastic process of vehicle velocity. The research results confirmed high susceptibility of the IC engine pollutant emission to the engine operation states, which endorses the usefulness of treating the conditions of operation of automotive engines as stochastic processes.

Key words: *internal combustion engines, pollutant emission, vehicle driving tests, stochastic processes*

Badania porównawcze emisji zanieczyszczeń z samochodowego silnika spalinowego z zastosowaniem testów jezdnych

Emisja zanieczyszczeń z samochodowych silników spalinowych jest bardzo wrażliwa na stany pracy silników zdeterminowane procesami prędkości samochodów. W niniejszej pracy przedstawiono wyniki badań porównawczych charakterystyk emisji drogowej zanieczyszczeń w różnych testach jezdnych. Do wyznaczania emisji drogowej zanieczyszczeń wykorzystano testy stosowane w procedurach homologacyjnych i testy specjalne oraz opracowane w Przemysłowym Instytucie Motoryzacji, traktowane jako realizacje procesu stochastycznego prędkości samochodu. Wyniki badań potwierdziły znaczną wrażliwość emisji zanieczyszczeń na stany pracy silnika spalinowego, co potwierdza celowość traktowania warunków pracy silników samochodowych jako procesów stochastycznych.

Słowa kluczowe: *silniki spalinowe, emisja zanieczyszczeń, testy jezdne, procesy stochastyczne*

1. Introduction

The pollutant emission from automotive internal combustion (IC) engines is highly susceptible to engine operation states [14], and to both the static engine operation states and the occurrence of dynamic states. For an automotive engine, the state of its operation is mainly determined by the vehicle velocity process. Therefore, the ecological properties of automotive engines in terms of pollutant emission are explored by carrying out empirical research using vehicle driving tests, developed to simulate the conditions of vehicle operation in real road traffic. Such tests have the form of running the engine under test in accordance with predefined time domains of vehicle velocity.

The vehicle driving tests may be formulated in accordance with specific criteria of similarity between the test parameters and the actual conditions of vehicle motion. The first vehicle driving tests were designed in accordance with the criterion of similarity between the characteristics, mostly point-type, of the test conditions and actual vehicle operation conditions, e.g. such as the vehicle velocity process, the similarity of extreme values, average value, variance, or probability density, and for the acceleration process, the similarity of extreme values, and average values of the positive and negative acceleration. This criterion was taken as a basis for the preparation of such tests as for e.g. NEDC (New European Driving Cycle), Japan 10-15 Mode [26, 27], BAC

1. Wstęp

Emisja zanieczyszczeń jest bardzo uzależniona od stanów pracy silników spalinowych [14] i to zarówno od stanów statycznych, jak i od występowania stanów dynamicznych. W odniesieniu do silników samochodowych stan ich pracy jest zdeterminowany przede wszystkim procesem prędkości samochodów. Z tego powodu w celu poznania właściwości ekologicznych silników samochodowych ze względu na emisję zanieczyszczeń prowadzi się badania empiryczne w testach jezdnych, opracowanych jako warunki symulujące użytkowanie trakcyjne pojazdów. Testy te stanowią przebiegi prędkości samochodu w dziedzinie czasu.

Testy jezdne można tworzyć z zastosowaniem określonych kryteriów podobieństwa właściwości testów i rzeczywistych warunków ruchu samochodów. Pierwsze testy jezdne były tworzone zgodnie z kryterium podobieństwa charakterystyk, najczęściej punktowych, warunków badań oraz rzeczywistego użytkowania pojazdów, np. podobieństwa dla procesu prędkości jazdy samochodu: wartości ekstremalnych, wartości średniej, wariancji, czy gęstości prawdopodobieństwa, a dla procesu przyspieszenia: wartości ekstremalnych i wartości średniej przyspieszeń dodatniego i ujemnego. Zgodnie z tym kryterium opracowano m.in. testy: NEDC (*New European Driving Cycle*) i Japan 10-15 Mode [26, 27], BAC (*Business Arterial Commuter*), WVU 5-Peak (*West Virginia University*), SRC (*Standard Road*

(Business Arterial Commuter), WVU 5-Peak (West Virginia University), SRC (Standard Road Cycle) [27], or Colombia Test [23]. Another method of designing the vehicle driving tests is faithful simulation in time domain. Examples of the tests designed in accordance with this criterion are FTP-75 (Federal Test Procedure), HWFET (Highway Fuel Economy Test), SFTP SC03 (Supplement Federal Test Procedure), or California UC (United Cycle) [27]. Other criteria of similarity, e.g. between spectral characteristics, can also be used [13, 14].

Usually, the ecological properties of automotive engines in terms of pollutant emission are assessed based on the results of tests carried out within type-approval procedures. However, the conditions of real vehicle operation may differ greatly from the type-approval conditions. Hence, the characteristics of IC engines, and above all the pollutant emission, may in certain circumstances significantly deviate from those determined in the conditions of type-approval tests, especially in the case of severe traffic difficulties, which frequently occur in the central parts of large urban agglomerations [3, 4] or at very heavy engine loads, e.g. during motorway drives [4]. Because of this, researchers also try to determine the characteristics of IC engines in conditions differing from those applied in the type-approval procedures [1–11, 13–25]. In some of the research works, attempts are also made to treat the properties of automotive IC engines as stochastic processes [1, 5, 8–11, 13–15, 17]. Another approach, having been dynamically developed in the recent period, is the examination of pollutant emission in the real conditions of operation of motor vehicles [2, 19–23].

The authors of this paper decided to verify the results of examination of pollutant emission from an automotive IC engine, obtained from selected type-approval tests and from special tests representing the conditions of street congestions and on motorways. For the said verification, results of special tests developed by the authors to simulate the motion of passenger cars in Polish conditions [9] were used.

2. Tests used to simulate the motion of passenger cars in Polish conditions

In the article [9], a task was undertaken to develop vehicle driving tests that would represent the typical mode of operation of motor vehicles in Polish conditions. With this goal in mind, a concept was adopted to treat the vehicle velocity processes in characteristic vehicle motion conditions, i.e. in street congestion, urban, extra-urban, and high-speed (motorway and fast road) traffic conditions, as stochastic processes. The tests, treated as realizations of stochastic processes, were designed in compliance with the rule of faithful simulation in time domain. The tests were defined based on the results of testing a Honda Civic passenger car operated on roads of Mazowieckie and Łódzkie Voivodships.

As a result of the investigations carried out, four PIMOT tests were prepared for each vehicle operation mode, with treating them as realizations of stochastic processes of vehicle velocity characterizing the vehicle operation modes in the following conditions:
– street congestions (denoted by "CT");

Cycle) [27], Colombia Test [23]. Innym sposobem tworzenia testów jezdnych jest wierna symulacja w dziedzinie czasu. Zgodnie z tym kryterium opracowano m.in. testy: FTP-75 (*Federal Test Procedure*), HWFET (*Highway Fuel Economy Test*), SFTP SC03 (*Supplement Federal Test Procedure*), czy California UC (*Unified Cycle*) [27]. Istnieje również możliwość zastosowania innych kryteriów podobieństwa, np. charakterystyk widmowych [13, 14].

Zazwyczaj do oceny właściwości ekologicznych silników samochodowych ze względu na emisję zanieczyszczeń wykorzystuje się wyniki badań w testach stosowanych w procedurach homologacyjnych. Rzeczywiste warunki użytkowania samochodów mogą jednak znacznie odbiegać od warunków homologacyjnych. W niektórych warunkach właściwości silników spalinowych, przede wszystkim emisja zanieczyszczeń, mogą – w związku z tym – znacznie odbiegać od właściwości w warunkach testów homologacyjnych, szczególnie w sytuacji dużych utrudnień w ruchu, co często występuje w centrach wielkich aglomeracji miejskich [3, 4], albo przy bardzo dużym obciążeniu silnika, np. w czasie jazdy na autostradach [4]. W związku z tym są podejmowane badania właściwości silników spalinowych w warunkach innych niż w procedurach homologacyjnych [1–11, 13–25]. W niektórych pracach są podejmowane próby potraktowania właściwości samochodowych silników spalinowych jako procesów stochastycznych [1, 5, 8–11, 13–15, 17]. Innym rodzajem badań, rozwijanym dynamicznie w ostatnim czasie, są badania emisji zanieczyszczeń w rzeczywistych warunkach użytkowania pojazdów samochodowych [2, 19–23].

Autorzy niniejszego artykułu postanowili zweryfikować wyniki badań emisji z samochodowego silnika spalinowego, uzyskane w wybranych testach homologacyjnych oraz w testach specjalnych, stosowanych do badań w warunkach zatorów ulicznych oraz na autostradach. Do weryfikacji tych wyników wykorzystano wyniki badań w specjalnych testach, opracowanych przez autorów w celu symulacji ruchu samochodów osobowych w warunkach polskich [9].

2. Testy do symulacji ruchu samochodów osobowych w warunkach polskich

W publikacji [9] przedstawiono opracowanie testów jezdnych, charakteryzujących sposób użytkowania samochodów w warunkach polskich. Przyjęto koncepcję, aby procesy prędkości w charakterystycznych warunkach ruchu samochodów, tzn. w zatorach ulicznych, w miastach, poza miastami oraz na autostradach i drogach ekspresowych, potraktować jako procesy stochastyczne. Do opracowania testów, stanowiących realizacje procesów stochastycznych, wykorzystano zasadę wiernej symulacji w dziedzinie czasu. Testy wyznaczano na podstawie wyników badań samochodu osobowego Honda Civic, eksploatowanego na drogach województw mazowieckiego i łódzkiego.

W wyniku przeprowadzonych badań opracowano po cztery testy PIMOT, stanowiące realizacje procesów stochastycznych prędkości samochodu, charakteryzujących jego użytkowanie w warunkach:
– zatorów ulicznych – CT,
– w miastach bez zatorów ulicznych – UT,

– urban traffic without congestions (denoted by "UT");
– extra-urban (rural) traffic (denoted by "RT");
– high-speed traffic (on motorways and fast roads, denoted by "HT").

Four realizations of the vehicle velocity process in the vehicle driving test have been presented in each of the graphs below (Figs 1 to 4).

The driving tests developed significantly differ from each other in their properties [7–11]. The average vehicle velocity values in individual realizations of the driving tests were:

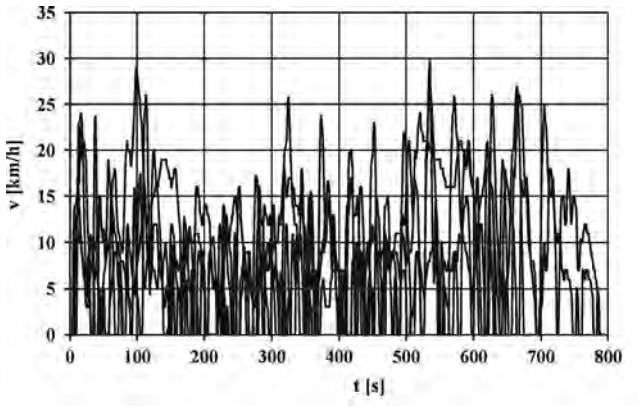

Fig. 1. Realizations of the process of vehicle velocity for test drives in street congestions – CT

Rys. 1. Realizacje procesu prędkości v w testach jazdy w zatorach ulicznych – CT

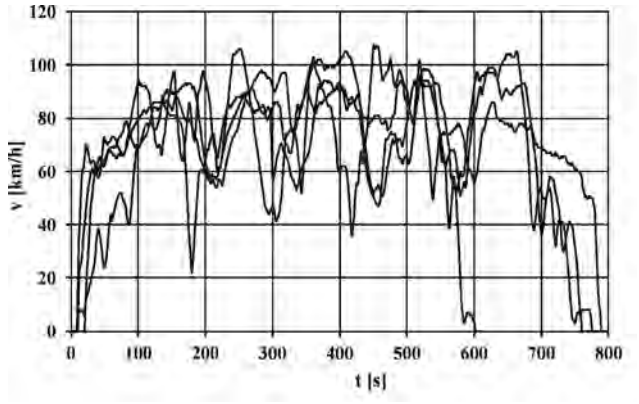

Fig. 3. Realizations of the process of vehicle velocity for test drives in extra-urban (rural) traffic – RT

Rys. 3. Realizacje procesu prędkości v w testach jazdy poza miastami – RT

about 8 km/h for the test drives in street congestions, about 36 km/h for the test drives in urban traffic without congestions, about 76 m/h for the test drives in extra-urban (rural) traffic, and about 134 km/h for the test drives in high-speed traffic (on motorways and fast roads).

3. Results of the examination of pollutant emission from a passenger car engine in the driving tests

The tests were carried out on a Honda Civic EJ9 passenger car (trade name of the car model: Civic 3D 1.4i) with a spark-

– poza miastami – RT,
– na autostradach i drogach ekspresowych – HT.

Na rysunkach 1–4 przedstawiono po cztery realizacje procesu prędkości w opracowanych testach jezdnych.

Opracowane testy jezdne znacznie różnią się właściwościami [7–11]. Prędkość średnia w poszczególnych realizacjach testów wynosi dla: jazdy w zatorach ulicznych około 8 km/h, w miastach bez zatorów ulicznych – około 36 km/h, poza miastami – około 76 km/h oraz na autostradach i drogach ekspresowych – około 134 km/h.

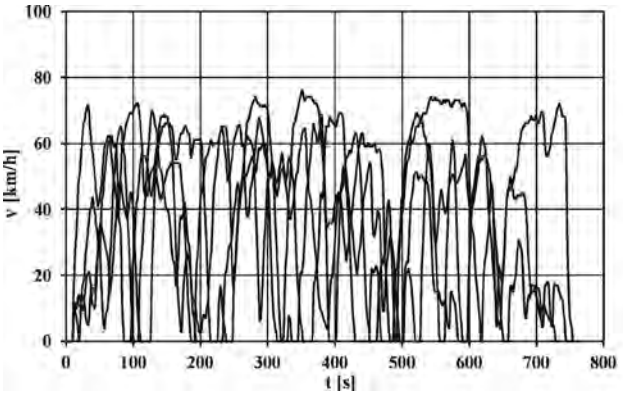

Fig. 2. Realizations of the process of vehicle velocity for test drives in urban traffic without congestions – UT

Rys. 2. Realizacje procesu prędkości v w testach jazdy w miastach bez zatorów ulicznych – UT

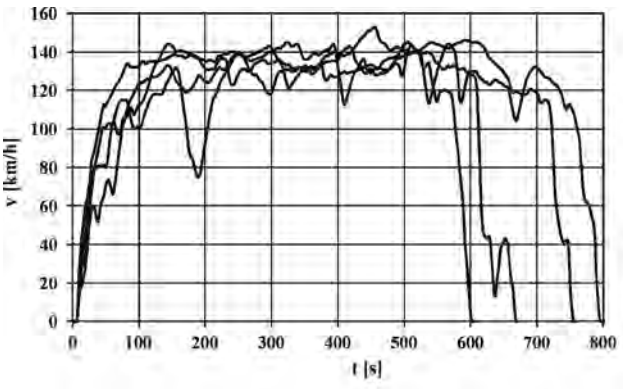

Fig. 4. Realizations of the process of vehicle velocity for test drives in high-speed traffic (on motorways and fast roads) – HT

Rys. 4. Realizacje procesu prędkości v w testach jazdy na autostradach i drogach ekspresowych – HT

3. Wyniki badań emisji zanieczyszczeń z silnika samochodu osobowego w testach jezdnych

Obiektem badań był samochód osobowy Honda Civic EJ9 (nazwa handlowa Civic 3D 1.4i) z silnikiem o zapłonie iskrowym o objętości skokowej 1396 cm^3, spełniający wymagania emisji zanieczyszczeń na poziomie Euro 3.

Badania samochodu prowadzono w stanie silnika spalinowego nagrzanego do ustabilizowanej temperatury. Badania przeprowadzono na stanowisku hamowni podwoziowej Schenk Komeg EMDY 48. Aparatura zastosowana do badań

ignition engine and a displacement of 1396 cm^3, meeting the requirements of the Euro 3 exhaust emission standard.

The car was tested with its engine having been heated to a stable temperature. The Honda Civic car was tested on a vehicle chassis dynamometer Schenk Komeg EMDY 48. The research equipment used for the tests meets the requirements of Directive 1999/96/EC of the European Parliament and of the Council. To examine the pollutant emission, an exhaust gas analysing test stand was used, which incorporated Horiba Mexa 7200 system provided with Horiba analysers to measure the concentrations of carbon monoxide (AIA-721A), hydrocarbons (FIA-725A), nitrogen oxides (CLA-755A), carbon dioxide (AIA-722), and oxygen (MPA-720).

The tests were carried out in compliance with type-approval procedures UDC (Urban Driving Cycle), EUDC (Extra Urban Driving Cycle), NEDC, FTP-75, Japan 10-15 Mode, and HWFET, special test procedures "Stop-and-Go" and "Autobahn" [4], and the PIMOT test procedure. The car tests according to the PIMOT procedure were carried out five times, with four realizations for each test.

Figures 5–8 show the average value and the standard deviation of specific distance pollutant emission in the UDC, EUDC, NEDC, FTP-75, Japan 10-15 Mode, and HWFET type-approval tests and in the "Autobahn" and "Stop-and-Go" special tests.

The average value and the standard deviation of the emission of pollutants determined for the whole sets of realizations of the PIMOT driving tests have been presented in Figs 9–12.

To assess the curves representing the relations between emission and average vehicle velocity in the type-approval and special driving tests and in the PIMOT driving tests, the mutually corresponding curves have been compared with each other in Figs 13–16.

The curves plotted as characteristics of specific distance emission of pollutants are consistent with the relations de-

spełniała wymagania dyrektywy 1999/96/WE Parlamentu Europejskiego i Rady. Do badań emisji zanieczyszczeń wykorzystano stanowisko do analizy spalin, w którego skład wchodzi system Horiba Mexa 7200 wyposażony w analizatory Horiba do pomiarów stężeń: tlenku węgla (AIA–721A), węglowodorów (FIA–725A), tlenków azotu (CLA–755A), dwutlenku węgla (AIA–722) i tlenu (MPA–720).

Jako testy homologacyjne przyjęto do badań: UDC (*Urban Driving Cycle*), EUDC (*Extra Urban Driving Cycle*), NEDC, FTP-75, Japan 10-15 Mode i HWFET, a jako testy specjalne: Stop and Go i Autobahn [4]. Badania w testach PIMOT odbywały się w czterech realizacjach dla każdego testu. Badania samochodu w każdym z testów wykonywano pięciokrotnie.

Na rysunkach 5–8 przedstawiono wartość średnią i odchylenie standardowe emisji drogowej zanieczyszczeń w testach homologacyjnych: UDC, EUDC, NEDC, FTP-75, Japan 10-15 Mode i HWFET oraz w testach specjalnych: Autobahn i Stop and Go.

Na rysunkach 9–12 przedstawiono wartość średnią i odchylenie standardowe emisji drogowej zanieczyszczeń w zbiorach testów PIMOT.

W celu oceny charakterystyk zależności emisji drogowej zanieczyszczeń od prędkości średniej w testach homologacyjnych i specjalnych oraz w testach PIMOT przedstawiono je na rysunkach 13–16.

Wyznaczone charakterystyki emisji drogowej zanieczyszczeń są zgodne z zależnościami wyznaczanymi na podstawie dostępnych wyników badań, np. na podstawie baz danych, zawartych w specjalistycznych oprogramowaniach, takich jak INFRAS [18], COPERT [16] oraz w pracach [11, 12, 14]. Ogólnie są spełnione pewne prawidłowości. Dla dużych utrudnień ruchu, dla których jest mała prędkość średnia, jest duża emisja drogowa zanieczyszczeń, szczególnie węglowodorów i tlenku węgla. Również jest znamienne zwiększanie się dla dużej prędkości średniej, odpowiadającej dużemu obciążeniu silników, emisji dro-

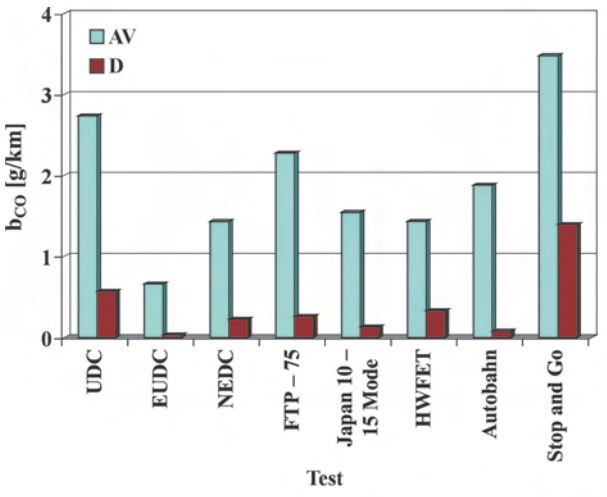

Fig. 5. Specific distance emission of carbon monoxide in the type-approval and special driving tests: AV – average value, D – standard deviation

Rys. 5. Emisja drogowa tlenku węgla w testach homologacyjnych i specjalnych: AV – wartość średnia, D – odchylenie standardowe

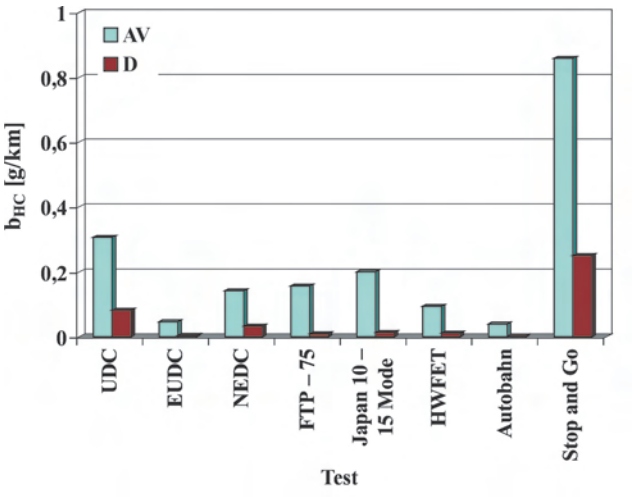

Fig. 6. Specific distance emission of hydrocarbons in the type-approval and special driving tests: AV – average value, D – standard deviation

Rys. 6. Emisja drogowa węglowodorów w testach homologacyjnych i specjalnych: AV – wartość średnia, D – odchylenie standardowe

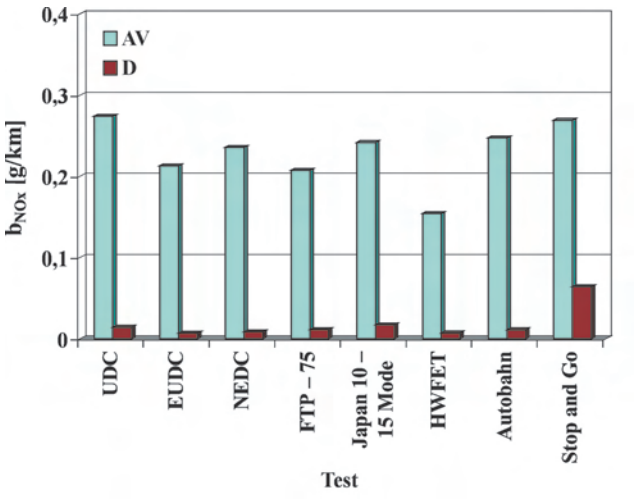

Fig. 7. Specific distance emission of nitrogen oxides in the type-approval and special driving tests: AV – average value, D – standard deviation

Rys. 7. Emisja drogowa tlenków azotu w testach homologacyjnych i specjalnych: AV – wartość średnia, D – odchylenie standardowe

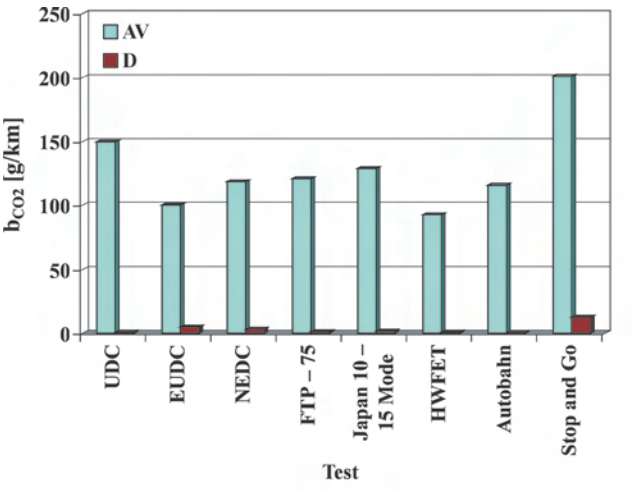

Fig. 8. Specific distance emission of carbon dioxide in the type-approval and special driving tests: AV – average value, D – standard deviation

Rys. 8. Emisja drogowa dwutlenku węgla w testach homologacyjnych i specjalnych: AV – wartość średnia, D – odchylenie standardowe

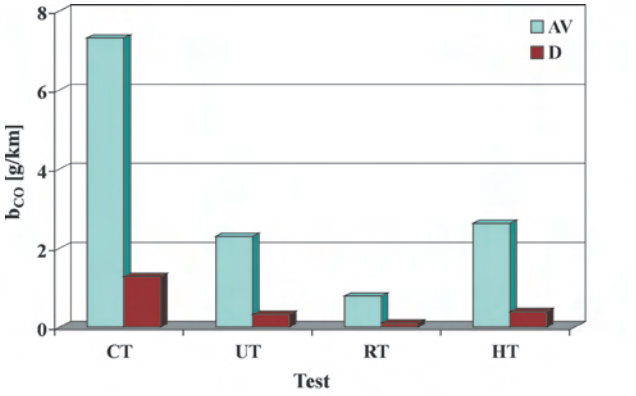

Fig. 9. Specific distance emission of carbon monoxide in the PIMOT driving tests: AV – average value, D – standard deviation

Rys. 9. Emisja drogowa tlenku węgla w testach PIMOT: AV – wartość średnia, D – odchylenie standardowe

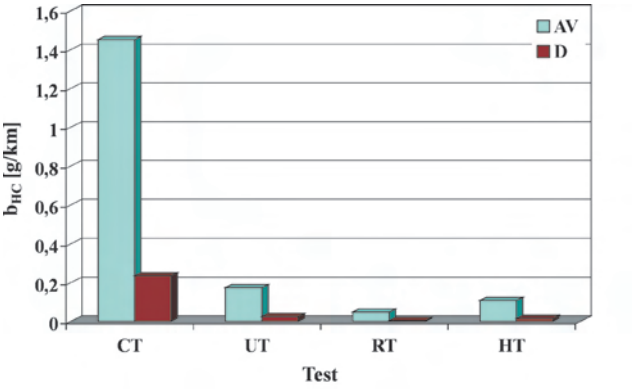

Fig. 10. Specific distance emission of hydrocarbons in the PIMOT driving tests: AV – average value, D – standard deviation

Rys. 10. Emisja drogowa węglowodorów w testach PIMOT: AV – wartość średnia, D – odchylenie standardowe

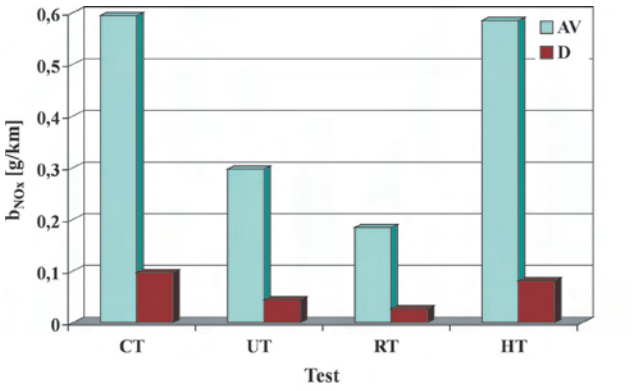

Fig. 11. Specific distance emission of nitrogen oxides in the PIMOT driving tests: AV – average value, D – standard deviation

Rys. 11. Emisja drogowa tlenków azotu w testach PIMOT: AV – wartość średnia, D – odchylenie standardowe

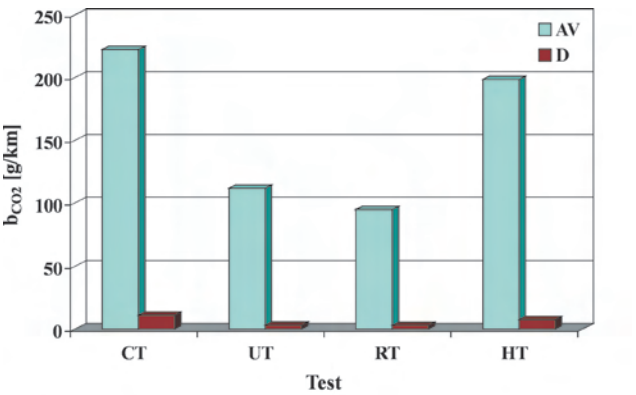

Fig. 12. Specific distance emission of carbon dioxide in the PIMOT driving tests: AV – average value, D – standard deviation

Rys. 12. Emisja drogowa dwutlenku węgla w testach PIMOT: AV – wartość średnia, D – odchylenie standardowe

termined from the available research results, e.g. from the databases incorporated in specialist computer programs such as INFRAS [18] or COPERT [16] or given in publications [11, 12, 14]. In general, some regularities can be observed in these characteristics. In the case of severe traffic difficulties, where the average vehicle velocity is low, the emission is high, especially the emission of hydrocarbons and carbon monoxide. It is also symptomatic that at high average velocity, corresponding to heavy engine loads, a growth is observed in the emission of nitrogen oxides, carbon dioxide, and, to a smaller extent, carbon monoxide.

Noteworthy is also the fact that: for the characteristic curves determined from the PIMOT tests, the differences between the emission values for low and high average vehicle velocity and for medium velocity are bigger than those observed in the characteristic curves plotted using the results of type-approval and special tests. This is even more interesting when taking into account that for some vehicle motion modes

gowej tlenków azotu i dwutlenku węgla i – w mniejszym stopniu – tlenku węgla

Jest znamienne, że dla charakterystyk wyznaczonych na podstawie testów PIMOT różnice między wartościami dla małych i dużych prędkości średnich samochodu oraz dla prędkości umiarkowanych są większe niż dla charakterystyk wyznaczonych na podstawie testów homologacyjnych i specjalnych. Jest to tym bardziej interesujące, że niektóre modele ruchu spośród testów homologacyjnych i specjalnych oraz testów PIMOT mają podobną prędkość średnią. Potwierdza to znany z badań emisji zanieczyszczeń z silników samochodowych fakt, że procesy emisji zanieczyszczeń są silnie zależne od przebiegów wielkości charakteryzujących stan pracy silnika, zdeterminowany przede wszystkim procesem prędkości pojazdu [4, 13, 14, 18]. Potwierdza to także celowość traktowania warunków ruchu pojazdów do celów oceny emisji zanieczyszczeń z silników samochodowych jako procesów stochastycznych.

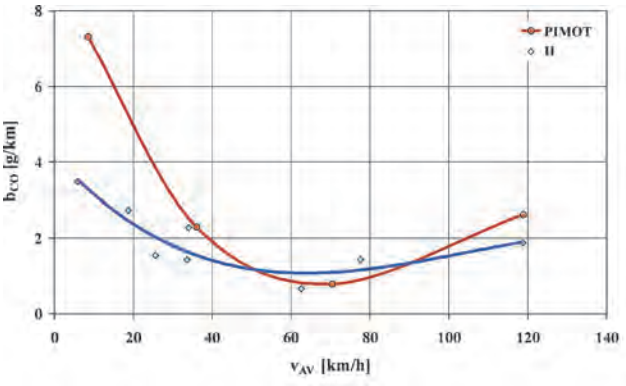

Fig. 13. Specific distance emission of carbon monoxide vs. average vehicle velocity curves, plotted for the type-approval and special driving tests (H) and for the PIMOT driving tests

Rys. 13. Porównanie zależności emisji drogowej tlenku węgla w testach homologacyjnych i specjalnych – H oraz w testach PIMOT od prędkości średniej

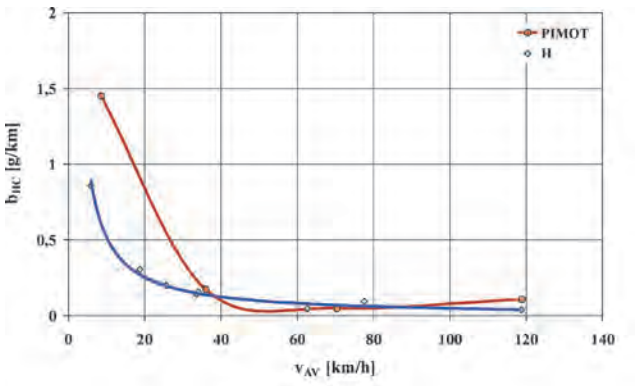

Fig. 14. Specific distance emission of hydrocarbons vs. average vehicle velocity curves, plotted for the type-approval and special driving tests (H) and for the PIMOT driving tests

Rys. 14. Porównanie zależności emisji drogowej węglowodorów w testach homologacyjnych i specjalnych – H oraz w testach PIMOT od prędkości średniej

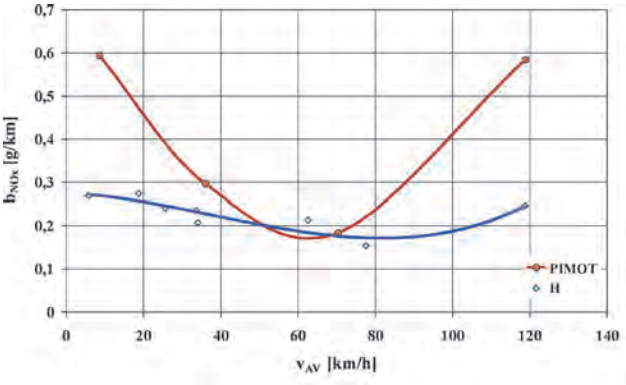

Fig. 15. Specific distance emission of nitrogen oxides vs. average vehicle velocity curves, plotted for the type-approval and special driving tests (H) and for the PIMOT driving tests

Rys. 15. Porównanie zależności emisji drogowej tlenków azotu w testach homologacyjnych i specjalnych – H oraz w testach PIMOT od prędkości średniej

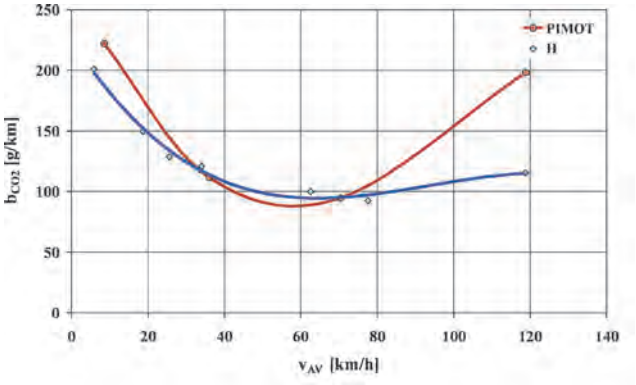

Fig. 16. Specific distance emission of carbon dioxide vs. average vehicle velocity curves, plotted for the type-approval and special driving tests (H) and for the PIMOT driving tests

Rys. 16. Porównanie zależności emisji drogowej dwutlenku węgla w testach homologacyjnych i specjalnych – H oraz w testach PIMOT od prędkości średniej

among those used in the type-approval and special tests and in the PIMOT tests, the average vehicle velocity takes similar values. This confirms the fact, known from other research works on the pollutant emission from automotive engines, that the pollutant emission processes are strongly dependent on changes of the quantities that characterize the engine operation state, determined above all by the vehicle velocity process [4, 13, 14, 18]. Thus, it should be considered useful to treat vehicle motion conditions as stochastic processes when they are analysed for the purposes of evaluation of pollutant emission from automotive engines.

Additionally, relations between the specific distance pollutant emission in type-approval, special, and PIMOT tests and the average vehicle velocity were determined (Figs 17–20). The sets of points were approximated by a polynomial function of the 3rd or 4th degree or by a power function (for hydrocarbons).

In the graphs above, differences, significant in some cases, between the pollutant emission values can be clearly seen in the sets of measurement results used; simultaneously, the curves that approximate the sets of test results, which

Dodatkowo wyznaczono zależności emisji drogowej zanieczyszczeń w testach homologacyjnych i specjalnych oraz w testach PIMOT od prędkości średniej – rysunki 17–20. Zbiory punktów aproksymowano funkcją wielomianową o stopniach 3 lub 4, albo funkcją potęgową (w odniesieniu do węglowodorów).

Na wykresach tych są wyraźnie widoczne znaczne niekiedy różnice wartości emisji drogowej zanieczyszczeń dla wykorzystywanych zbiorów wyników pomiarów, jednocześnie linie aproksymujące zbiory wyników badań, będące sumami zbiorów, pochodzących z badań w testach homologacyjnych i specjalnych oraz w testach PIMOT, wykazują tendencje zbieżne z charakterystykami wyznaczanymi dla poszczególnych pojazdów [12, 16, 18] oraz dla kategorii pojazdów [12, 16, 18].

4. Podsumowanie

Poziom nieokreśloności stanów pracy silników spalinowych użytkowanych w pojazdach samochodowych uzasadnia traktowanie warunków pracy tych silników jako przypadkowych. W związku z tym zaproponowano wyzna-

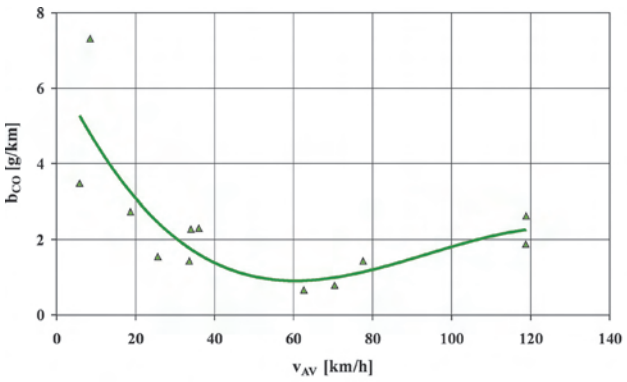

Fig. 17. Relation between the specific distance emission of carbon monoxide and the average vehicle velocity in type-approval, special, and PIMOT tests

Rys. 17. Zależność emisji drogowej tlenku węgla w testach homologacyjnych i specjalnych oraz w testach PIMOT od prędkości średniej

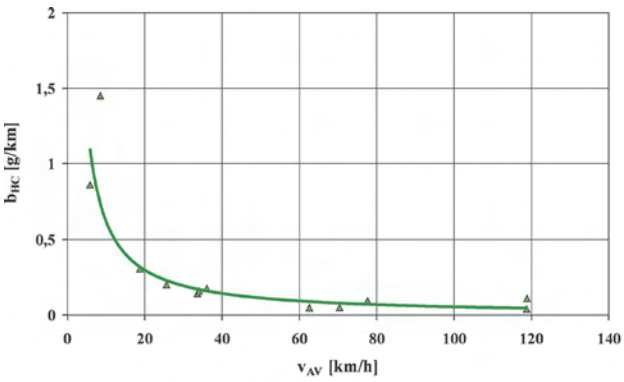

Fig. 18. Relation between the specific distance emission of hydrocarbons and the average vehicle velocity in type-approval, special, and PIMOT tests

Rys. 18. Zależność emisji drogowej węglowodorów w testach homologacyjnych i specjalnych oraz w testach PIMOT od prędkości średniej

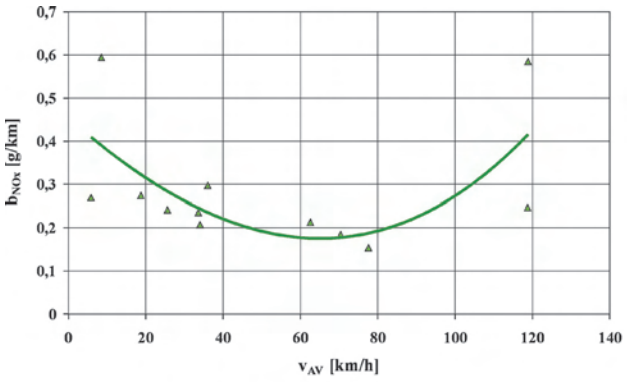

Fig. 19. Relation between the specific distance emission of nitrogen oxides and the average vehicle velocity in type-approval, special, and PIMOT tests

Rys. 19. Zależność emisji drogowej tlenków azotu w testach homologacyjnych i specjalnych oraz w testach PIMOT od prędkości średniej

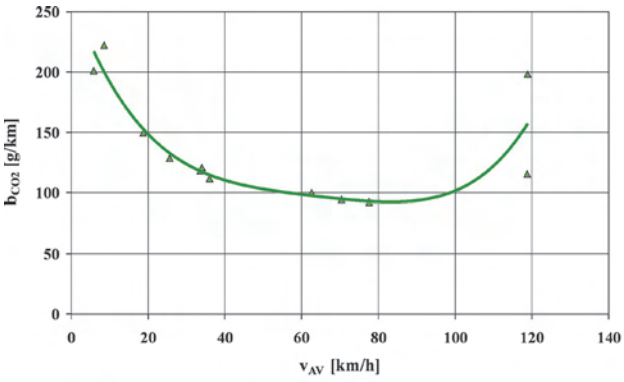

Fig. 20. Relation between the specific distance emission of carbon dioxide and the average vehicle velocity in type-approval, special, and PIMOT tests

Rys. 20. Zależność emisji drogowej dwutlenku węgla w testach homologacyjnych i specjalnych oraz w testach PIMOT od prędkości średniej

are sums of the sets derived from the tests carried out to the type-approval, special, and PIMOT test procedures, show trends coinciding with the characteristic curves determined for individual vehicles [12, 16, 18] and vehicle categories [12, 16, 18].

4. Conclusions

The level of indeterminacy of the states of operation of IC engines used in motor vehicles provides grounds for treating the conditions of operation of such engines as varying on a random basis. Therefore, a proposal was made to develop driving tests that would represent the conditions of motion of motor vehicles as realizations of stochastic processes. The tests of this type, named PIMOT tests, were designed in accordance with the criterion of faithful simulation in time domain, based on results of empirical determination of the velocity of a passenger car. To simulate the vehicle motion, models representing the vehicle operation modes in the conditions of street congestions, urban traffic, extra-urban traffic, and high-speed traffic on motorways and fast roads were adopted.

The pollutant emission was examined on a chassis dynamometer in PIMOT tests, type-approval tests (UDC, EUDC, NEDC, HWFET, and Japan 10-15 Mode), and special tests simulating the conditions of vehicle drive in street congestions ("Stop-and-Go") and on motorways ("Autobahn").

The research results revealed high dependence of the pollutant emission from an IC engine on the engine operation conditions. It is important to note the fact that even in tests with similar values of the average vehicle velocity, significant differences occur in the emission of individual pollutants. This confirms the usefulness of treating the conditions of operation of automotive IC engines as stochastic processes.

For both the PIMOT and other test types, the characteristic curves plotted as representing the relation between pollutant emission and average vehicle velocity show regularity and consistency with the current state of knowledge. However, there are differences between the curves being compared. This confirms high dependency of the pollutant emission from IC engines on both the static and dynamic states of engine operation.

czanie testów jezdnych, charakteryzujących warunki ruchu pojazdów samochodowych, jako realizację procesów stochastycznych. Testy te, nazwane testami PIMOT, wyznaczono zgodnie z kryterium wiernej symulacji w dziedzinie czasu na podstawie wyników badań empirycznych prędkości samochodu osobowego. Przyjęto modele ruchu samochodów w warunkach: zatorów ulicznych, w miastach, poza miastami oraz na autostradach i drogach ekspresowych.

Badania emisji zanieczyszczeń na hamowni podwoziowej przeprowadzono w testach PIMOT oraz w testach homologacyjnych (UDC, EUDC, NEDC, HWFET i Japan 10-15 Mode) i specjalnych, symulujących jazdę w zatorach ulicznych – Stop and Go i na autostradach – Autobahn.

Wyniki badań wykazały znaczną wrażliwość emisji zanieczyszczeń na warunki pracy silnika spalinowego. Jest znamienne, że nawet dla testów o zbliżonej wartości średniej prędkości bywają znaczne różnice wartości średniej emisji drogowej zanieczyszczeń. Potwierdza to celowość traktowania warunków pracy samochodowych silników spalinowych jako procesów stochastycznych.

Wyznaczone charakterystyki emisji zanieczyszczeń w zależności od wartości średniej wykazują dla obydwu rodzajów testów regularność i zgodność ze stanem wiedzy, jednocześnie jednak występują między porównywanymi charakterystykami różnice. Potwierdza to znaczną wrażliwość emisji zanieczyszczeń zarówno na statyczne, jak i dynamiczne stany pracy silników.

This paper was based on results of tests carried out as a part of research project No. N N509 556440 entitled "Sensitivity of pollutant emission and fuel consumption to the conditions of use of a spark-ignition engine for mobile applications", sponsored by the National Science Centre.

Artykuł opracowano na podstawie wyników badań realizowanych w pracy N N509 556440 „Wrażliwość emisji zanieczyszczeń i zużycia paliwa na warunki użytkowania trakcyjnego silnika o zapłonie iskrowym", finansowanej ze środków Narodowego Centrum Nauki.

Bibliography/*Literatura*

[1] Abou Zeid M., Chabini I., Nam E.K., Cappiello A. Probabilistic modeling of acceleration in traffic networks as a function of speed and road type. Proceedings of the IEEE 5th International Conference on Intelligent Transportation Systems, Singapore, September 2002, 472–478.

[2] Arregle J., Bermudez V., Serrano J.R., Fuentes E. Procedure for engine transient cycle emissions testing in real time. Experimental Thermal And Fluid Science 2006, 30 (5), 485–496.

[3] Beevers S.D., Carslaw D.C. The impact of congestion charging on vehicle emissions in London. Atmospheric Environment 2005, 39 (1), 1–5.

[4] BUWAL, INFRAS AG. Luftschadstoffemissionen des Strassenverkehrs 1950-2010. BUWAL–Bericht Nr. 255, 1995.

[5] Cappiello A., Chabini I., Nam E. K., Lue A., Abou Zeid M. A statistical model of vehicle emissions and fuel consumption. Proceedings of the IEEE 5th International Conference on Intelligent Transportation Systems, Singapore, September 2002, 801–809.

[6] Chin A.T.H. Containing air pollution and traffic congestion: transport policy and the environment in Singapore. Atmospheric Environment 1996, 30 (5), 787–801.

[7] Chłopek Z., Biedrzycki J., Lasocki J., Wójcik P. Emisja zanieczyszczeń z silnika samochodu w testach jezdnych symulujących rzeczywiste użytkowanie trakcyjne. Zeszyty Naukowe Instytutu Pojazdów 2013, 92 (1), 65–74.

[8] Chłopek Z., Biedrzycki J., Lasocki J., Wójcik P. Investigation of pollutant emissions from a motor vehicle engine in tests simulating real vehicle use in road traffic conditions. Combustion Engines 2013, 154 (3), 202–207.

[9] Chłopek Z., Biedrzycki J., Lasocki J., Wójcik P. Report of research project No. N N509 556440 "Sensitivity of pollutant emission and fuel consumption to the conditions of use of a spark-ignition engine for mobile applications". Warszawa 2013 (not published, in Polish).
[10] Chłopek Z., Biedrzycki J., Lasocki J., Wójcik P. Investigation of the motion of motor vehicles in Polish conditions. The Archives of Automotive Engineering – Archiwum Motoryzacji 2013, 60 (2), 3–20.
[11] Chłopek Z., Laskowski P. Pollutant emission characteristics determined using the Monte Carlo Method. Eksploatacja i Niezawodność – Maintenance and Reliability 2009, 42 (2), 42–51.
[12] Chłopek Z., Zimakowska M. Charakterystyki emisji zanieczyszczeń z samochodowych silników spalinowych (Characteristics of pollutant emission (from) vehicle internal combustion engines). A chapter in the monograph "Współczesne problemy inżynierii i ochrony środowiska (Present-day problems of environmental engineering and protection)". Prace Naukowe Politechniki Warszawskiej – Inżynieria Środowiska, Oficyna Wydawnicza Politechniki Warszawskiej (Publishing House of the Warsaw University of Technology), Warszawa 2009, 55, 53–66.
[13] Chłopek Z. Metody badań właściwości silników spalinowych w warunkach przypadkowych modelujących użytkowanie (Methods of examining the properties of internal combustion engines in random conditions modelling the real engine operation). Archiwum Motoryzacji 2001, 4, 187–210.
[14] Chłopek Z. Modelowanie procesów emisji spalin w warunkach eksploatacji trakcyjnej silników spalinowych (Modelling of exhaust emission processes in the conditions of operation of combustion engines in mobile applications). Prace Naukowe Politechniki Warszawskiej – Mechanika, Oficyna Wydawnicza Politechniki Warszawskiej (Publishing House of the Warsaw University of Technology), Warszawa, 173/1999.
[15] Chłopek Z. The research of the probabilistic characteristics of exhaust emissions from vehicle engines. Combustion Engines – Silniki Spalinowe 2011, 144 (1), 49–56.
[16] COPERT IV – Methodology and Emission Factors. European Environment Agency. European Topic Center on Air Emission, 2000.
[17] Frey H.C., Zheng J. Probabilistic analysis of driving cycle–based highway vehicle emission factors. Environmental Science & Technology 2002, 36 (23), 5184–5191.
[18] INFRAS AG. Handbuch für Emissionsfaktoren des Strassenverkehrs. Version 3.1. Bern 2010.
[19] Merkisz J., Gis W. Exhaust emission from vehicles under real conditions. Proceedings of the Ninth Asia–Pacific International Symposium on Combustion and Energy Utilization: APISCEU. Beijing, 02–06 November 2008.
[20] Merkisz J., Pielecha J., Gis W. Comparison of vehicle emission factors in NEDC cycle and road test. Proceedings of the Ninth Asia–Pacific International Symposium on Combustion and Energy Utilization: APISCEU. Beijing, 02–06 November 2008.
[21] Romaniszyn K., Nowak A. Analiza wpływu parametrów ruchu pojazdu na zużycie paliwa i emisję zanieczyszczeń przy przejeździe przez Bielsko–Białą (An influence of car motion parameters on fuel consumption and the emission of pollutants). Zeszyty Naukowe OBRSM BOSMAL 2004, 23 (1), 43–49.
[22] Romaniszyn K., Nowak A. Wpływ parametrów ruchu pojazdu na zużycie paliwa i emisję zanieczyszczeń przy przejeździe przez Bielsko–Białą (Influence of car motion parameters on fuel consumption and pollutant emissions during a test drive through Bielsko-Biała). Zeszyty Naukowe – Inżynieria Włókiennicza i Ochrona Środowiska, University of Bielsko-Biała, 2004, Series No. 5: Konferencje, 14, 176–182.
[23] Rostkowski J., Brady J., Torres J. Exhaust emissions testing of fifteen buses in Santafe de Bogotá, D.C. Operating with 1000 and 3000 ppm sulphur diesel. Technical report. Environment Canada, Environmental Technology Centre, Emissions Research Measurement Division and Empresa Colombiana de Petróleos and Instituto Colombiano del Petroleo ECOPETROL. Ottawa 2000.
[24] Sturm P.J. Boulter P., Haan P., Joumard R., Hausberger S., Hickman J., Keller M., Niederle W., Ntziachristos L., Reiter C., Samaras Z., Schinagl G., Schweizer T., Pischinger R. Instantaneous emission data and their use in estimating passenger car emissions. MEET project: Methodologies for estimating air pollutant emissions from transport. Final report COST 319 A2. Technical University of Graz. Graz, Austria 1998.
[25] Wang J., Storey J., Domingo N., Huff S., Thomas J., West B. Studies of diesel engine particle emissions during transient operations using an engine exhaust particle size. Aerosol Science and Technology 2006, 40 (11), 1002–1015.
[26] Worldwide emission standards. Passenger cars and light duty vehicles. Delphi. Innovation for the real world. 2012/2013.
[27] www.dieselnet.com.

Prof. Zdzisław Chłopek, DSc., DEng. – professor at the Faculty of Automotive and Construction Machinery Engineering at Warsaw University of Technology.

Prof. dr hab. inż. Zdzisław Chłopek – profesor na Wydziale Samochodów i Maszyn Roboczych Politechniki Warszawskiej.

e-mail: *zchlopek@simr.pw.edu.pl*

Jacek Biedrzycki, MEng. – head of Laboratory of Engines and Chassis in the Automotive Industry Institute in Warsaw.

Mgr inż. Jacek Biedrzycki – kierownik Pracowni Badań Silników i Podwozi w Przemysłowym Instytucie Motoryzacji w Warszawie.

e-mail: *j.biedrzycki@pimot.eu*

Jakub Lasocki, DEng. – doctor at the Faculty of Automotive and Construction Machinery Engineering at Warsaw University of Technology.

Dr inż. Jakub Lasocki – adiunkt na Wydziale Samochodów i Maszyn Roboczych Politechniki Warszawskiej.

e-mail: *j.lasocki@simr.pw.edu.pl*

Piotr Wójcik, MEng. – scientific and technical specialist in the Automotive Industry Institute in Warsaw.

Mgr inż. Piotr Wójcik – specjalista badawczo-techniczny w Przemysłowym Instytucie Motoryzacji w Warszawie.

e-mail: *p.wojcik@pimot.eu*

Przemysłowy Instytut Maszyn Rolniczych

60-963 POZNAŃ, ul. Starołęcka 31
tel. (+48 61) 871-22-00, fax (+48 61) 879-32-62
e-mail: office@pimr.poznan.pl, http://www.pimr.poznan.pl

Instytut już blisko 70 lat prowadzi prace naukowo-badawcze i badawczo-rozwojowe tworząc postęp techniczny w budowie i eksploatacji maszyn oraz urządzeń roboczych, wdraża wyniki badań do praktyki gospodarczej, współpracuje z licznymi instytucjami, uczelniami oraz przemysłem krajowym i zagranicznym.

Szereg rozwiązań (maszyn, urządzeń i technologii) opracowanych przez Instytut i wdrożonych w zakładach przemysłowych jest eksploatowanych w kraju i zagranicą.

Jednym z ostatnich sukcesów PIMR jest:

- *Maszyna i zestaw urządzeń umożliwiający usuwanie roślinności inwazyjnej na obszarach wodno-błotnych cennych przyrodniczo, którą wyróżniono szeregiem nagród:*

PIMR OFERUJE

- ***nowoczesne projektowanie i wirtualne modelowanie maszyn***
- ***badania symulacyjne i eksploatacyjne maszyn***
- ***badania obciążeniowe maszyn i urządzeń roboczych***
- ***szybkie prototypowanie - „rapid prototyping”***
- ***technologię produkcji biopaliw na potrzeby gospodarstw rolnych***
- ***badania „zgodności typu" i analizę zagrożeń maszyn***

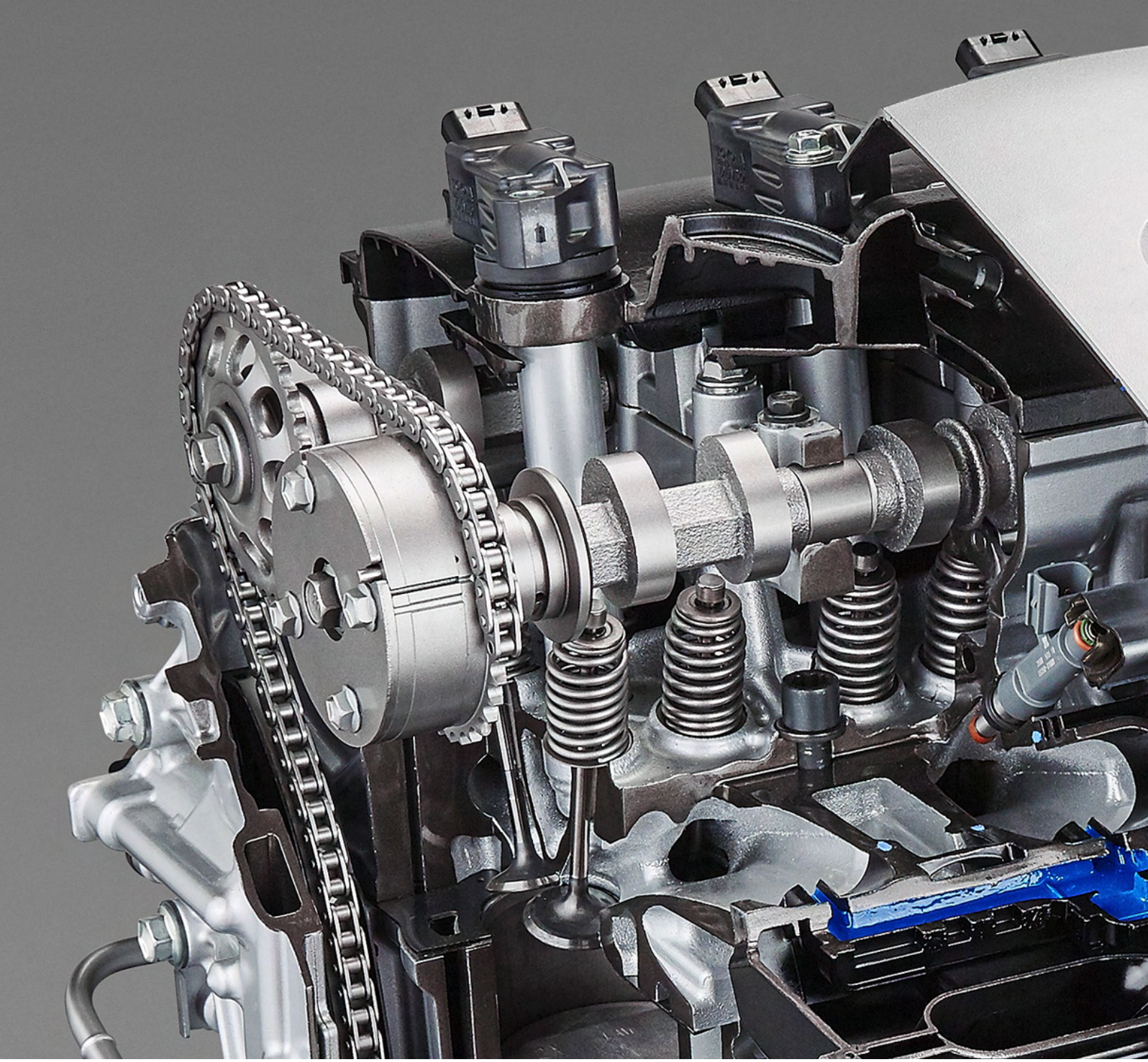

Publisher:

Polish Scientific Society of Combustion Engines

Combustion Engines

Polskie Towarzystwo Naukowe Silników Spalinowych

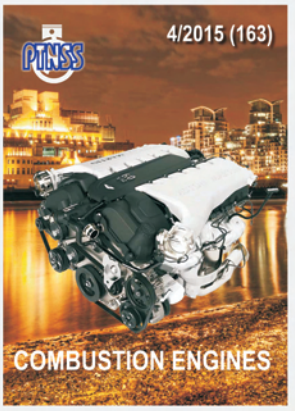

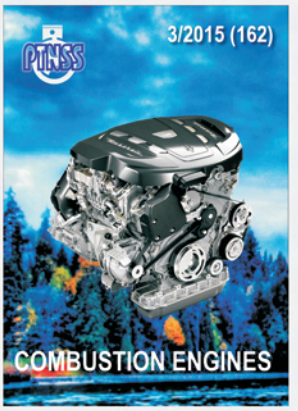

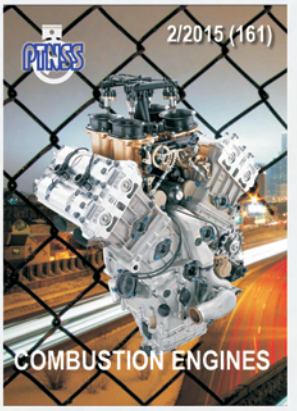

ISSN: 2300-9896

www.combustion-engines.eu